Synthesis and Characterisation of Layered Double Hydroxides and their Application for Water Purification

Discipline of Nanotechnology and Molecular Science, School of Chemistry, Physics and Mechanical Engineering, Science and Engineering Faculty, Queensland University of Technology, Brisbane Queensland 4001, Australia.

Frederick. L. Theiss
BAppSc(chem)

This thesis is submitted as part of the assessment requirements of the Master of Applied Science Degree at the Queensland University of Technology

2012

Keywords

Layered double hydroxides, hydrotalcites, anionic clays, water purification, sulfate, nitrate, fluoride, iodine, iodide, stichtite, powder X-ray diffraction, thermogravametric analysis, thermogravimitry, evolved gas analysis, evolved gas mass spectrometry.

Abstract

Layered doubly hydroxides (LDHs) also known as hydrotalcites or anionic clays are a group of clay minerals that have shown promise for the removal of toxic anions from water through both anion exchange and a process known as the reformation effect. This project has involved the preparation and characterisation of LDH materials as well as the investigation of their ability to remove selected anions from aqueous solutions by the reformation effect.

The LDH materials were successfully prepared from magnesium, aluminium, zinc and chromium chloride salts using the co-precipitation method. Samples were characterised using powder X-ray diffraction (XRD) and thermogravimetry (TG) to confirm the presence of LDHs. Powder XRD revealed a characteristic LDH structure for all LDH samples. Thermal Analysis showed decomposition usual occurred through a three or four step process as expected for LDHs. Preliminary investigations of the removal of sulfate, nitrate and fluoride by an Mg/Al LDH were carried out, and the products were characterised using XRD and TG which showed that an LDH material similar to the original hydrotalcite was formed after reformation.

A Zn/Al LDH was investigated as a potential sorbent material for the removal of iodine and iodide from water. It was found that the LDH was a suitable adsorbent which is able to remove almost all of the iodine present in the test solutions. Again, the products were characterised by XRD, TG and evolved gas mass spectrometry (EGMS) in an attempt to better understand

the iodine removal process. Powder XRD showed successful reformation of the LDH structure and TG/EGMS showed that only a small amount of iodine species were lost during thermal decomposition. Finally, the mineral stichtite a Mg/Cr LDH was successfully synthesised and investigated using XRD, TG and EGMS. Unfortunately, due to lack of time it was not possible to identify any new uses for the mineral stichtite in the current project.

Table of Contents

List of Figures

List of Tables

Statement of Original Authorship

The work contained in this thesis has not been previously submitted to meet requirements for an award at this or any other higher education institution. To the best of my knowledge and belief, the thesis contains no material previously published or written by another person except where due reference is made.

_____ _____

Frederick L. Theiss (Author) Date

Acknowledgments

I would like to thank and acknowledge the following individuals and organisations. My supervisors Emeritus Professor Ray Frost and Professor Godwin Ayoko. I would also like to thank Dr. Sara Couperthwaite for her considerable assistance as well as Dr. Wayde Martens for his assistance with the thermogravametric analysis and Mr. Tony Raftery for his help with powder XRD. I also wish to thank Mr. Michael J. Sear-Hall for his assistance with the experimental work in chapter three and everyone else at the Discipline of Chemistry, Faculty of Science and Technology, Queensland University of Technology.

List of publications

Accepted Publications

Frederick L. Theiss, Sara J. Palmer, Godwin A. Ayoko, and Ray L. Frost, *"Sulfate Intercalated Layered Double Hydroxides Prepared by the Reformation Effect"*, published in print *"Journal of Thermal Analysis and Calorimetry"*, (2011) 107, pp.1123-1128.

Available from: http://eprints.qut.edu.au/48760/

Frederick L. Theiss, Michael J. Sear-Hall, Sara J. Palmer and Ray L. Frost, *"Zinc Aluminium Layered Double Hydroxides for the Removal of Iodine and Iodide from Aqueous Solutions"* published in print *"Desalination and Water Treatment"*, (2012) 39(1-3), pp. 166-175.

Available from: http://eprints.qut.edu.au/50293/

Collaboration with other Authors

Frost, Ray L., Palmer, Sara J., Theiss, Frederick *"Synthesis and Raman spectroscopic characterisation of hydrotalcites based on the formula* $Ca_6Al_2(CO_3)(OH)_{16}\cdot 4H_2O$*"*, published in print *"Journal of Raman Spectroscopy"*, (2011), 42(5), 1163-1167.

Conferences Presentations

Frederick Theiss, Sara J. Palmer, Godwin A. Ayoko and Ray L. Frost, *"Application of Layered Double Hydroxides for Water Purification"* Poster and abstract presented at the Australian Clay Mineral Society conference 2010, 07-08-2010 to 08-08-10

Chapter One:

Introduction to Layered Double Hydroxides

Chapter 1: Introduction to Layered Double Hydroxides

1.1 Introduction

Layered double hydroxides (LDHs) also known as anionic clays or hydrotalcite like materials have found many uses including medical applications, additives in polymers, the formation of composite nano-materials, precursors to mixed metal oxide catalysts and the removal of environmental hazards [1-3]. LDHs are based on the structure of brucite ($Mg(OH)_2$) in which magnesium ions occupy octahedral positions in a complex layered structure. In LDHs, varying amounts of the divalent cation, such as Mg^{2+}, is substituted with a trivalent cation, such as Al^{3+}, in the case of hydrotalcite, which was one of the first examples of the LDHs to be discovered. LDHs have been prepared using many combinations of divalent trivalent cations including magnesium, aluminium, zinc, nickel, chromium, iron, copper, indium, gallium, and calcium [4-35]. LDHs can be described by the general formula:

$$\mathbf{[M_{1-x}^{2+}M_x^{3+}(OH)_2]^{x+}[A^{n-}]_{x/n}\cdot \mathit{m}H_2O} \qquad (1.1)$$

Where M^{2+} and M^{3+} are the divalent and trivalent layer cations respectively, $0.2 < x < 0.33$ and A^{n-} is the exchangeable anion [3, 30, 36]. The layers of a LDH carry a net positive charge that is balanced by anions that are either intercalated between the layers or attracted to the surface. This structure gives LDHs natural anion exchange properties that make them unique amongst the clay minerals, most of which exhibit negatively charged layers with cation exchange properties. One application of LDHs, which has received considerable attention in recent years is their ability to be used as

sorbents for the removal anions from aqueous solutions. LDHs are able to remove anions from water by two different mechanisms; 1) anion exchange [2, 37, 38] and 2) the reformation effect [2, 3, 38]. As this chapter will show, LDHs are able to remove a wide range of anions from water. LDHs occur in nature but are also cheap and simple to produce, making them an attractive option for water purification. The main disadvantage of LDHs it that they are not selective to particular anions, meaning that all anions in solution must be removed not just the anions of interest.

1.2. Review of Previous Literature

The wide range of layered double hydroxides, as well as the numerous applications for which they can be used, means that much of the available literature is not directly relevant to this project. This review aims to provide a sample of the available literature that contains relevant or required background information necessary to understand this project.

1.2.1. Sorption of Anions by Ion Exchange

As previously mentioned LDHs exhibit anion exchange properties in their natural state [37]. This property can be used for the removal of anionic contaminants from water, however, superior results are usually obtained if the LDH is thermally activated. If the LDH is to be used as an anion exchange material it is important to select an anion that the LDH has lower affinity for than the target anion [37, 38]. As a result carbonate containing LDHs are not optimum anion exchange materials due to the strong affinity they exhibit for the carbonate anion. Care must be taken when using non-

carbonate containing LDHs to ensure that adsorption of carbonate from the atmosphere or dissolved in water is minimised [2, 37].

An important investigation into the ion exchange properties of LDHs was carried out by Miyata in 1983 [37]. Miyata began by preparing three different Mg/Al LDHs each containing a different interlayer anion. The anions chosen for investigation were nitrate, chloride and sulfate. Samples of the LDH were then treated with a number of different anion solutions including F^-, Br^-, I^-, OH^-, CO_3^{2-}, SO_4^{2-} and the anionic dye Naphthol Yellow S (NYS^{2-}) with the chemical formula $C_{10}H_4N_2Na_2O_8S{\cdot}3H_2O$. The flasks containing the mixtures were maintained at a constant temperature of 25°C overnight with constant shaking before separation of the mixture by filtration. The anion concentration was quantified by analysing the filtrate using various wet chemical and instrumental techniques [37].

Miyata plotted ion exchange isotherms for each sample and used them to calculate selectivity coefficients (K_{ANO3}) with respect to the nitrate containing LDH. The order of anion selectivity for monovalent anions was $OH^- > F^- > Cl^- > Br^- > NO_3^- > I^-$. The order of anion selectivity for divalent anions was $CO_3^{2-} > NYS^{2-} > SO_4^{2-}$. All samples except for the iodide containing LDH were found to fit the Langmuir type adsorption isotherm [37].

1.2.2. Sorption of Anions by the Reformation Effect

Thermal activation (TA) requires heating the LDH to between 300-500°C. This removes the interlayer water and anions resulting in the formation of a

mixed metal oxide [39, 40]. An unusual property of thermally activated layered double hydroxides (TA-LDH) is that when they are exposed to water and a source of anions the LDH structure can be re-formed through the sorption of anions and water. This process is known as the reformation (or memory) effect [2, 3, 38].

To maximise the reformation effect the maximum number of anions possible must be removed during thermal activation. It is therefore important to choose anions that can be easily removed at elevated temperatures forming stable non-toxic decomposition products [41]. Carbonate is an ideal anion for this purpose. As a carbonate containing LDH decomposes it releases carbon dioxide and water vapour which are both stable and non-toxic (in low concentrations). LDHs also have a higher affinity for carbonate than any other anion and this can reduce the likelihood of non-removable anions being exchanged during long term storage and eliminates the need for precautions to prevent non-carbonate containing LDHs from adsorbing carbonate from the atmosphere or dissolved in water [37, 38].

As previously mentioned it is desirable to remove as many interlayer anions as possible during thermal activation as this will result in better performance of the TA-LDH sorbent. However, using an excessively high thermal activation temperature may result in the partial decomposition of the LDH structure into oxides that cannot undergo reformation. This will results in a reduction of anion sorption efficiency as part of the adsorbent is no longer

usable. For these reasons, the thermal activation temperature is an important factor that must be carefully considered. Optimum anion sorption efficiency is achieved by balancing these two factors [40]. The optimum thermal activation temperature depends on the stability of the individual LDH and is usually determined experimentally. It is typically between 300 and 800°C depending on the LDH [2, 3, 38].

1.2.3. Synthesis of Layered Double Hydroxides

Several methods have been developed for the synthesis of LDHs. These include co-precipitation [42], the urea method [40, 42], the sol gel method [42], the microwave irradiation method [42] and the alkali metal method [42]. Each method has its own unique advantages and disadvantages when compared to the other methods [42, 43]. The co-precipitation method is the simplest and most commonly used of all methods for the preparation of LDHs, and is the only method that will be described in detail here. This method involves the preparation of two solutions, the first containing the desired metal cations as salts (usually of chloride or nitrate) dissolved in solution in their desired stoichiometric ratio; and the second solution is a caustic solution at a pH of 9 or greater. The caustic solution may also contain the desired interlayer anions depending on the co-precipitation method chosen. The LDH is then prepared by delivering the two solutions to each other dropwise from a burette, separating funnel or a peristaltic pump. The metal cations will co-precipitate then the solution reaches super saturation. Super saturation is achieved by addition of the caustic solution which causes the solution pH to increase. When the solution pH exceeds the

pH at which the most soluble hydroxide of the metals in solution is precipitated the LDH will precipitate. The precise identity of the base is not particularly important, however, anions such as OH^- may be competitively intercalated into the interlayer of the LDH. Once the solutions are combined the hydrotalcite will form as a precipitate that can be collected by filtration. The precipitate must be dried to remove excess water and ground to a uniform consistency before it can be used. The co-precipitation method is often preferred as it is simple to carry out and does not require any volatile solvents or other harsh and expensive chemicals or apparatus [42, 43]. Unfortunately, LDHs prepared by co-precipitation often suffer from poor crystalinity and the presence of impurities. In contrast a method like the urea method (which is in many ways similar to co-precipitation) allows better control of particle size and higher crystallinity than other methods [44]. However, the urea method is only suitable for preparation of LDHs with high charge density, meaning is cannot be used to prepare LDHs containing Cu^{2+} or Cr^{3+}.

1.2.4. Techniques used for Characterisation of LDHs

Many techniques are used to characterise LDHs and assess their effectiveness as anion adsorbent. These techniques often include Powder X-ray diffraction (powder XRD), energy-dispersive X-ray spectroscopy (EDX), infrared spectroscopy (IR) near infrared spectroscopy (NIR), Raman spectroscopy (Raman) and thermal analysis techniques such as: theromgravametric analysis (TGA), differential thermal analysis (DTA), differential scanning calorimitry (DSC), and nitrogen BET surface area

measurements (BET). Only some of these techniques will be mentioned in greater detail.

1.2.4.1. Powder XRD

Powder X-ray diffraction is a useful technique for the characterisation of LDHs and allows for phase identification of crystalline materials [2, 45, 46]. As LDH materials have a similar layered structure, they all share a similar characteristic XRD pattern. Crystalline impurities in samples can be readily identified using powder XRD by simply comparing their characteristic diffraction pattern to a reference library of patterns. Additional information can be obtained by examining changes in the $d_{(003)}$ spacing of the LDH. The $d_{(003)}$ spacing of a LDH corresponds to the distance between the cation layers. When the interlayer anions in a LDH are changed, a corresponding change in the $d_{(003)}$ spacing should be observed. This change will indicate if the new anions have been successfully intercalated into the LDH or simply adsorbed onto the surface of the material [8, 38].

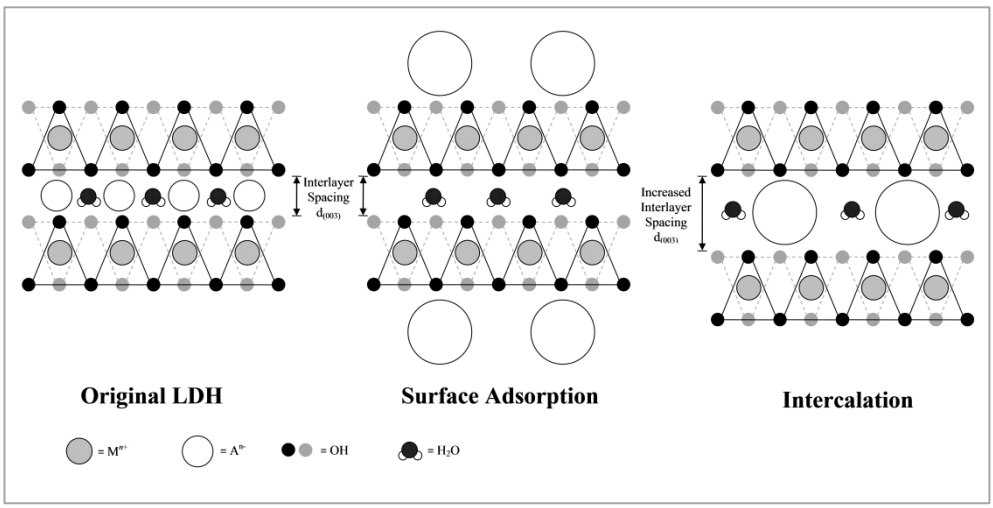

Figure. 1.1: Intercalation of anions in a LDH material.

Thermally activated LDHs have a very different diffraction pattern compared to non-activated LDH. They are often dominated by highly intense peaks corresponding to metal oxides formed during decomposition of the LDH.

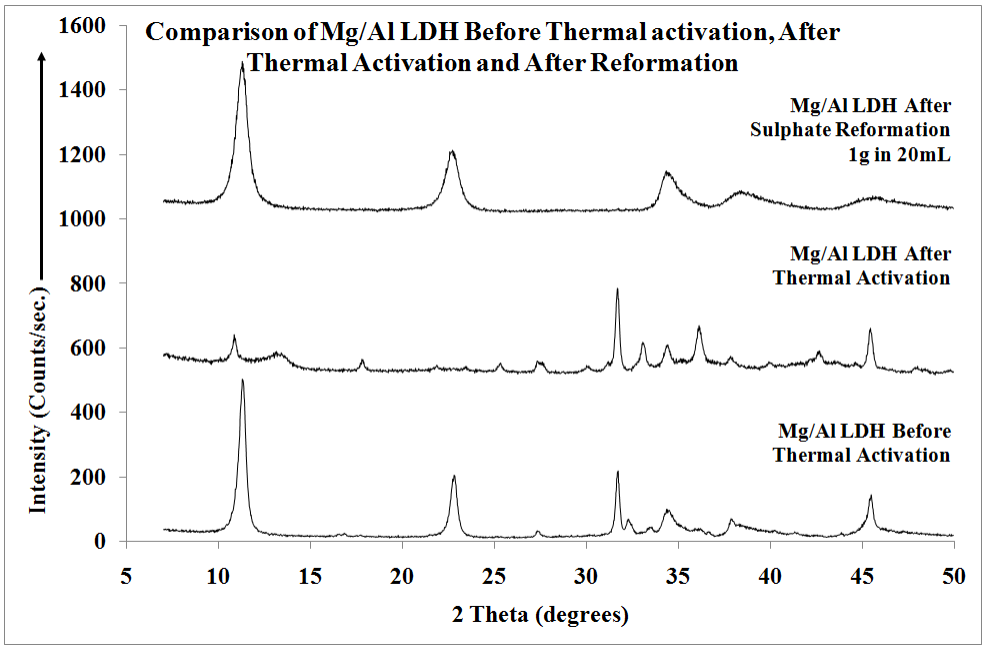

Figure. 1.2: Powder XRD pattern of Mg/Al LDH before thermal activation (Bottom), after thermal activation (middle) and reformation after treatment of 1g of Mg/Al LDH in 20mL of sodium sulfate solution (top).

At lower thermal activation temperatures various partially decomposed oxides and hydroxides will be observed in the sample, however, the exact composition of the product will depend on the LDH that has been thermally activated.

1.2.4.2. Thermal Analysis of Layered Double Hydroxides

Thermogravimetry (TG) also known as thermogravimetric analysis (TGA) is the most common thermal analysis technique used in LDH research. In TG, a sample is heated so that the temperature increases slowly over time. The change in the mass of the sample is recorded and plotted against temperature to produce a TG curve [2, 33, 47]. As the sample is heated, processes such as the evolution of a gas may occur which can result in an observable loss of mass.

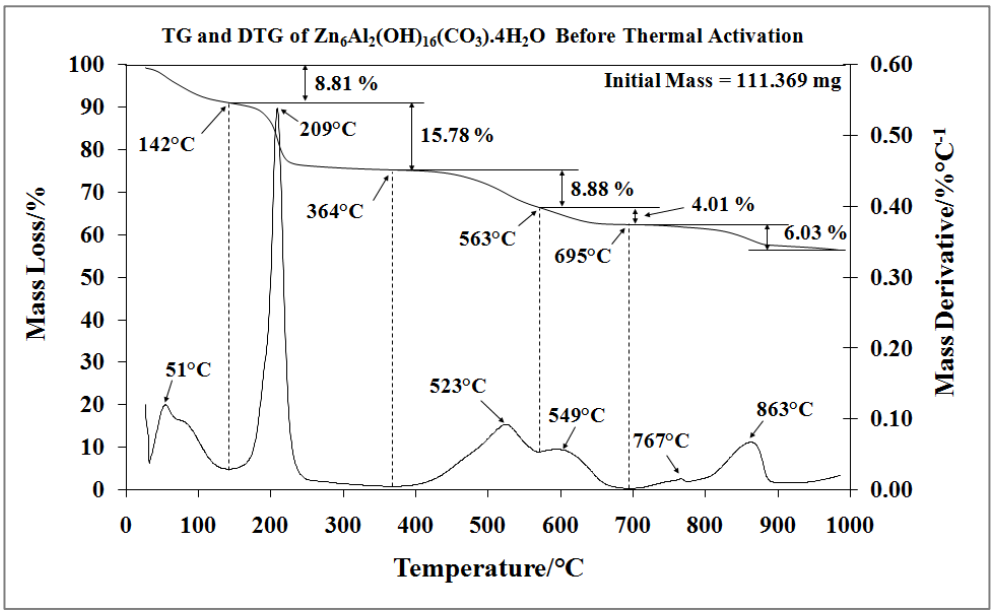

Figure. 1.3: TG and DTG curve for the thermal decomposition of a Zn/Al LDH.

It is common to examine TG results using a differential thermogravimetry (DTG) curve. The DTG curve is obtained by differentiating the TG curve obtained from the experiment (this is usually done automatically by the instrument's software package). In the DTG curve, mass losses which occur as points of inflection in the TG curve are transformed into local maxima which helps to show the changes in mass more clearly. The significant

disadvantages of TG (and DTG) is that it is unable to identify processes that may occur during decomposition of the sample that do not result in a change in mass (an example of this is a phase change). To obtain information on these types of processes other thermal analysis techniques such as differential thermal analysis (DTA) or differential scanning calorimetry (DSC) must be used. Another disadvantage of TG is that the technique does not directly identify the gases evolved, however, this difficulty can be overcome by coupling the thermogravimetric analyser to an instrument capable of detecting and/or identifying gases. Evolved gas detection (EGD) is concerned with simply detecting at what temperatures gases are evolved from the sample while evolved gas analysis (EGA) is used to identify any evolved gases.

When a sample undergoes decomposition or desorption, gases can be evolved. Evolved gas detection (EGD) is often coupled with TG, DTA and DSC to provide additional information about the decomposition of the sample [33, 47]. As the instruments furnace is usually purged with a purge gas (which depends on the experiment), the outgoing gas stream exiting the furnace can be directed to a detector similar to those used in gas chromatography. Detectors that can be used include flame ionisation, thermal conductivity and gas density detectors [33, 48]. These simple detectors only register when a gas has been evolved, they do not provide information on the identity of that gas. If the evolved gas is to be identified then evolved gas analysis (EGA) must be used.

Evolved gas mass spectrometry (EGMS) is currently most popular method for EGA [48]. In this technique evolved gases are identified by their molecular mass using a mass spectrometer [33, 48]. Historically there has been difficulty coupling these two techniques. Mass spectrometers can only operate under low pressure, which is required to reduce the number of collisions between ions as they pass through the mass analyser and reach the detector (low pressures provide a longer mean free path). As previously mentioned in thermal analysis pressurised gas is usually used to constantly purge the furnace and remove and transport the gaseous decomposition products of interest. As most attempts at developing low-pressure thermal analysis have been unsuccessful a jet separator, heated capillary or similar device must be used to overcome this significant incompatibility [48].

A mass spectrometer can be operated in two modes [48]. The mass spectrometer can be scanned resulting in a mass spectrum. This technique is useful for obtaining information on all the components of the sample however, a large amount of data is recorded and must be processed. Single ion monitoring is more commonly used for evolved gas analysis. In this method the mass analyser is set to allow only ions with a specific charge to mass ratio to reach the detector. Single ion monitoring only allows for the detection and identification of one or more specifically chosen gases however, as decomposition products of interest can often be predicted this technique may be preferable [48]. Evolved gas mass spectrometry suffers from the same drawbacks as every other form of mass spectrometry. As ions are separated by their charge to mass ratio rather than any chemical method

different chemical species or isotopes may overlap. Interference from the purge gas will also be observed no matter which gas is chosen. Despite these disadvantages EGMS is by far the best available technique for analysis of evolved gases.

A second method that is commonly used for evolved gas analysis is infrared spectroscopy (IR). This technique utilises a specialised gas flow cell that may be fitted to the instrument. The main advantage of using IR spectroscopy for evolved gas analysis is that it requires simpler and cheaper apparatus than EGMS, however, the technique has a significant disadvantage. Numerous common decomposition products such as O_2 and N_2 do not contain a net dipole and therefore are not IR active. Consequently, some of the decomposition products may not be identified by this technique. The popularity of this technique has declined in recent years in favour of EGMS.

A third method for identification of evolved gases is gas chromatography (GC). This technique works by identifying gases by their retention times on GC columns [48]. This method does however suffer from a significant disadvantage. As chromatographic separation in a GC column takes time intermittent sampling must be used with the column completely purged between samples, resulting in rapid events may being completely missed [48]. Identification of evolved gases by GC has also become less popular in recent years as the availability and affordability of dedicated mass spectrometry has increased.

Differential scanning calorimetry (DSC) and differential thermal analysis (DTA) are two similar techniques that have also been applied to the study of LDHs in the past. DSC and DTA are two of the most common thermal analysis techniques used in the world today [33, 49]. Unlike TG which provides information on the mass loss of a sample DTA and DSC provides information on exothermic and endothermic thermal events that occur in the sample during thermal decomposition. DTA and DSC curves provide information that is complementary to that of TG and DTG curves.

The instrumentation for DTA and DSC is similar. In both cases, the furnace must contain both a sample and a reference material. In DTA, the temperature of the furnace is varied and the temperature difference (ΔT) between the sample and the reference is recorded and plotted against the furnace temperature (T). [48]

$$\mathbf{\Delta T = T_S - T_R} \tag{1.2}$$

In DSC, the sample and reference are heated at different rates so that there is no difference in temperature between them. The power needed for heating the samples is recorded and plotted instead of measuring the temperature difference between the sample and the reference material as in DTA.

$$\mathbf{\Delta T = T_S - T_R = 0} \tag{1.3}$$

1.2.5. Summary of Previous Work on the Removal of Selected Anions from Water

1.2.5.1. Removal of Fluorine Containing Species

There have been numerous investigations into the removal of fluoride from potable water. In many parts of the world, water naturally contains levels of fluoride in excess of the World Health Organisation's (WHO) maximum acceptable concentration of 1.5mg/L with the highest naturally occurring reported as 2800mg/L [50, 51]. High concentrations of fluoride in water is often due to the presence of fluoride containing minerals including fluorspar (CaF_2), cryolite ($Na_3[AlF_6]$) and fluorapatite ($Ca_5[PO_4]_3F$) [50]. Fluoride may also enter the environment through industrial waste (such as aluminium refining and the burning of high fluoride coal) and is found in most foodstuffs (tea can be particularly high in fluoride) and is often added to dental products.

Fluoride is an essential element for humans at low concentrations for optimal health. Fluoride is often deliberately added to drinking water or table salt in low concentrations to protects against dental caries (medical them for dental cavities, tooth decay). Long term exposure to high concentrations of fluoride (above the WHO standard) may lead to mottling of the teeth. More severe exposure can cause skeletal fluorosis, which is a serious and possibly crippling medical condition [50]. Current methods for the removal of fluoride from potable water are complex and costly. LDHs may provide a simpler and more economical method for removing fluoride from drinking water. Due to the significant number of publications on this topic and the limitations of this particular, document it is impossible to

vigorously review every recent paper, therefore only a few significant publications will be reviewed. The following publications may be of interest to the reader: [33, 50, 51]

Liang et. al investigated the removal of fluoride from solution using Mg/Al LDH adsorbents [40]. Mg/Al LDH materials with varying cationic ratios (2.0, 3.0 and 4.0) were prepared and characterised by various techniques. The interlayer anion chosen in these experiments was carbonate as the LDH was to be thermally activated. LDH samples (2.0g) were treated with fluoride solutions of varying concentration and fluoride concentration was measured using a fluoride selective electrode.

Fluoride adsorption was found to increase with thermal activation temperature to a maximum of 500°C. The adsorption loading at this calcination temperature was 80mg/g [40]. The maximum amount if interlayer carbonate is removed at this calcinations temperature. It was determined that if the material is heated to higher temperatures it will decompose to a spinel phase that does not exhibit reformation. The LDH with the molar ratio of 2.0 was found to be the most effective fluoride sorbent [40]. This effect was attributed to greater specific surface area observed for the 2.0 sample when compared to the others. Optimum fluoride adsorption of 88.0% occurred at a pH of 6.0. The slightly acidic conditions remove OH^- as a competing anion improving fluoride sorption. At higher pH the thermally activated LDH may partly dissolve. The optimum

adsorbent dose was found to be 2.0g/1.8L of 100mg/L fluoride solution and the optimum initial fluoride concentration was 200mg/L [40].

Wang et. al also investigated the removal of fluoride from aqueous solution using Mg/Al LDH materials [41]. This time fluoride sorption was investigated using Mg/Al LDHs and thermally activated Mg/Al LDHs. Again, carbonate was the chosen interlayer anion. Fluoride removal by LDHs without any thermal treatment were lower than those obtained from thermally activated adsorbents. A removal efficiency of 29.8% was observed for a solution at pH 7 with initial fluoride concentration of 10mg/L. The maximum fluoride removal of 33.8% occurred with a solution with an initial fluoride concentration of only 3.31mg/L [41]. Thermal activation improved fluoride sorption to 55.0% under similar conditions to those stated above. The LDH thermally activated at a temperature of 130°C was found to be the most efficient adsorbent with a maximum fluoride removal of 75.8% [41]. This temperature is significantly lower than the one reported by Liang et. al [40]. These papers show that Mg/Al LDHs show promise for use as fluoride adsorbents in water treatment.

1.2.5.2. Removal of Nitrate

Absorption of nitrate by a TA Zn/Al LDH was investigated by Frost et. al. [52]. The LDH was prepared by the co-precipitation method from aluminium nitrate (0.25M), zinc nitrate (1M) and a caustic solution of sodium hydroxide (2M) and sodium carbonate. The reaction was performed under a nitrogen atmosphere. The LDH was characterised by powder XRD

and phase composition was determined. The LDH was thermally activated to a temperature of 255°C before treatment with an excess of decarbonated 0.1M sodium nitrate solution (350mL). 50mL aliquots of solution where removed at regular intervals. The solid LDH was collected by vacuum filtration, then washed with decarbonated water in preparation for further characterisation by powder XRD as well as IR and Raman spectroscopy [52].

The results of powder XRD indicated the materials prepared conformed to an accepted reference pattern of a LDH. When the Zn/Al LDH was thermally activated the characteristic LDH pattern was not observed, instead the pattern closely resembled that of zinc oxide. The $d_{(003)}$ spacing of the LDH was observed to decrease from 0.79nm in the original carbonate containing material to 0.76nm in the nitrate containing LDH [52]. Vibrational spectroscopy (IR and Raman) was used for identification of the type of bonding of the interlayer anions. As carbonate and nitrate have characteristic vibrations in known regions of the spectrum, the composition of the interlayer can be determined by these techniques. Examination of the Raman spectrum showed bands at 1060 and 1062cm^{-1} attributed to carbonate symmetric stretching modes. Bands at 1055 and 1045cm^{-1} were attributed to nitrate symmetric stretching modes. It was proposed that two forms of carbonate and nitrate exist in the LDH structure with the band at 1068cm^{-1} assigned to carbonate bonded to the hydroxyl groups at the surface of the LDH and the second band at 1062cm^{-1} caused by carbonate strongly hydrogen bonded to interlayer water. Similarly, the two nitrate

bands can be attributed to nitrate bonded to the hydroxyl groups at the surface and nitrate free in solution. Similar bands in the IR spectrum confirm this conclusion [52]. Though this work does not present quantitative results on the uptake of nitrate anions by LDHs it does attempt to uncover the mechanism of nitrate sorption and determine the composition of the product.

1.2.5.3. Removal of Phosphate

Although phosphate is an essential nutrient for living things, excessive phosphate content in waterways may result in eutrophication caused by blooming of phytoplankton. Phosphate may enter the aquatic environment naturally, however, there are many man-made sources including agricultural runoff as well as industrial and domestic wastewater. Many methods have been developed for removal of phosphates from water though only a few are used commercially [53].

One important aspect of phosphate removal that has previously been overlooked is the recovery of phosphate from adsorbents for future re-use in agriculture. It is estimated that total depletion of all known reserves of phosphorous baring rocks will occur at some time in the next 50 to 400 years [54, 55]. The most recent estimates are at the higher end of this timeframe and have been revised up due to improvements in phosphorous recovery rates during mining has made the processing of lower grade rock more viable [55]. Other factors such as improvements in technology, discovery and exploitation of new deposits as well as improved farming

practices may extend this timeframe further. Truly sustainable agriculture capable of feeding the world's growing population will inevitably rely on the recovery and recycling of phosphorous. LDHs may have the potential to not only remove phosphates from water, but due to their anion exchange properties it is conceivably possible to recover the phosphate which may be a suitable precursor for the production of inorganic fertilisers.

Iron containing LDH materials have shown promise as efficient phosphate sorbents. Seida and Nakano [56] investigated sorption of phosphate by iron containing LDHs by anion exchange. The aim of this work was to develop alternative and safer materials for phosphate removal. Iron was chosen as the trivalent anion in the LDH as there has recently been some concern that aluminium may accelerate the onset of Alzheimer disease [50]. Two LDH materials with the formula $Mg_aFe_b(OH)_{2(a+b)}CO_3^{2-}{}_{b/2}\cdot mH_2O$ and $Ca_aFe_b(OH)_{2(a+b)}CO_3^{2-}{}_{b/2}\cdot mH_2O$ were prepared. Phosphate removal from stock solutions ranging in concentration from 1 to 1500mg P/L are then analysed, using 0.05g of LDH and 10mL of solution. The mixtures were left for 24 hours with constant shaking. Phosphate removal was determined using inductively coupled Plasma atomic emission spectroscopy (ICP-AES) [56]. Adsorption isotherms were prepared and a good fit was obtained by fitting the Langmuir model. The maximum removal (q_{max}) was calculated from the Langmuir plot and was found to be 15.5 and 28.8mg/g for the Mg and Ca LDHs respectively. It was also found that removal of phosphate increased with increasing phosphate concentration. pH of the solution was

also measured and found to increase. This was attributed to partial dissolution of the LDH releasing metal cations and hydroxides [56].

Next, the effect of solution pH was investigated. A phosphate concentration of 100mg P/L (grams of phosphorous per litre of solution) was chosen and the pH was varied using hydrochloric acid. The samples were otherwise treated by the same method described above [56]. Phosphate removal was found to increase with increasing initial pH. More dissolved metal cations were observed in the lower pH solutions. This is not unexpected as LDHs are basic in nature. Finally, phosphate removal from a real world effluent sample was investigated using a column packed with LDH and a flow rate of 20mL/h. Phosphate was determined by the molybdenum-blue method. It was found that over 80% of phosphate in the effluent could be recovered under these conditions [56].

More recently Triantafyllidis et. al [57] investigated the removal of phosphate from water using a thermally activated Mg/Fe LDH sorbent. Three Mg/Al LDHs were prepared using the co-precipitation method. LDH1 contained only carbonate in the interlayer and was prepared by a standard co-precipitation method using nitrate salts. LDH2 was prepared using a similar method, however the amount of carbonate used in the synthesis was significantly reduced. LDH3 was prepared using a similar method to that of LDH2, however, chloride salts were used instead of nitrate salts and also contained the lowest concentration of carbonate. The LDHs were modified after synthesis to totally or partly substitute the Al^{3+} in the LDH cation

layers for Fe^{3+}. Once again, samples of the LDH were used to remove anions from solution, this time by anion exchange. The phosphate solution used was prepared by dissolving the required amount of potassium dihydrogen phosphate in water to produce solutions with concentrations ranging from 10 to 500mg P/L. The pH of the solutions were not adjusted [57].

Maximum uptake of phosphate by the unmodified LDH1 was found to be 15mg P/L. LDH2 and LDH3 had a similar value of approximately 28mg P/L. This effect is not unexpected due to the high affinity LDHs exhibit for carbonate, which was already present in the interlayer of the LDHs. LDH3 was found to have the highest adsorption capacity at low concentrations [57]. Substitution of the Al^{3+} by Fe^{3+} in the LDH structure resulted in a decrease in phosphate sorption as Fe^{3+} content increased. This was attributed to the Fe^{3+} causing an increase in the LDH's affinity for carbonate by increasing the positive surface charge of the LDH layers [57]. Samples of the LDH were thermally activated by heating at 450°C in air for a period of 4 hours. Powder XRD revealed the presence of magnesium oxide in the TA-LDH which may indicate the sample has been overheated and some of the sample has decomposed beyond the ability to reform. Sorption efficiency was found to increase with thermal activation in all samples. LDH1 was found to be the most efficient of the Mg/Al LDH materials for phosphate sorption with a maximum uptake of 220mg/g. LDH2 showed a similar result, while LDH3 was the least effective of the Mg/Al LDHs. A different trend was observed in the Fe^{3+} substituted samples. It was found that

sorption efficiency increased with Fe^{3+} content. The Fe^{3+} substituted LDH was found to be the most efficient phosphate sorbent overall with a maximum loading capacity of approximately 300mg milligrams of phosphorous per gram of adsorbent compared to 44mg/g observed for the Mg/Al LDH [57].

In this thesis the candidate aims to:

- To investigate the application of layered double hydroxides for the removal of selected toxic and unwanted anions including sulfate, nitrate, fluoride and iodide from water via the reformation effect.

- To prepare synthetic hydrotalcite, the Mg/Al LDH and characterise the prepared hydrotalcite by powder X-ray diffraction and thermogravametric analysis.

- To prepare layered double hydroxides containing zinc and chromium metal cations and characterise the products by powder X-ray diffraction and thermogravametric analysis.

- To conduct preliminary experiments to investigate the removal of sulfate, nitrate, fluoride from water using thermally activated Mg/Al LDH.

- To characterise LDH materials recovered after anion sorption by powder X-ray diffraction and thermogravametric analysis in an

attempt to better understand the mechanisms of the reformation effect.

- To design and carry out preliminary experiments to investigate the potential of a Zn/Al LDH for capture and storage of radioactive iodine species.

- To prepare and investigate synthetic equivalents of the mineral stichtite in an attempt to find useful applications for an often overlooked Australian LDH mineral.

Chapter Two:

Synthesis and Applications for the removal of Sulfate, Nitrate and Fluoride by Mg/Al Layered Double Hydroxides

Chapter 2: Synthesis and Applications for the removal of Sulfate, Nitrate and Fluoride by Mg/Al Layered Double Hydroxides

2.1. Introduction

As previously mentioned, hydrotalcite contains aluminium as the trivalent cation that partially substitutes magnesium in the positively charged brucite layers. Many methods are available in literature for the preparation of hydrotalcite, and as a result it has become common to compare results obtained from other LDHs with those of hydrotalcite [2, 3, 43, 58-61]. This chapter contains work on the synthesis and characterisation of a sample of synthetic hydrotalcite prepared by the co-precipitation method and its application for the removal of sulfate (SO_4^{2-}), Nitrate (NO^{3-}) and fluoride (F^-) from aqueous solution.

2.2. Preliminary Synthesis of Hydrotalcite by the Co-Precipitation Method

A test batch of 7.36g of $Mg_6Al_2(OH)_{16}(CO_3)\cdot 4H_2O$ (Mg/Al LDH) was prepared by the co-precipitation method as described below. A mixed metal solution was prepared by dissolving aluminium chloride hexahydrate (15.0893g, 0.0935mol) and magnesium chloride hexahydrate (38.1187g, 0.3092mol) in deionised water (250mL). The caustic solution was prepared by slowly dissolving sodium hydroxide (approximately 20g) and sodium carbonate (42.396g) in deionised water (250mL). The caustic solution (100mL) was added dropwise to the mixed metal solution (100mL) with continuous stirring.

As the caustic solution was added, hydrotalcite immediately formed as a white precipitate. The mixture was covered and left overnight with stirring. The hydrotalcite precipitate was collected by vacuum filtration and washed with deionised water (50mL). The result was a white paste that was dried in an oven overnight at approximately 80°C and a clear filtrate which was discarded. After drying, the hydrotalcite had reduced in size considerably and had the appearance of a flaky white solid. A small quantity of hydrotalcite was ground with a mortar and pestle for IR and powder XRD analysis. The total mass of hydrotalcite obtained was 7.36g.

Table 2.1: Details of the preliminary synthesis of Mg/Al LDH.

Reagent	Theoretical Mass (g)	Mass Weighed (g)	Solution Volume (mL)
Mixed metal solution			
Magnesium chloride hexahydrate	38.118 (0.3091mol)	38.1187 (0.3092mol)	250
Aluminium chloride hexahydrate	15.0894 (0.09348mol)	15.0893 (0.09348mol)	
Caustic solution			
Sodium hydroxide	20.000	20	250
Sodium carbonate	42.396	42.396	
Total Mass of Product			
Hydrotalcite	28.23	7.36	---

It was possible to calculate the maximum theoretical yield of hydrotalcite using the aluminium chloride as the yield limiting reagent. It was assumed that all aluminium chloride hexahydrate was converted to hydrotalcite with the ideal formula of $Mg_6Al_2(OH)_{16}CO_3 \cdot 4H_2O$. The total percentage yield was therefore 26.07%.

2.3. Bulk Synthesis of Hydrotalcite by the Co-Precipitation Method

Once the exploratory experimentation was completed a larger batch of hydrotalcite was prepared using a similar procedure. Due to the large volumes of solution needed (10000mL of both mixed metal and caustic) 5000mL volumetric flasks where used. It was therefore necessary to prepare each solution in two parts. The exact masses and volumes of solution used are outlined in Table 2.2. All reagents where weighed on a top pan balance as large masses were involved.

Table 2.2: Details of the bulk synthesis of Mg/Al LDH.

Reagent	Theoretical Mass (g)	Mass Weighed (g)	Solution Volume (mL)
Mixed metal solution 1			
Magnesium chloride hexahydrate	762.376 (6.183mol)	762.37 (6.183mol)	5000
Aluminium chloride hexahydrate	301.788 (1.870mol)	301.79 (1.870mol)	
Mixed metal solution 2			
Magnesium chloride hexahydrate	762.38 (6.183mol)	762.36 (6.183mol)	5000
Aluminium chloride hexahydrate	301.79 (1.870mol)	301.77 (1.869mol)	
Caustic solution 1			
Sodium hydroxide	400	400.07	5000
Sodium carbonate	847.92	847.93	
Caustic solution 2			
Sodium hydroxide	400	400.09	5000
Sodium carbonate	847.92	842.92	
Total Mass of Product			
Hydrotalcite	---	990.37	---

One difference from the previous experiment was that the mixed metal solution (10000mL) was added dropwise to the caustic solution (10000mL). The pH of the solution was monitored using a general laboratory pH probe and found to average at 12.2. Additional sodium hydroxide was added first

in granular form then in a solution to keep the pH above 10. Hydrotalcite was collected by vacuum filtration as previously described. Due to the large volumes of solution involved (20L) the filtering step took approximately two weeks to complete. The filtered hydrotalcite was washed in a 0.1M sodium carbonate solution (10L) overnight and collected by vacuum filtration over the course of a few days. The hydrotalcite precipitate was collected in a number of filtrations, with each filtration resulting in a wet hydrotalcite "cake" that was dried at approximately 80°C.

After all the "cakes" of hydrotalcite were dried and ground, it was homogenised by combining all the samples into a large glass dish and thoroughly mixed. Additional hydrotalcite was recovered from the filtrate by allowing the solid particles to settle, which were then decanted off the clear solution. The remaining solution containing the fine hydrotalcite particles was evaporated in an oven at aproximatly 80°C to yield dry hydrotalcite. These samples of hydrotalcite were not used in further experiments as they were not homogenised.

Table 2.3: Details of the total yield of the bulk synthesis of Mg/Al LDH.

Date Collected	Approximate Mass (g)
01-04-10	163.19
06-04-10	260.81
07-04-10	216.59
08-04-01	287.10
Sub Total	927.69
29-04-10 (filtrate)	62.68
Total	990.37

2.4. Thermal Activation of Synthetic Hydrotalcite

An initial batch of Mg/Al LDH was thermally activated to a maximum temperature of 380°C. The rate of heating averaged at 20°C/minute up to the set temperature. The sample was held at the set temperature for 60 minutes. The mass losses are tabulated below. The percent mass loss was found to be 22.37%. The thermally activated Mg/Al LDH was used for testing the adsorption of sulfate and is detailed later in this chapter.

Table 2.4: Mass losses during thermal activation

Crucible Number	Mass Mg/Al LDH Before Thermal Activation (g)	Mass Mg/Al LDH After Thermal Activation (g)
1	50.03	39.83
2	50.06	38.27
3	50.01	38.42
Total	150.1	116.52

2.5. Treatment of Mg/Al LDH with Anion Solutions

Three 1000ppm solutions were prepared by dissolving the required quantity of either sodium sulfate, sodium nitrate or sodium fluoride in ultrapure water. Samples of the Mg/Al LDH (3g) were each treated with a 20mL aliquot of one of the three 1000ppm anionic solutions. Each sample was stirred for 30 minutes before separation by vacuum filtration. Recovered LDH was dried in an oven at approximately 80°C for approximately two days to remove excess water. Sulfate, nitrate and fluoride were chosen because they were three readily available anions with charges and numbers of atoms. Typically, LDHs are reported to have a high affinity for multi-atomic anionic species with multiple charges. Sulfate is an example of this type of anion while fluoride is an example of an anion which LDHs are

expected to have low affinity for. Nitrate was chosen because it is multi-atomic but only carries a single charge.

2.6. Characterisation of Mg/Al LDH samples by Powder X-ray diffraction

All Powder X-ray diffraction (PXRD) patterns were collected using a Philips X'pert wide angle X-Ray diffractometer, with Cu Kα radiation (1.54052 Å). Powder XRD of the Mg/Al LDH samples before thermal activation or after treatment with an anionic solution are presented in Figure. 3.1, and indicate the successful formation of a LDH structure. The XRD patterns correspond well to a reference pattern of synthetic hydrotalcite (00-041-1428). Other phases identified in the sample were sodium chloride (NaCl) and sodium carbonate hydrate ($Na_2CO_3 \cdot 2H_2O$), which were expected bi-products of the synthesis procedure. Powder XRD patterns indicate that the hydrotalcite needs further washing and re-chracterisation before it can be used in future experiments The average $d_{(003)}$ spacing is 7.81 Å, which is consistent with a LDH structure. [2, 3]

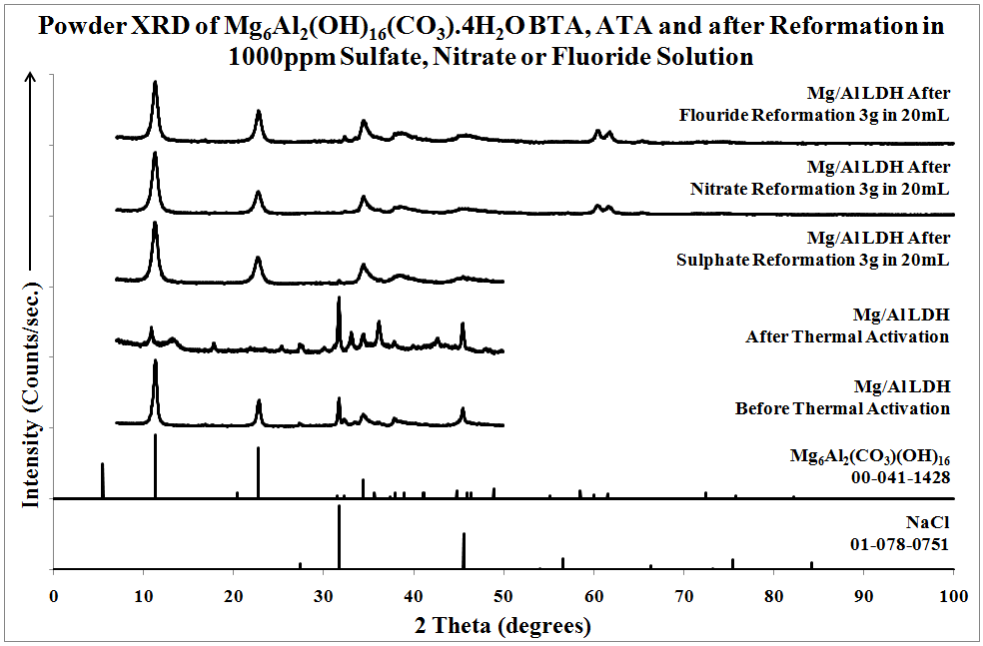

Figure. 2.1: XRD pattern of Mg/Al LDH before thermal activation, after treatment of 3g of Mg/Al LDH in 20cm3 of sodium sulfate, nitrate or fluoride solutions and references.

Thermal activation resulted in the destruction of the layered structure of the LDH material (expected). When the patterns obtained before and after thermal activation are compared (Figure. 2.1) a clear difference is observed. Phase identification was carried out on the thermally activated hydrotalcite and the results are presented in Figure. 2.2. Phases found after thermal activation are NaCl, $Na_3Mg(CO_3)_2Cl$, AlO(OH) and $Na_2Mg(CO_3)_2$.

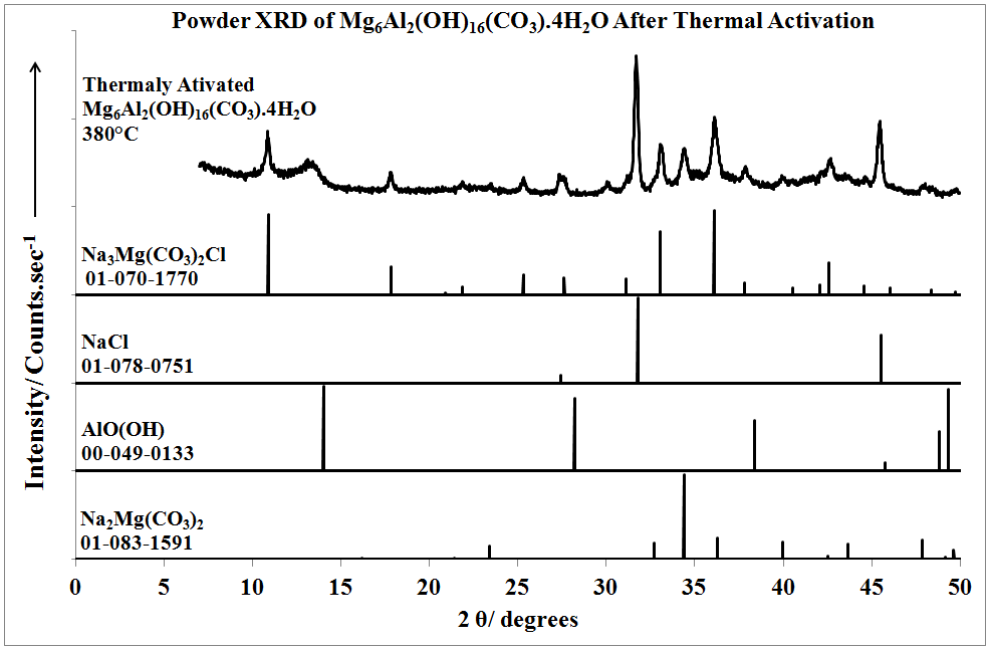

Figure. 2.2: XRD pattern of Mg/Al LDH after thermal activation with references of possible phases.

After reformation in the various anionic solutions, all three LDH samples reformed a structure similar to that of the original material. The samples also appeared to contain similar phases to that of the original hydrotalcite. However, the NaCl impurity was reduced in all reformed samples. The $d_{(003)}$ spacing was once again investigated and the results are reported in Table 2.5. The $d_{(003)}$ spacing of all samples are within the accepted range of a LDH material. This indicates reformation has occurred successfully suggesting that intercalation of some anion from solution has occurred. However, due to the nature of powder XRD it is impossible to determine the composition of the interlayer anions using this technique alone.

The $d_{(003)}$ spacing in the original hydrotalcite and those recovered after treatment with either SO_4^{2-} or F^- solutions show remarkable similarity. This likely indicates that any anions removed from solution have been adsorbed

on the surface of the hydrotalcite rather than intercalated into the interlayer. Further investigation into this is still required.

Table 2.5: $d_{(003)}$ spacing of the various LDHs prepared.

Anion	d_{003} Spacing Observed (Å)
Carbonate (CO_3^{2-})	7.81
Sulfate (SO_4^{2-})	7.83
Nitrate (NO_3^-)	8.31
Fluoride (F^-)	7.81

2.7. Characterisation of Mg/Al LDH samples by Thermal Analysis

Thermogravimetry (TG) is commonly used to understand the decomposition mechanisms of LDH materials. Thermal analysis was carried out using a TA® Instrument incorporated with a high resolution thermogravimetric analyser (series Q500) under a flowing nitrogen atmosphere (40mL/min). The samples were placed in an open platinum pan and heated from room temperature to a maximum temperature of 1000°C at a rate of 2.50°C/min. TG and DTG curves were obtained, however, a mass spectrometer was not available for the analysis of the evolved gases.

Six mass losses were observed during the decomposition of hydrotalcite before thermal activation (BTA) shown in Figure. 2.3. The decomposition mechanism proposed for the hydrotalcite sample has been previously reported [62]. The first two mass losses were observed at 39 and 68°C. Due to the low temperatures of these features it can be safely assumed that they correspond to the removal of weakly adsorbed water from the external surface of the hydrotalcite. These mass losses accounted for 11.51% of the total mass loss. The next mass loss occurred at 170°C and accounted for

4.40% of the mass loss. This temperature is high enough for the removal of interlayer water. Thus, the following decomposition steps are proposed:

$$Mg_6Al_2CO_3(OH)_{16}{\cdot}xH_2O \rightarrow Mg_6Al_2CO_3(OH)_{16}{\cdot}4H_2O + (x\text{-}4)H_2O \quad (3.1)$$

$$Mg_6Al_2CO_3(OH)_{16}{\cdot}4H_2O \rightarrow Mg_6Al_2CO_3(OH)_{16} + 4H_2O \quad (3.2)$$

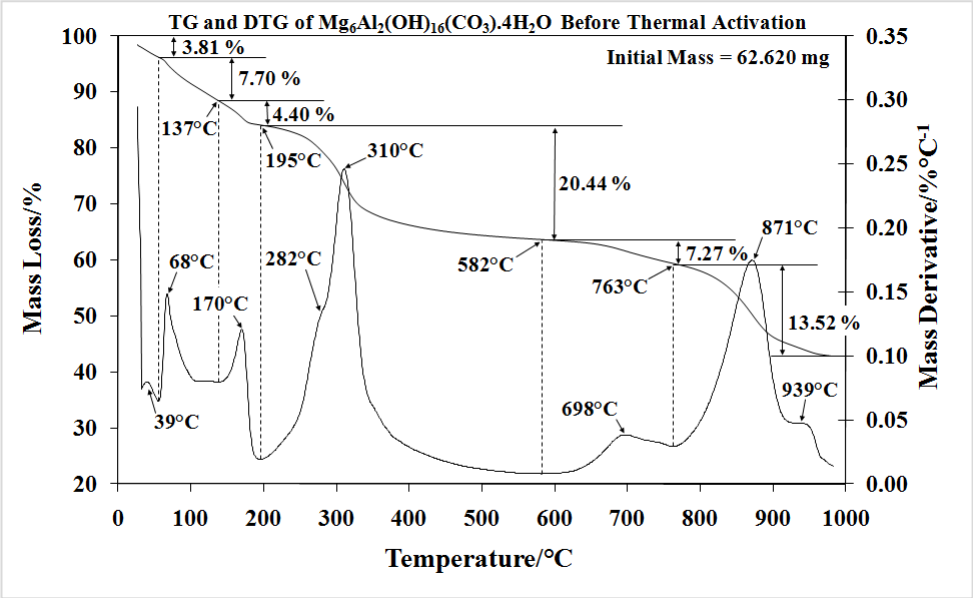

Figure. 2.3: TG and DTG curves of Mg/Al LDH before thermal activation or absorption experiments.

The fourth and largest mass loss (20.44%) occurred at 310°C and was most likely caused by the loss of hydroxyl groups (dehydroxylation) and interlayer anions, in this case carbonate (decarbonation). Typically, these two decomposition steps occur almost simultaneously in this temperature region. Examination of the DTG curve revealed asymmetry in the peak caused by the presence of two overlapping peaks (OH and CO_2). The main peak occurred at 310°C, while a shoulder was observed at a lower temperature of 282°C. Literature summarised in [2] suggests that the feature at 282°C corresponds to the Al-OH dehydroxylation, while the main peak

corresponds to both Mg-OH dehydroxylation and decarbonation.Dehydroxylation and the removal of interlayer anions are usually the largest contributor to the mass loss in LDH structures at elevated temperatures. The following decomposition steps are proposed for the dehydroxylation and decarbonation of hydrotalcite [63]:

$$Mg_6Al_2CO_3(OH)_{16} \rightarrow Mg_6Al_2O_8CO_3(OH)_2 + 6H_2O + H_2 \quad (3.3)$$

$$Mg_6O_8Al_2CO_3(OH)_2 \rightarrow Mg_6Al_2O_8(OH)_2 + CO_2 + \tfrac{1}{2}O_2 \quad (3.4)$$

Further mass losses were observed at higher temperatures, however, as these temperatures were too high for reformation of the LDH they were not investigated further. It was proposed these could be the result of the decomposition of the mixed metal oxides into a spinel phase or simply due to the presence of an impurity.

$$Mg_6O_8Al_2(OH)_2 \rightarrow Mg_6Al_2O_8 + H_2O + \tfrac{1}{2}O_2 \quad (3.5)$$

$$Mg_6O_8Al_2 \rightarrow 5MgO + MgAl_2O + O_2 \quad (3.6)$$

Three mass losses occurred for the LDH that regenerated after treatment with the 100ppm sulfate solution (Figure 2.4). A mass loss occurred arround 125°C and accounted for a 14.53% mass loss. This broad feature is likely due to the removal of both adsorbed (external surface) and interlayer water. As the exact composition of anions in the interlayer is not known, mechanisms for the decomposition of hydrotalcite treated with sulfate, nitrate and fluoride are based on equimolar quantities of carbonate and the anion of interest in the interlayer.

$$Mg_{12}Al_4(OH)_{32}(CO_3, SO_4)\cdot xH_2O \rightarrow Mg_{12}Al_4(OH)_{32}(CO_3, SO_4)\cdot 8H_2O + (x\text{-}8)H_2O \quad (3.7)$$

$$Mg_{12}Al_4(OH)_{32}(CO_3, SO_4)\cdot 8H_2O \rightarrow Mg_{12}Al_4(OH)_{32}(CO_3, SO_4) + 8H_2O \quad (3.8)$$

The second mass loss at 352°C is attributed to the dehydroxylation and removal of interlayer anions. This feature accounted for 28.47% of the total mass lost. It is important to note that this decomposition step occurred at a higher temperature than the temperature for the corresponding decomposition step for the BTA sample. The temperature of dehydroxylation is often used to compare the thermal stability of different LDHs. The increase in dehydroxylation temperature indicates that the LDH reformed in the sulfate solution has a greater thermal stability than the BTA sample. This provides some evidence to suggest that sulfate anions have been successfully intercalated into the regenerated hydrotalcite. Once again, two overlapping peaks were observed in the DTG curve for this temperature region.

$$Mg_{12}Al_4(OH)_{32}(CO_3, SO_4) \rightarrow Mg_{12}O_{16}Al_4(CO_3,SO_4) + 16H_2O \quad (3.9)$$

$$Mg_{12}O_{16}Al_4(CO_3, SO_4) \rightarrow Mg_{12}O_{16}Al_4O_2CO_3 + SO_2 \quad (3.10)$$

$$Mg_{12}O_{16}Al_4O_2CO_3 \rightarrow (MgO)_{12}(Al_2O_3)_2 + CO_2 + \tfrac{1}{2}O_2 \quad (3.11)$$

A third and final mass loss occurred between 632 and 1000°C accounting for a 3.13% mass loss. Again due to the high temperature of this feature these peaks were not investigated further.

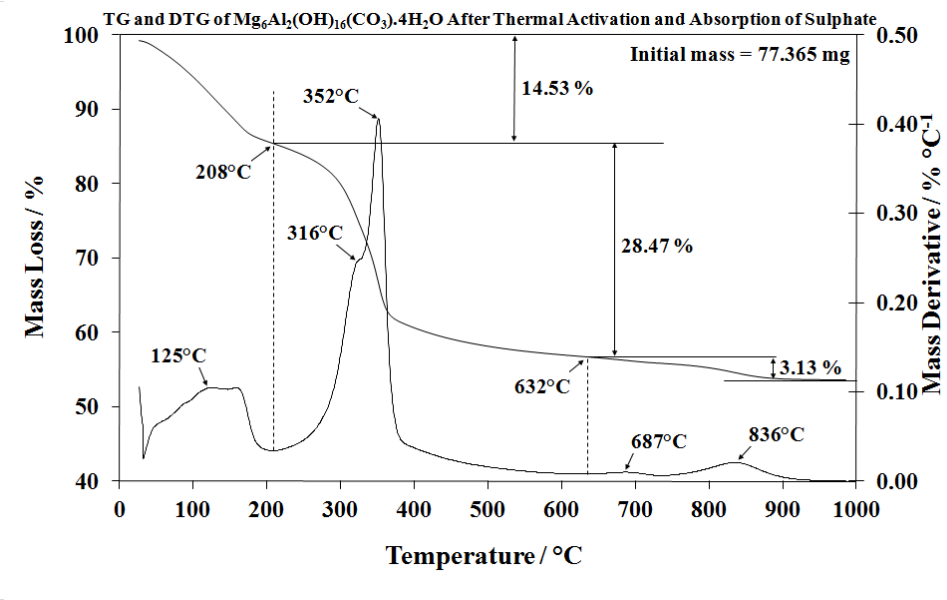

Figure. 2.4: TG and DTG curves of Mg/Al LDH After thermal activation and reformation by treatment of 3g of Mg/Al LDH with 1000ppm sodium sulfate solution (20mL).

Thermal decomposition of a sample of the Mg/Al LDH treated with a 1000ppm nitrate solution was also investigated. Four mass loss steps were observed in the TG curve of this sample shown in Figure. 2.5. The first mass loss occurring at 124°C accounted for 11.84% of the total mass loss. The DTG curve shows a single broad feature likely caused by several overlapping decomposition processes, such as adsorbed water on external surfaces and more strongly held interlayer water.

$$Mg_{12}Al_4CO_3(NO_3)_2(OH)_{16}{\cdot}xH_2O \rightarrow Mg_{12}Al_4CO_3(NO_3)_2(OH)_{32}{\cdot}8H_2O + (x\text{-}8)H_2O \quad (3.13)$$

$$Mg_{12}Al_4CO_3(NO_3)_2(OH)_{32}{\cdot}8H_2O \rightarrow Mg_{12}Al_4CO_3(NO_3)_2(OH)_{32} + 8H_2O \quad (3.14)$$

The next mass loss occurred at 346°C accounting for 30.03%, which is the largest mass loss observed in this sample. This mass loss is attributed to the

dehydroxylation and removal of interlayer anions in the LDH structure. The DTG reveals only a sharp peak in this temperature region, with a small shoulder at lower temperatures. It is also of interest to note that the temperature of this peak has increased from 310°C in the original sample to 346°C. It is therefore possible to conclude that the LDH prepared by reformation in nitrate solution has a greater thermal stability than that of the original CO_3^{2-} hydrotalcite. This increase may indicate the successful intercalation of nitrate anions. An increase in the $d_{(003)}$ spacing (discussed previously) continues to support the notion that nitrate anions have been intercalated and not adsorbed to the external surface.

$$\mathbf{Mg_{12}Al_4CO_3(NO_3)_2(OH)_{32} \rightarrow Mg_{12}O_{16}Al_4CO_3(NO_3)_2(OH)_4 + 12H_2O + 4H_2} \quad (3.15)$$

$$\mathbf{Mg_{12}O_{16}Al_4CO_3(NO_3)_2(OH)_4 \rightarrow Mg_{12}Al_4O_{16}(OH)_4 + CO_2 + 2NO_2 + 1½O_2} \quad (3.16)$$

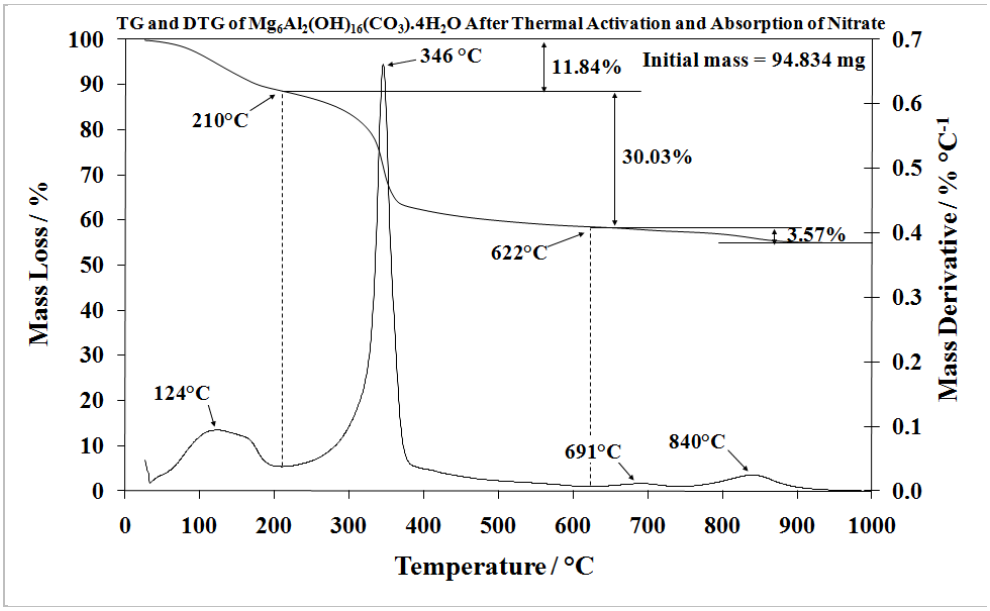

Figure. 2.5: TG and DTG of Mg/Al LDH, after thermal activation and reformation with the adsorption of nitrate solution (20mL, 1000ppm).

The final mass losses occurred at around 690 and 840°C and accounted for a 3.57% mass loss. Again these mass losses were not investigated further, but they are likely due to the decomposition of impurities identified by XRD.

Only three mass loss steps were observed in the TG curve of the sample after treatment in fluoride solution (Figure. 3.6). Examination of the DTG curve shows a single broad feature at 126°C with a mass loss of 11.54% of the total mass loss. This mass loss is likely due to the overlapping loss of both weakly adsorbed surface water and interlayer water. Similar features were observed for the sulfate and nitrate reformed hydrotalcite samples.

$$Mg_{12}Al_4CO_3(F)_2(OH)_{16}{\cdot}xH_2O \rightarrow Mg_{12}Al_4CO_3(F)_2(OH)_{32}{\cdot}8H_2O + (x\text{-}8)H_2O \quad (3.19)$$

$$Mg_{12}Al_4CO_3(F)_2(OH)_{32}{\cdot}8H_2O \rightarrow Mg_{12}Al_4CO_3(F)_2(OH)_{32} + 8H_2O \quad (3.20)$$

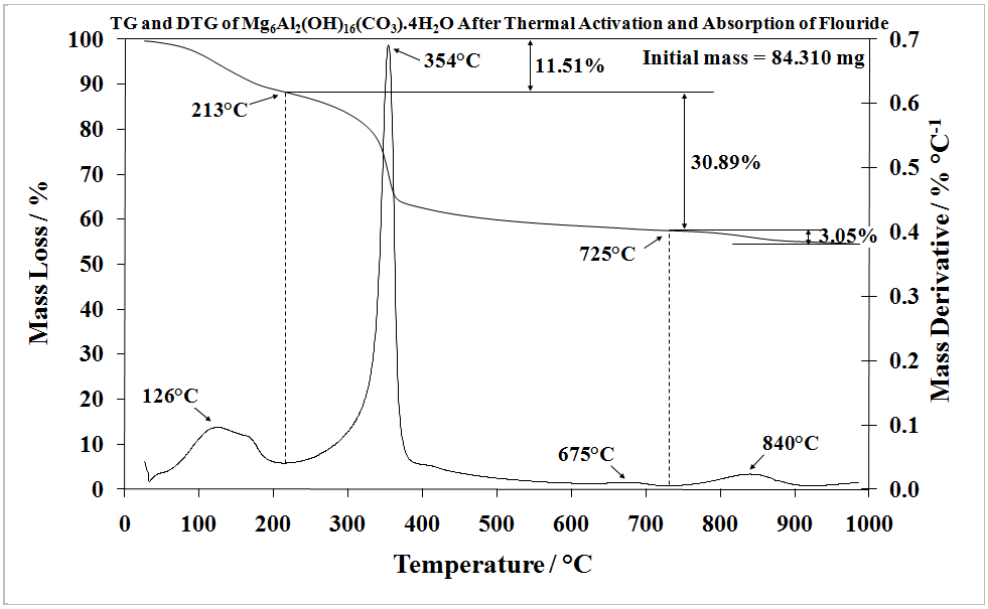

Figure. 2.6: TG and DTG of Mg/Al LDH, after thermal activation and reformation with the adsorption of fluoride solution (20mL, 1000ppm).

The second mass loss occurs at 354°C and accounts for 30.89% of total mass loss. This mass loss is attributed to the dehydroxylation and removal of interlayer anions. The DTG curve for this region only reveals one sharp peak, as seen previously for SO_4^{2-} and NO^{3-}, and an increase in decomposition temperature is observed. This peak corresponds to the dehydroxylation and decarbonation of the reformed LDH structure. The sample treated with fluoride has greater thermal stability than the original LDH structure.

$$Mg_{12}Al_4CO_3(F)_2(OH)_{32} \rightarrow Mg_{12}O_{16}Al_4CO_3(F)_2 + 16H_2O \quad (3.21)$$

$$Mg_{12}O_{16}Al_4CO_3(F)_2 \rightarrow (MgO)_{12}Al_4O_5(F)_2 + CO_2 \quad (3.22)$$

The final mass loss occurred at 840°C accounting for 3.05% mass loss, and has again not been investigated because it does not involve the reformed LDH structure.

2.8. Conclusions/ Discussion

Synthetic hydrotalcite was successfully prepared by the method described in this chapter. Powder XRD was used to confirm that the material that was prepared was synthetic hydrotalcite. The pattern obtained yielded a good match to an accepted pattern for synthetic hydrotalcite (00-041-1428). The material exhibited a $d_{(003)}$ spacing of 7.81 Å, which was consistent with other LDH materials. Additional phases such as sodium chloride and sodium carbonate hydrate were identified in the sample as by-products of the synthesis process.

The thermal activation process dehydrates the original hydrotalcite structure to $Mg_6Al_2O_8(OH)_2$. This mixed metal hydroxide is able to adsorb anions and water molecules after thermal activation to reform a LDH structure. Heating the hydrotalcite to temperatures greater than 500°C will decompose this mixed metal oxide to its corresponding oxide counterparts and reformation will not be possible. Powder XRD analysis of the LDH after thermal activation revealed the destruction of the characteristic layered structure of the material. A clear difference can be observed between the two patterns (Figure. 2.2). Phase identification was carried out on a sample of the Mg/Al LDH that was thermally activated to a maximum temperature of 380°C as was previously described in this chapter. The sample was

found to contain NaCl, $Na_3Mg(CO_3)_2Cl$, AlO(OH) and $Na_2Mg(CO_3)_2$. This confirms the LDH has begun to decompose into a mixed metal oxide with thermal activation.

Reformation in the various anion solutions resulted in the formation of LDH materials with a similar structure to that of the original hydrotalcite. Powder XRD clearly shows the similarity between the patterns of samples treated with sulfate, nitrate, fluoride and the original BTA sample (Figure. 3.1). All these samples were found to contain similar phases and have similar $d_{(003)}$ spacing (Table 2.5). The remarkable similarity in the powder XRD patterns and the TG curves may suggest that the majority of anions intercalated into the LHD during reformation were carbonate ions. However, the change in the decomposition temperature indicates that at least a small quantity of SO_4^{2-}, NO_3^{2-} or F^- has been intercalated. Only the material treated with nitrate solution showed a significant change in the $d_{(003)}$ spacing. The presence of carbonate could possibly be identified by its characteristic vibrational modes using IR spectroscopy. It is likely that the samples contain interlayer carbonate that could originate from a number of sources including incomplete decarbonation of the original LDH, adsorption of carbon dioxide from the atmosphere during transport and storage and adsorption of carbonate dissolved in the ultrapure water used in the experiments.

All samples appeared to decompose by a similar mechanism involving the removal of adsorbed and interlayer water followed by dehydroxylation and

removal of interlayer anions. All LDHs recovered after reformation in the anion solutions showed a greater thermal stability than the BTA sample. Thermal stability of the LDH appeared to increase with treatment of sulfate, nitrate and fluoride. It is possible that the presence of these anions has improved the thermal stability of the LDH or that the increased stability results from the thermal activation process.

The theoretical mass losses calculated for dehydroxylation and decarbonation of the LDHs used in this chapter (not shown) are greater than the experimental results obtained by this investigation. It is proposed that the hydrotalcite did not fully decompose to the mixed metal hydroxide at the temperature used for thermal activation (i.e. not all the hydroxide and carbonate anions were removed at this temperature). The mechanism proposed is that of an ideal sample. The presence of impurities such as those previously identified as well as anions other than carbonate in the interlayer of the LDH (particularly chloride) is likely to affect the mass losses during thermal decomposition. It is therefore reasonable to expect that observed mass losses will be slightly different to those predicted by the mechanism.

Chapter Three:

Synthesis and Characterisation of Zn/Al Layered Double Hydroxides: Applications for Removal and Storage of Iodine Species.

Chapter 3: Synthesis and Characterisation of Zn/Al Layered Double Hydroxides: Applications for Removal and Storage of Iodine Species.

3.1. Introduction

Iodide is essential for normal thyroid development with an estimated daily intake between 80-150mg/day, there is currently no WHO standard for iodine or iodide in drinking water [50]. One of the toxic by-products of uranium fission is ^{129}I. This isotope of iodine is radioactive with an extremely long half-life, which can be absorbed by the body resulting in a detrimental effect on human health [50]. The recent incident at the Fukushima nuclear power station in Japan has shown that developing materials for the safe removal and storage of radioactive iodine (also known as radioiodine) is a priority if nuclear power is to be expanded as an alternative energy source to replace fossil fuels. Numerous attempts to capture and store iodine waste has been reported using Mg/Al LDHs as adsorbents [2, 64, 65]. In this chapter, experiments were conducted in an attempt to remove iodine species from water by the reformation effect using a Zn/Al LDH as a sorbent. To the best of our knowledge this is the first time that the removal of iodine species using a Zn/Al LDH has been reported.

3.2. Previous Investigations into the Removal of Iodide Containing Species

There have been only a few publications regarding the removal of iodide species from water using Mg/Al layered double hydroxides. The early work dealing with sorption of iodide by LDHs was carried out by Fetter et. al. in 1997 [65] and determined that sorption of iodide required thermal activation

of the hydrotalcite with very little iodide removal occurring in non-thermally activated samples. This indicated that hydrotalcites have a lower affinity for iodide than carbonate or sulfate, which were the interlayer anions present in the LDHs.

More recent work on the removal of iodide using Mg/Al LDHs was performed by Liang et. al. [64] in 2006. This paper reported up to 97.6% iodide removal using LDH (4.0g/L). The effect of LDH structure, LDH dosage, initial iodide concentration and the presence of competing anions were all examined. The optimum cationic ratio of Mg:Al was found to be 4:1 with an uptake capacity of 96.1mg/g. This was attributed to the large atomic radius of the iodide ion having greater affinity for the lower charge density of the 4:1 substituted LDH. Thermal activation was found to improve uptake capacities. Uptake increased with thermal activation temperature with a maximum occurring at 500°C. The optimum dose of LDH was found to be 1.0g/L resulting in a 96.5% removal of iodide ions. Increasing the dosage beyond this point was found to produce only minor improvements.

The effect of initial iodide concentration was also investigated. It was found that the uptake capacity increases with the equilibrium concentration of iodide and the maximum uptake capacity was found to be 376mg/g. The Langmuir model was able to be applied to the experimental data to yield an acceptable fit. Using the Langmuir constant it was possible to calculate the Gibbs free energy of the process which was found to be -23.8kJ/mol

confirming the spontaneity of the process. Finally, the effect of competing anions on the sorption of iodide was tested. The percentage removal of iodide decreased as the concentration of competing anions increased. This demonstrates that the LDHs investigated in this paper have a lower affinity for iodide than the other anions.

Kulyukhin et. al. [66] continued to work on the removal of iodide and also investigated the removal of the iodate anions (IO_3^-) from water by Mg/Al LDHs. It was proposed that I^- and IO_3^- are the major iodide species present in water contaminated with radioiodine as iodine (I_2) disproportionates in water [66]. It was determined that LDHs were not able to remove IO_3^- and I^- by anion exchange. This is most likely due to the low affinity of LDHs to the anions as well as competition of other with higher affinity such as carbonate which can be introduced from the atmosphere. The authors of the paper proposed that the sorption of iodine species may be the result of steric hindrance. Another potential cause of this apparent low affinity may result from the charge density of the LDH adsorbent. Liang et. al in [64] determined that iodide uptake was greatest in a LDH with a Mg/Al ratio of 4:1 providing support for this explanation. Thermally activated LDHs where found to be more effective for removing the IO_3^- and I^- anions from solution.

Further investigation into the sorption of iodine and iodide contaminants by LDHs and TA-LDHs is required and to the best of our knowledge nothing has been published in literature concerning the removal of iodide by LDHs

containing layer cations other than magnesium or aluminium. LDHs intercalated with other interlayer anions (such as chloride, nitrate, hydroxide) may have greater affinity for iodide than those that have already been tested and may be more suitable for industrial applications. There has also never been any attempt to remove iodine directly from solution. Experiments need to be conducted that prove whether or not iodine dissociates sufficiently in water and what effect, if any, this equilibrium would have on the uptake of iodine. It is also important to consider whether LDHs are suitable materials for the long term storage of radioiodine wastes. The possibility of anion exchange resulting in de-sorption of iodide species in different chemical environments must also be investigated.

3.3. Previous Investigations into the Removal of Halides by Zn/Al LDHs

A considerable amount of research concerning the application of Mg/Al LDHs as anion sorbents is currently available in the scientific literature (see chapter 1). In contrast, nowhere near as much interest has been directed towards the possible application of Zn/Al LDHs for removal of unwanted anions from aqueous solution.

3.3.1 Removal if Fluoride by Zn/Al LDHs

Das et al. [33] investigated fluoride removal using a thermally activated Zn/Al LDH with as Zn:Al ratio of 2:1 prepaired by co-precipitation at constant pH. Characterisation by a range of techniques including: powder XRD, TGA, DTA, FTIR, BET and elemental analysis determined that the product of the synthesis was the desired Zn/Al LDH. the LDH was

thermally activated by calcinations at 450°C for 8 hours. Fluoride sorption experiments were carried out using synthetic fluoride solutions prepared to the desired concentration by dissolution of sodium fluoride (AR grade) in deionised water. Fluoride concentration was measured using an Elico digital pH metre with a fluoride selective glass electrode [33].

First, the effect of contact time with the fluoride solution was investigated. Fluoride removal increased with time reaching a maximum after 4 hours using an adsorbent dose of 1g/L and an initial fluoride concentration of 10mg/L. The percentage removal at 4 hours was 85.5% [33]. Next, the effect of pH on fluoride removal was tested. The desired solution pH was achieved using nitric acid or sodium hydroxide. No buffer was used to avoid competition with other anions. Fluoride uptake was found to increase with pH, reaching a maximum at pH 6.0 before decreasing. The increase in fluoride uptake was attributed to the reduction in competing hydroxide anions in the solution [33].

The effect of adsorbent dose and initial concentration of fluoride was also investigated. A maximum loading capacity of 13.43mg/g was obtained using an adsorbent dose of 0.2g/L. Loading capacity of the LDH was found to decrease as adsorbent does increased indicating that the surface sites of the thermally activated LDH were heterogeneous [33]. Adsorption density increased fluoride concentration to a maximum of 60mg/L of fluoride, before remaining constant. Again this suggests the surface sites of the thermally activated LDH were heterogeneous [33].

Increasing the temperature at which fluoride removal took place reduced fluoride adsorption, indicating that the fluoride adsorption process was exothermic in nature. The adsorption data was fitted to a linearly transformed Langmuir equation indicating that fluoride sorption was a surface phenomenon [33]. The effect of competitive sulfate and phosphate anions was investigated. Fluoride sorption was found to remain almost constant when sulfate concentration was below 30mg/L. At higher sulfate concentrations fluoride sorption decreased, reaching 15.44% when the sulfate concentration was 100mg/L. In contrast fluoride sorption decreased at phosphate concentration above 10mg/L. A fluoride removal of 24.34% was observed at a phosphate concentration of only 50mg/L [33].

3.3.2 Removal if chloride by Zn/Al LDHs

Lv et al. [67] investigated the removal of chloride from aqueous solution using the anion exchange properties of selected Zn/Al LDHs prepared by co-precipitation. All LDHs prepared were characterised by powder XRD, FTIR and ICP-AES. Firstly the effect of altering the composition of the cation layers was investigated. The LDH with a Zn:Al ratio of approximately 2:1 was found to be the overall for the sorption of chloride with 64.20% chloride removal [67]. Optimum contact time for the Zn/Al LDH was investigated and found to be 4 hours. The maximum amount of chloride adsorbed at this point was 64.1% [67]. Next, the effect of pH on anion removal was investigated. Anion uptake was stable between pH 4.0 and 9.0 with a maximum uptake of 19.84 at pH 7.0 [67]. It was proposed

that anion uptake is low at high pH because of the presence of competing hydroxide ions, and a due to partial dissolution of the LDH layers at low pH. The dose of LDH required for optimum removal of chloride with an initial concentration of 100mg/L was 2.5g/L [67].

Equilibrium isotherms were investigated at 25, 30, 35, 40, 45 and 60°C. Anion exchange capacity increased with temperature, indicating that chloride mechanism uptake is endothermic in nature. Isotherms could be fitted to the Langmuir isotherm model. The Gibbs free energy (ΔG^0) was calculated and found to be negative at all temperatures confirming the spontaneity of the adsorption process. The positive value of ΔH^0 confirms the endothermic nature of chloride sorption while positive value of ΔS^0 indicates increased randomness at the solid/solution interface [67]. Finally the kinetics of chloride sorption was investigated and found to follow the pseudo-second order kinetics model. The activation energy was calculated using the Arrhenius equation and found to be 10.27kJ/mol.

3.4 Preliminary Synthesis of Zn/Al LDH by the Co-Precipitation Method

A preliminary sample of Zn/Al LDH ($Zn_6Al_2(OH)_{16}(CO_3)\cdot 4H_2O$) was synthesised, using a similar method to the one reported for the Mg/Al LDHs (chapter 2) in which the magnesium was substituted by zinc as described in Table 3.1. A mixed metal solution was prepared by dissolving zinc chloride (45.8269g, 0.2788mol) and aluminium chloride (15.0896g, 0.09347mol) in deionised water (250mL). The same caustic solution (98mL) used in the synthesis of $Mg_6Al_2(OH)_{16}(CO_3)\cdot 4H_2O$ was used for this experiment. The

caustic solution was added dropwise to the zinc containing mixed metal solution (98mL) with stirring resulting in the formation of a white precipitate. Once all the caustic solution was added the mixture was stirred for approximately 24 hours. The LDH was collected by vacuum filtration, washed with deionised water and dried overnight in an oven at approximately 70°C. The LDH was weighed and a sample ground for analysis.

Table 3.1: Details of the preliminary synthesis of Zn/Al LDH

Reagent	Theoretical Mass (g)	Mass Weighed (g)	Solution Volume (mL)
Mixed metal solution			
Zinc chloride hexahydrate	45.8271 (0.2788mol)	45.8269 (0.2788mol)	250
Aluminium chloride hexahydrate	15.0894 (0.09348mol)	15.0896 (0.09347mol)	
Caustic solution			
Sodium hydroxide	20.000	20	250
Sodium carbonate	42.396	42.396	
Total Mass of Product			
$Zn_6Al_2(OH)_{16}(CO_3)\cdot 4H_2O$	---	13.75	---

3.5 Bulk Synthesis of Zn/Al LDH by the Co-Precipitation Method

Further synthesis and adsorption experiments reported here were carried out in collaboration with a colleague Mr Michael J. Sear-Hall who carried out much of the synthesis and adsorption testing described in this chapter. A larger quantity of 3:1 Zn/Al layered double hydroxide was prepared by scaling up the co-precipitation described above.

Table 3.2: Details of the bulk synthesis of Zn/Al LDH.

Reagent	Mass Weighed (g)	Solution Volume (mL)
Mixed metal solution		
Zinc chloride hexahydrate	183.33 (1.1357mol)	250
Aluminium chloride hexahydrate	60.36 (0.3672mol)	
Caustic solution		
Sodium hydroxide	80.05	250
Sodium carbonate	170.00	
Total Mass of Product		
$Zn_6Al_2(OH)_{16}(CO_3)\cdot 4H_2O$	169.03	---

A mixed metal solution was prepared by dissolving Aluminium chloride (60.36g, 0.3672mol) and zinc chloride hexhaydrate (183.33g, 1.1357mol) in ultrapure water (1000mL) as before. The caustic solution was prepared by dissolving sodium hydroxide (80.05g) and sodium carbonate (170.00g) in ultrapure water (1000mL). The solutions were combined by adding the caustic solution (1000mL) dropwise to the mixed metal solution (1000mL) with constant stirring. Combination of the two solutions resulted in the precipitation of white LDH. The mixture was allowed to stir for approximately two hours before the solids were removed by vacuum filtration. The recovered LDH (169.03g) was collected and dried overnight in an oven at 80°C before being ground to a fine powder using a mortar and pestle. A sample of the Zn/Al LDH was thermally activated at a temperature of 280°C. The furnace reached a maximum temperature of 371°C before slowly decreasing to approximately 310°C over the period of one hour. The maximum temperature reached during thermal activation was considerably higher than originally intended, however, as many papers report optimal

thermal activation temperatures around 500°C it was decided to continue with the experiment. The mass loss during thermal activation was found to be 27.09%. The sample was observed to change colour after thermal activation. The sample changed from white to light green colour.

3.6 Removal of iodine and iodide from aqueous solutions using Zn/Al LDH

A solution containing iodide (0.09M) was prepared by dissolving the required mass of potassium iodide in ultra pure water. Iodine was also required for this experiment. The solution was freshly prepared before each test by dissolving potassium iodide (approximately 0.56g) and potassium iodate (approximately 0.14g) in deionised water (20mL). Three drops of concentrated hydrochloric acid was added to cause iodine to form in solution.

Initial experiments were designed to determine the mass of TA LDH required to completely remove iodide and iodine from solution. Various combinations of 1, 2 and 3g samples of LDH were treated with iodine or iodide solution (20mL). The mixture was stirred for 30 minutes before separation. An iodometric titration was used to determine if any iodine/iodide remained after treatment with LDH. Sodium thiosulfate solution was prepared for use in the iodometric titrations. The solution was standardised by titration with iodine and found to be 0.0292M. No iodide was observed to remain in solution after treatment with three consecutive 3g applications of LDH. In contrast, only two 3g applications were required before all iodine was removed from solution.

Table 3.3: Results of the titration of iodide solution after treatment with Zn/Al LDH

Titration Number	Initial Concentration of KI Solution (M)	Mass of Zn/Al LDH (g)	Volume of $S_2O_3^{2-}$ solution required (mL)
1	0.089	1.0381	17.2
2	0.089	1.09.2	19.8
3	0.089	1.0714	18.8
Average	0.089	1.0816	18.6

Quantification of results was achieved by treating 1g samples of LDH with 20mL aliquots of iodide or iodine solutions using the method described above. An iodometric titration was used to determine iodine remaining in solution. Measurements were carried out in triplicate (Table 3.3 and 3.4). It was found that 1g of LDH was able to remove 36.8% of the iodide initially present in solution. However, the same mass of LDH was able to remove 99.5% of iodine initially present in the solution with an initial concentration of 0.1M. The LDH was collected and retained for further analysis. A colour change was observed, whereby the LDH became a grey yellow colour after treatment with iodide and a faint yellow brown after treatment with iodine.

Table 3.4: Results of the titration of iodine solution after treatment with Zn/Al LDH

Titration Number	Mass of Zn/Al LDH (g)	Mass KI Measured (g)	Mass KIO_3 Measured (g)	Solution Volume (mL)	Volume of Thiosulfate (mL)
1	1.03	0.5836	0.1412	20	6.0
2	1.03	0.5870	0.1424	20	6.8
3	1.04	0.5675	0.1428	20	6.5
Average	1.03	0.5794	0.1421	20	6.4

3.7 Characterisation of Synthetic Zn/Al LDH Samples by Powder X-ray Diffraction

Powder X-ray diffraction (XRD) was carried out on samples of Zn/Al LDH collected before thermal activation, after thermal activation, after the sorption of iodide and iodine. A Philips X'pert wide angle X-ray diffractometer, with Cu Kα radiation (1.54052 Å) was used to collect the XRD patterns. The XRD patterns obtained from BTA as well as iodide and iodine treated samples are presented in Figure. 3.1.

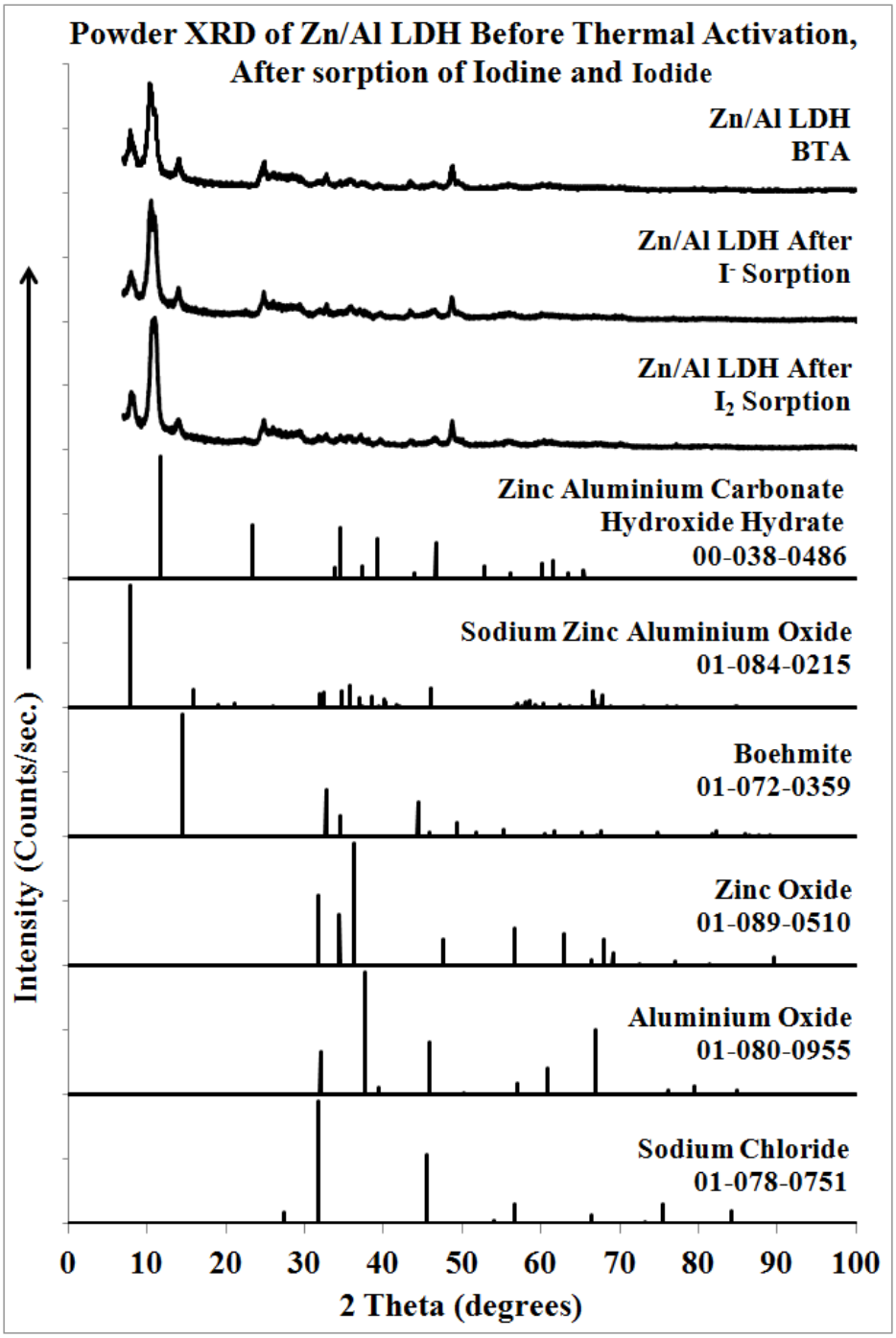

Figure. 3.1: Powder XRD pattern of Zn/Al LDH before thermal activation and after reformation in iodide or iodine solution with references.

Major peaks in the BTA sample corresponds to an accepted reference for a Zn/Al LDH (00-038-0486). Distinct shifts in peak positions are observed in the pattern of the BTA LDH when compared to the reference material. This indicates that there is a difference in the interlayer spacing. The d_{003} spacing

was investigated and found to be 8.07Å, which is within the acceptable range of a LDH structure. The sample also contained additional phases including sodium zinc aluminium oxide, boehmite, zinc oxide and aluminium oxide. These impurities and the overall poor crystalinity of the sample may result from poor control of the pH during the synthesis. There are methods that can be used to improve the yield of LDH such as ageing of the LDH in its mother liquor or hydrothermal treatment [44]. The major by-product of the synthesis process is sodium chloride, however, it was not observed. This indicates that it was successfully removed during washing.

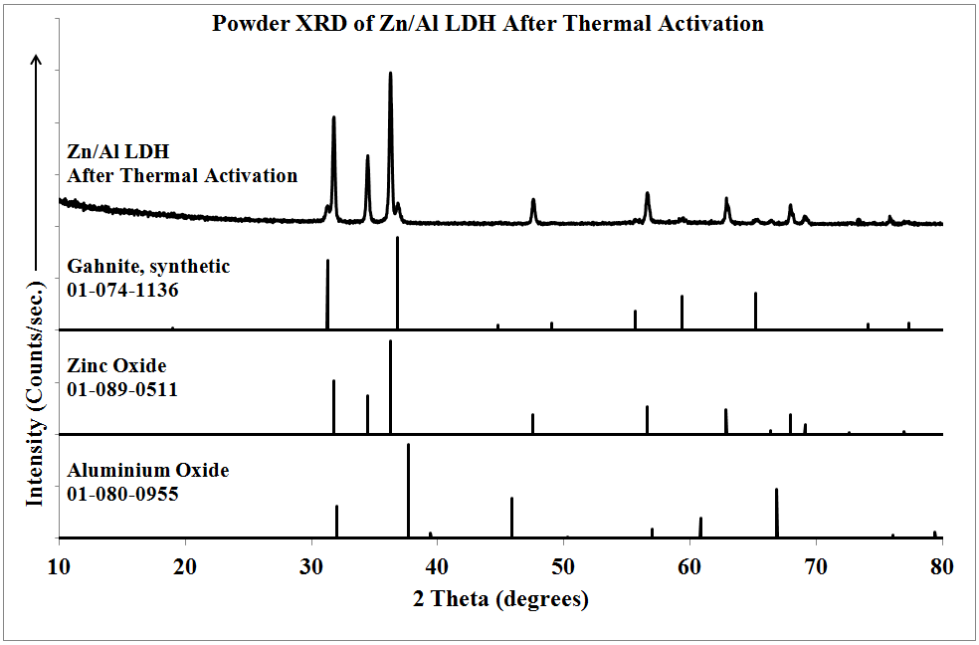

Figure. 3.2: Powder XRD pattern of Zn/Al LDH after thermal activation with references.

The powder XRD pattern of the LDH thermally activated to a maximum temperature of 371°C is presented in Figure. 3.2, lacks peaks corresponding to the characteristic LDH structure. This pattern was found to correspond well to references of zinc and aluminium oxides and gahnite ($ZnAl_2O_4$). The

presence of more intense peaks corresponding to zinc and aluminium oxides than gahnite indicate that the sample may have been partially decomposed during thermal treatment to a point that reformation may not occur. Using lower thermal activation temperatures (200 to 250°C) may be necessary to improve anion sorption by the reformation effect.

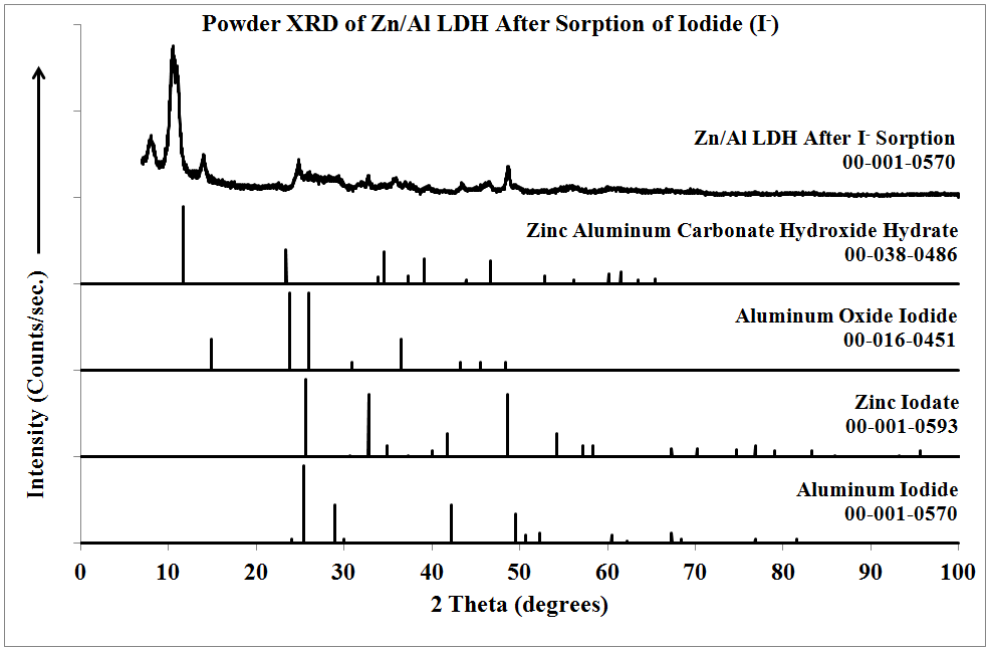

Figure. 3.3: Powder XRD pattern of Zn/Al LDH treatment with iodide solutions with references.

The LDH material recovered after sorption of iodide or iodine was also characterised by powder XRD. It was hoped that this technique would provide valuable information on the structure of the product and the mechanism of sorption of iodine species. The results (also presented in Figure. 3.1) show that both materials exhibit a similar LDH structure to that of the original BTA sample and the reference pattern for a Zn/Al LDH (00-038-0486). The similarities of the patterns may indicate that successful reformation of the LDH has occurred. Additional phases including

aluminium oxide iodate, zinc iodate and aluminium iodate were observed (Figure. 3.3 and Figure. 3.4). The d_{003} was found to be 8.59 and 8.41Å for the iodide and iodine treated samples, respectively. This value is only slightly larger than that of the original value.

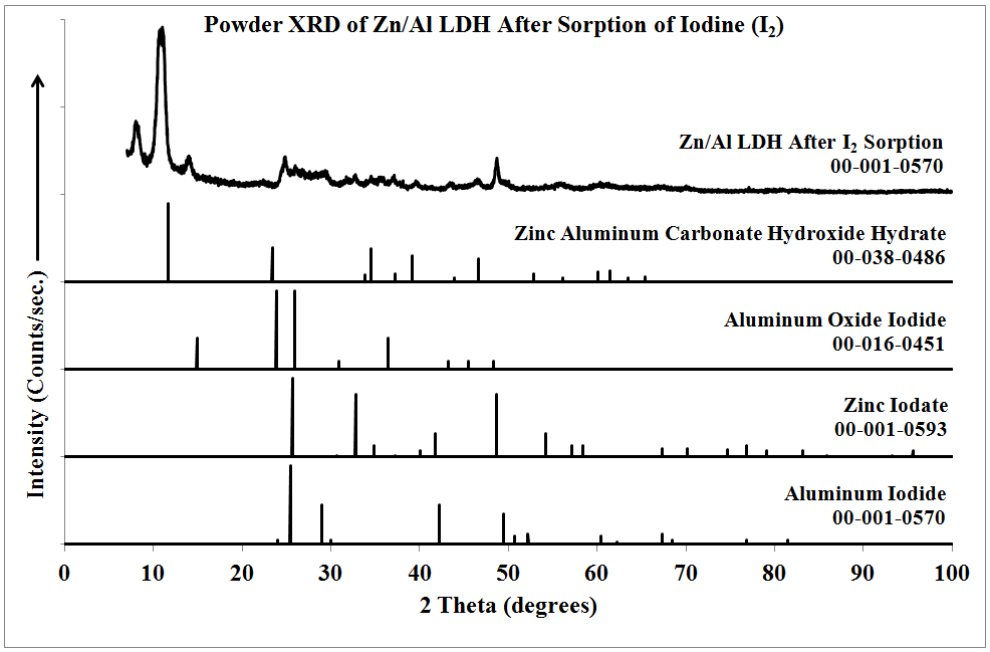

Figure. 3.4: Powder XRD pattern of Zn/Al LDH treatment with iodine solutions with references.

3.8. Characterization of Synthetic Zn/Al LDH Samples by Thermal Analysis

Thermogravimetric (TG) analysis was carried out on samples of Zn-LDH before and after thermal activation as well as after treatment with the iodide and iodine solutions. A TA® Instruments incorporated high resolution thermogravimetric analyser (series Q500) was used for thermal analysis experiments. The runs were carried under a flowing nitrogen atmosphere ($40cm^3$/min). Samples were placed in an open platinum pan and heated from room temperature to a maximum temperature of 1000°C at a rate of

2.50°C/min. TG and DTG curves were obtained. The TG analysis was repeated on selected samples to allow for evolved gas mass spectrometry. It was hoped this technique would provide further information on the thermal decomposition mechanism of the LDHs. The TA® Instruments thermogravimetric analyser was coupled to a Balzers (Pfeiffer) mass spectrometer for evolved gas analysis. The mass spectrometer was configured to analyse only selected gases. The gases selected included carbon dioxide, nitrogen/ carbon monoxide, oxygen and water as well as numerous iodine species such as I, I_2, IO, IO_2, IO_3, IO_4, and IO_5.

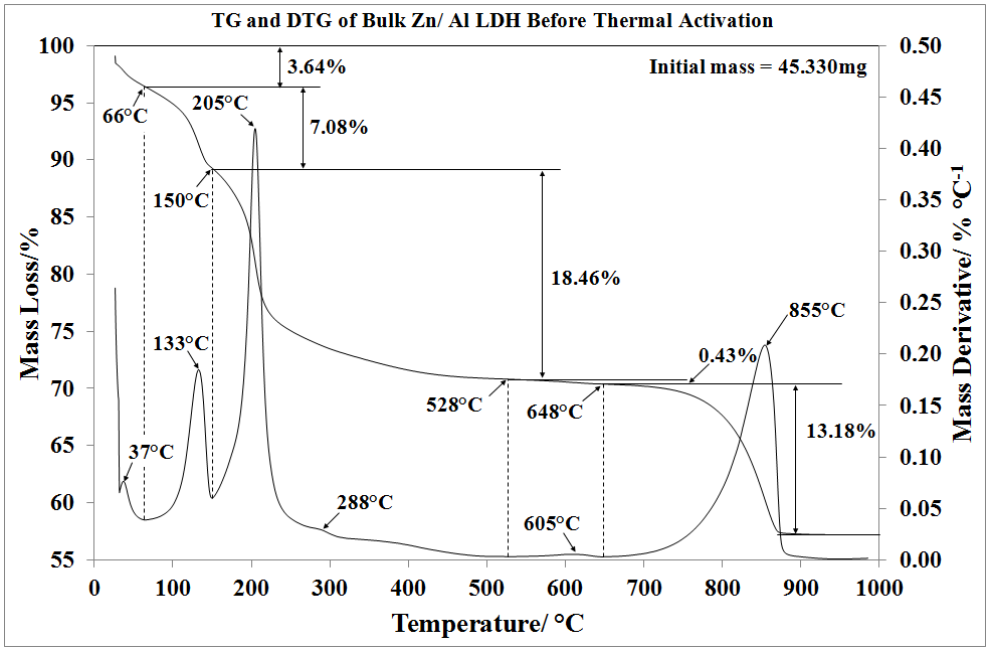

Figure. 3.5: TG and DTG of Bulk Zn/Al LDH before thermal activation

TG analysis was carried out on a sample of the bulk Zn/Al LDH BTA. The results are presented in Figure. 3.5. Thermal decomposition of Zn/Al LDH was investigated by Frost et. al. [68] who proposed a mechanism for its thermal decomposition. Four mass losses were observed during thermal

decomposition of the BTA sample. The first mass loss occurred at 37°C. This mass loss accounted for 3.64% of the total mass loss and was attributed to the loss of weakly adsorbed water due to the low temperature at which it occurred.

$$Zn_6Al_2CO_3(OH)_{16}\cdot xH_2O \rightarrow Zn_6Al_2CO_3(OH)_{16}\cdot 4H_2O + (x\text{-}4)H_2O \quad (3.1)$$

The second mass loss occurred at 133°C and was most likely due to the loss of interlayer water.

$$Zn_6Al_2CO_3(OH)_{16}\cdot 4H_2O \rightarrow Zn_6Al_2CO_3(OH)_{16} + 4H_2O \quad (3.2)$$

The third mass loss was also the largest. It occurred at 205°C and accounted for 18.46% of total mass lost. Asymmetry of the corresponding peak in the DTG curve indicates that two different processes are occurring simultaneously. This mass loss was therefore attributed to dehydroxylation and decarbonation, which usually occur almost simultaneously in this temperature region.

The results of powder XRD measurements of this sample do not completely support the mechanism proposed by Frost et. al, which has been reproduced below (equations 3.3-3.5). Powder XRD characterisation of samples were not reported in the original paper [68].

$$Zn_6Al_2CO_3(OH)_{16} \rightarrow Zn_6OAl_2CO_3(OH)_{14} + H_2O \quad (3.3)$$

$$Zn_6OAl_2CO_3(OH)_{14} \rightarrow Zn_6O_8Al_2CO_3 + 7\ H_2O \quad (3.4)$$

$$Zn_6O_8Al_2CO_3 \rightarrow (ZnO)_6Al_2O_3 + CO_2 \quad (3.5)$$

The presence of gahnite ($ZnAl_2O_4$) as an intermediary species is observed in the XRD pattern of the thermally activated LDH and indicates that the reactions reported in equations 3.6-3.8 better describe the decomposition of the Zn/Al LDH.

$$\mathbf{Zn_6Al_2CO_3(OH)_{16} \rightarrow Zn_6O_8Al_2CO_3 + 8H_2O} \quad (3.6)$$

$$\mathbf{Zn_6O_8Al_2CO_3 \rightarrow ZnAl_2O_4 + 5ZnO + CO_2} \quad (3.7)$$

$$\mathbf{ZnAl_2O_4 \rightarrow Al_2O_3 + ZnO} \quad (3.8)$$

Three additional features were observed in the DTG curve of the LDH sample collected (BTA). The first is a small feature at 288°C and the second occurred at 605°C. It was possible to determine that the second feature accounted for 0.43% of the total mass lost. The feature at 288°C could not be distinguished from the dehydroxylation/decarbonation peak. It was therefore not possible to estimate the percentage mass lost due to this feature alone.

A final mass loss occurred at 855°C which accounted for 12.61% of the total mass lost. The temperature at which this mass loss occurred was too high for reformation to reliably occur. For this reason, the feature was not investigated any further.

By making certain reasonable assumptions, it is possible to estimate the theoretical mass loss due to removal of interlayer water, dehydroxylation and decarbonation (or removal of whatever anions are present). The first essential assumption is that the formula of the Zn/Al LDH was

$Zn_6Al_2CO_3(OH)_{16}\cdot 4H_2O$ and that the sample analysed by TG is pure. The theoretical mass loss resulting from the removal of interlayer anions was calculated to be 13.88% compared to an observed result of 10.72% (a difference of 2.22%). The predicted mass loss of dehydroxylation and decarbonation was also calculated. The result obtained was 36.22%, compared to the observed value of only 18.46% (a difference of 15.31%). The discrepancy between the theoretical and observed mass losses may be due to the presences of impurities in the sample. The discrepancy between the total % mass loss observed and predicted was only 7.31%. This provides further evidence that the decomposition of this sample did not exactly follow the mechanism proposed by Frost et. al. [68].

The TG curve of the LDH collected after thermal activation and sorption of iodide (Figure. 3.6) shows six mass losses. The first mass loss at 43°C accounted for 1.49% of the total mass loss and was attributed to the loss of weakly absorbed water. The second and largest mass loss occurred next at 145°C accounting for 5.89% mass loss and assigned to the removal of interlayer water. A third mass loss at 191°C that accounted for 5.51% of total mass lost was attributed to dehydroxylation. The peaks in the DTG curve that correspond to the mass looses at 145 and 191°C overlap but can still be clearly separated. Three additional mass losses also occurred at 450, 635 and 752°C. These peaks account for 1.49, 1.63 and 1.67% of the total mass lost respectively. Again, these mass losses were not investigated further due to the high temperature at which they occurred.

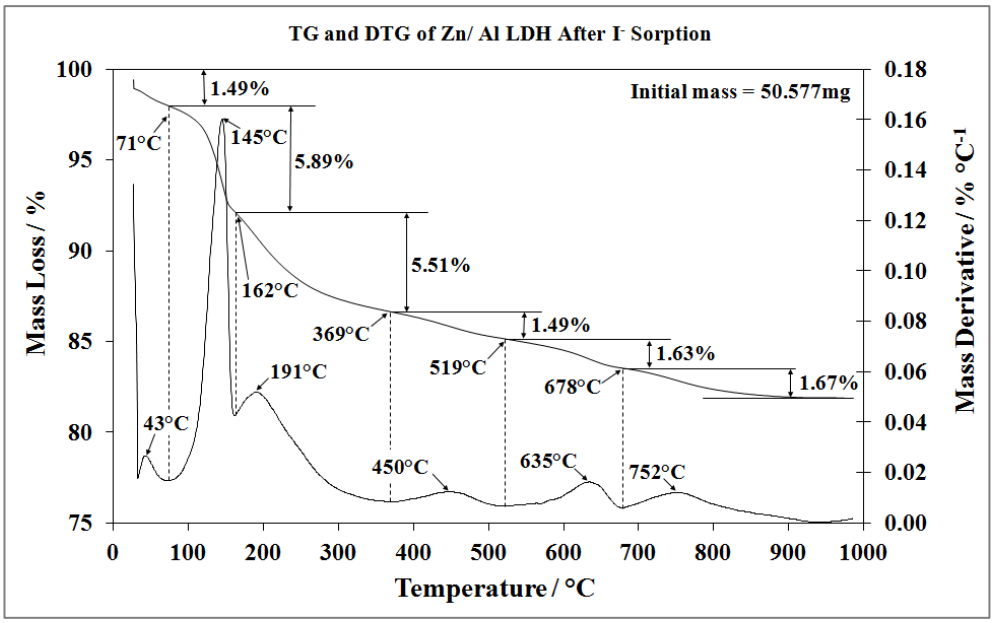

Figure. 3.6: TG and DTG of Bulk Zn/Al LDH after reformation in iodide solution

The theoretical mass loss resulting from the removal of interlayer water, dehydroxylation as well as the removal of interlayer anions was determined. Again, some assumptions had to be made. It was assumed that iodide was the only anion present in the interlayer. The theoretical mass loss for removal of interlayer water was to be 6.89%, which compared well to the observed result of 5.89%. The theoretical mass loss for dehydroxylation was estimated to be 13.78% compared to the observed result of 5.51%. This discrepancy may result from the partial decomposition of the sample into zinc and aluminium oxides, which do not exhibit the property of reformation.

The TG curve of Zn/Al LDH after treatment with iodine solution (Figure. 3.7) showed five mass losses. The first mass loss at 40°C accounted for 1.93% total mass lost and was attributed to the removal of weakly adsorbed water. The next mass loss occurred at 139°C accounting for 5.51% of the

total mass lost and is attributed to the removal of interlayer water. The third and largest mass loss occurred at 226°C and accounted for 8.38% of the total mass lost and is attributed to the dehydroxylation of the LDH. Two additional mass losses were also observed; 1) occurred at 498°C and accounted for 4.53% mass loss, and 2) at 732°C and accounted for 2.08% of total mass lost.

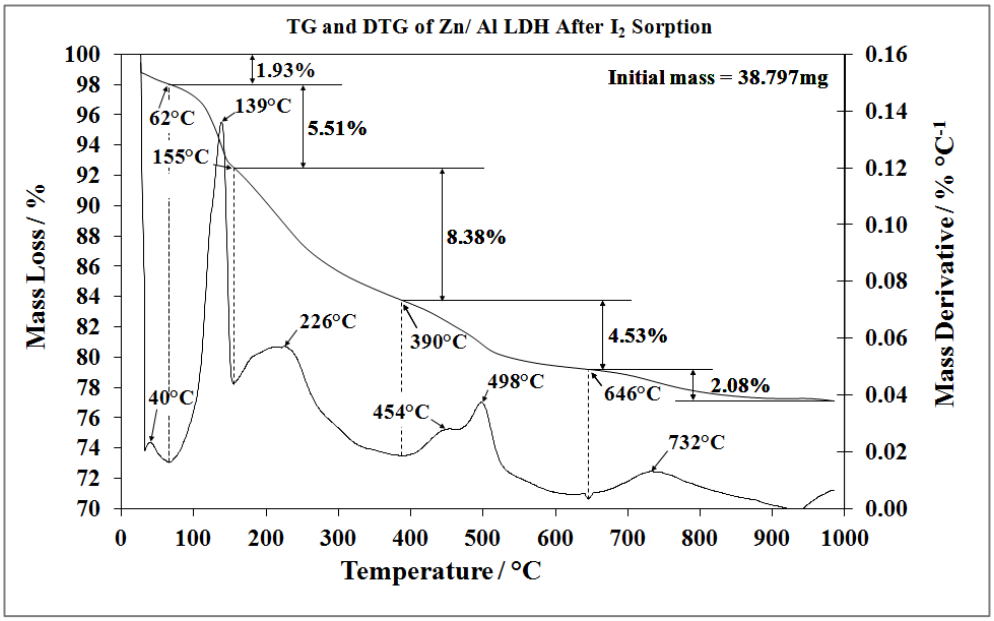

Figure. 3.7: TG and DTG of Bulk Zn/Al LDH after reformation in iodine solution

Once again the expected theoretical mass losses were calculated. It was again assumed that iodine was present in the interlayer in the form of iodide anions and that iodide is the only anion present in the sample. The theoretical mass loss for the removal of interlayer water was found to be 6.81%. This value compares well to the observed result of 6.89%. The theoretical mass loss of dehydroxylation was found to be 13.79% which was significantly larger than the observed value of 8.38%.

The TG patterns of the materials recovered after treatment of the TA LDH with iodide or iodine solution were very similar. They are also similar to the TG pattern obtained from the BTA Zn/Al LDH. Only a small change in the temperature of dehydroxylation was observed between the three samples. The temperature of dehydroxylation can be used as a measure of the thermal stability of a LDH. Therefore, it appears that Zn/Al LDHs containing intercalated iodine species have similar thermal stabilities to those containing only carbonate in the interlayer. [2]

Table 3.5: Comparison of the observed and theoretical mass losses for all three samples analysed by TG. The theoretical mass loss of the I^- and I_2 intercalated samples was determined by combining the loss of interlayer water and dehydroxylation only. No removal of interlayer anions was included.

Sample	Total Observed Mass Loss (%)	Theoretical Observed Mass Loss (%)	Difference (%)
BTA	42.79	50.10	-7.31
I^- Sorption	17.68	20.64	-2.96
I_2 Sorption	22.43	20.68	+1.75

The total mass loss observed for both the iodine and iodide samples (17.68% after iodide sorption and 22.43% after iodine sorption) was lower than the total mass loss of the original Zn/Al LDH BTA (42.79%). Both the iodide and iodine treated samples match the theoretically determined values if the removal of interlayer iodide is ignored (Table 3.5). This evidence suggests that Zn/Al LDHs containing iodine species undergo decomposition through more complex mechanisms than those described by Frost et. al. for a carbonate containing Zn/Al LDH [34]. This also indicates that iodine species may not be removed from Zn/Al LDHs during thermal

decomposition. The TG analysis of the LDH recovered after treatment with iodide and iodine solution was repeated to allow for evolved gas mass spectrometry. The iodide treated sample shown in Figure. 3.8 appeared to lose water at three distinct temperatures.

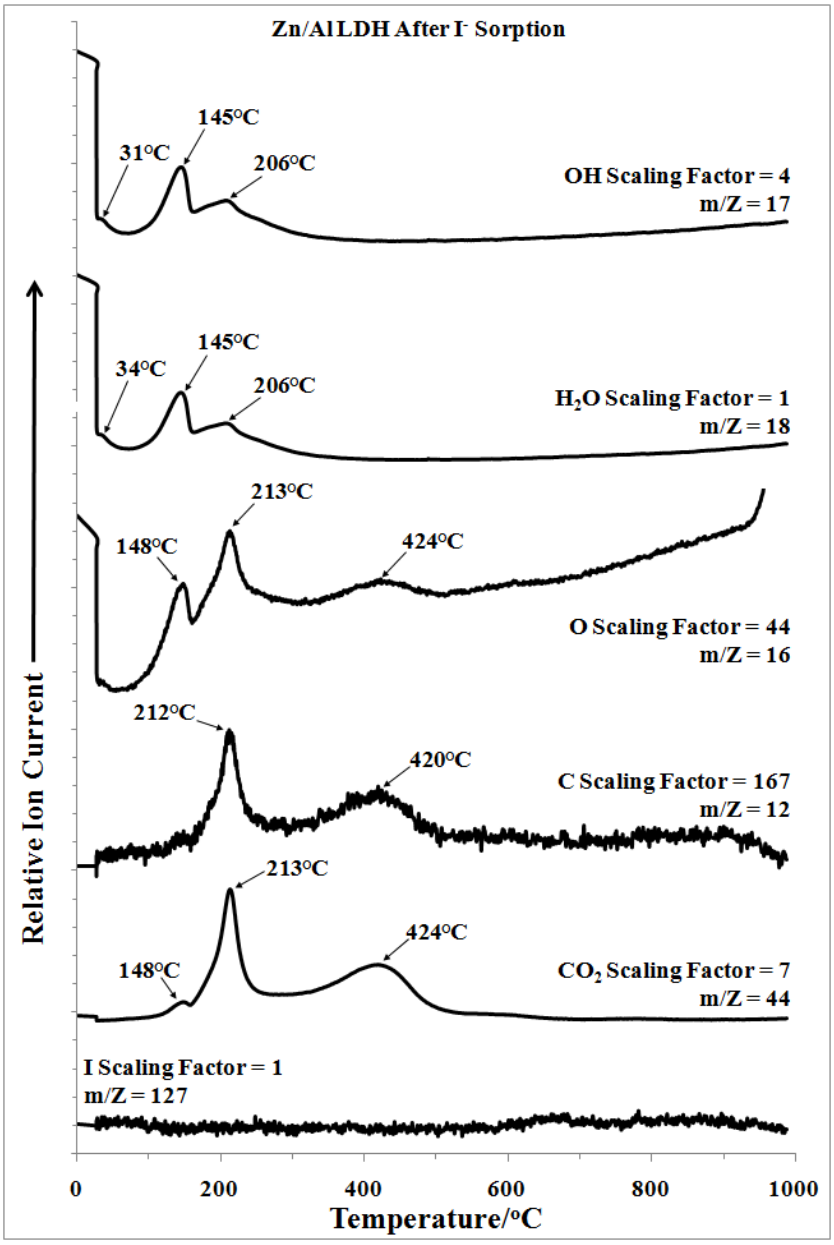

Figure. 3.8: Evolved gas mass spectrometry of selected ions evolved during the thermal decomposition of Zn/Al LDH treated with iodide solution.

Weakly adsorbed water was lost at 34°C followed by interlayer water at 145°C and dehydroxylation at 206°C. Two distinct losses of carbon dioxide were observed at 213 and 424°C. Oxygen was also lost at three temperatures 148, 213 and 424°C. Almost all mass losses above 600°C appeared to be a loss of oxygen (Figure. 3.8). More importantly, no iodine containing gases investigated were released during thermal decomposition.

Similar results were obtained for the decomposition of the material recovered after treatment with iodine solution. Ion current curves shown in Figure. 3.9 revealed three distinct losses of water at 47, 143 and 212°C. Two distinct forms of carbon dioxide were also observed to be lost, one at 224 and the other at 443°C. Oxygen was detected at 145, 224, 519 and above 600°C. A small additional peak in the ion current curves of water, carbon dioxide, oxygen and hydroxide at 176-177°C was also observed. However, the most significant difference between the two samples was that iodine (m/Z = 127) was observed between approximately 200-700°C with two distinct features at 295 and 519°C. It is not yet entirely clear why iodine is lost from this sample and not the one treated with iodide solution.

It is possible that less stable iodine species have formed in the interlayer or on the surface of the LDH treated with iodide solution. Another explanation is that there may simply be a greater number of iodine containing molecules adsorbed by the LDH. Some of these molecules may therefore occupy sites of higher binding energy and be lost more easily. Iodine may also be lost in a form that the mass spectrometer was not set to detect.

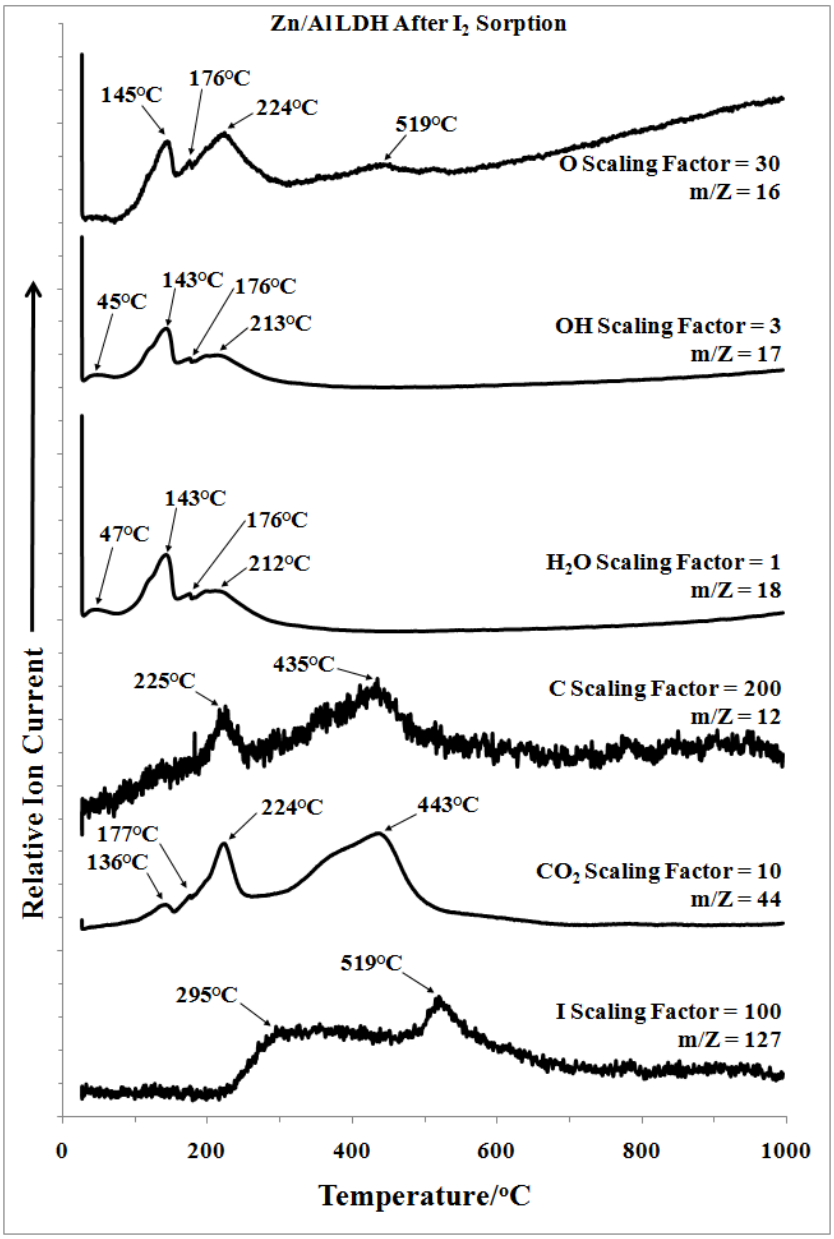

Figure. 3.9: Evolved gas mass spectrometry of selected ions evolved during the thermal decomposition of Zn/Al LDH treated with iodine solution.

It is important to note that due to the presence of significant impurities it is impossible to know the exact starting mass of the LDH. Consequently, the calculated results based on the TGA data presented in this chapter may be unreliable, however, the best possible attempts were made given the

circumstances. These experiments should be repeated to confirm the accuracy of results.

3.9. Conclusions / Discussion

Zinc aluminium layered double hydroxides show promise as potential sorbents for the removal of harmful iodine species from water. Successful anion sorption was achieved using batch processes with relatively short mixing times and without any attempt to reduce sorption of carbonate (a competing anion which LDHs are known to have a strong affinity for). Zn/Al LDHs appear more efficient at removing iodine (prepared by the reaction of potassium iodate and potassium iodide under acidic conditions) from solution when compared to a solution containing only iodide (in the form of potassium iodide). The LDH removes an estimated 99.5% of iodine from solution compared to only 36.8% for the removal of iodide.

Powder XRD confirmed the destruction of the original LDH during thermal activation and the successful reformation of similar structures in the material recovered after sorption of both iodine and iodide. Powder XRD also indicated that the LDH may have been partially decomposed to a mixed metal oxide during thermal activation reducing its efficiency as an anion sorbent. Using a lower thermal activation temperature may produce better results. The XRD patterns obtained from samples collected after treatment with the iodine solutions corresponded well to the reference (00-038-0486) for a Zn/Al LDH. Other phases that may have been present in the sample included aluminium oxide iodate, zinc iodate and aluminium iodate. The

d_{003} spacing increased after sorption of iodide and iodine (8.59 and 8.41Å respectively). The change in the d_{003} spacing suggests that intercalation did indeed occur. The XRD patterns indicated that the thermally activated LDH adsorbent successfully underwent reformation, forming a structure similar to that of the original Zn/Al LDH material. Furthermore, this may indicate a similar composition of anions in the interlayer and therefore a similar mechanism of sorption in both samples.

The thermal decomposition of all samples investigated appear to occur through a similar mechanism. A new mechanism for the thermal decomposition of a Zn/Al LDH has been proposed. This mechanism is similar to the one previously described in the literature [68, 69]. A significant observation was made while investigating the thermal decomposition of samples of LDH recovered after sorption of iodide and iodine. The total percentage mass loss observed for samples of LDH treated with iodine (22.43%) and iodide (17.68%) was significantly lower than that of the original LDH (42.79%). It is possible that iodine species form non-removable anions when intercalated into the Zn/Al LDH structure. Comparison of the theoretical and observed mass losses also appeared to confirm the hypothesis. This effect may be advantageous for the long-term storage of radioactive iodine in LDH materials. Further investigations are required into the desorption of iodine species, as well as the possibility of decomposing LDHs containing iodine species to mixed metal oxides at high temperatures (in excess of 1000°C) which should inhibit the reformation and anion exchange properties [2, 3]. However, as previously stated, the

calculated results based on the TGA data presented in this chapter may be unreliable due to the presence of impurities.

If iodine species cannot be removed by thermal decomposition of the LDH the efficiency of anion removal of the LDH would be significantly decreased after each subsequent thermal activation and reformation cycles. An anion-exchange step using a removable anion in solution (such as carbonate) would likely be required to make the Zn/Al LDH an effective, reusable sorbent material. Again, further investigation is required.

Evolved gas mass spectrometry was used to further investigate the decomposition of the LDH materials recovered after treatment with iodide and iodine solutions. No iodine species were observed to be lost as gases during the decomposition of iodide treated LDH sample, however, iodine in its elemental form (m/Z = 127) was observed to be lost at temperatures between 200-700°C during decomposition of the sample treated with iodide solution. The scaling factor of this ion current curve (Figure. 3.9) suggests only a small quantity of iodine was observed when compared to the amount of water. The loss of iodine may be due to the presence of different iodine containing anions in the interlayer of the LDH or, simply the greater number present in the sample. This could also be the result of variations in experimental conditions.

It is well established that iodine can react with water resulting in numerous anions which often react further to give a wide range of iodine species that

may be present in solution [70]. Given the correct conditions a complex equilibrium of numerous anionic species containing iodine may exist. If this is the case only a small quantity of anions to which the LDH has a high affinity are required. As the anion is removed by the adsorbent, the equilibrium will shift to favour the generation of more of the anion. Again, a lot more investigation is required before the sorption of iodine species by Zn/Al LH materials is completely understood.

Chapter Four:

Synthesis and Characterisation of Mg/Cr Layered Double Hydroxides: New Applications for the Mineral Stichtite.

Chapter 4: Synthesis and Characterisation of Mg/Cr Layered Double Hydroxides: New Applications for the Mineral Stichtite.

4.1. Introduction

The mineral stichtite is a chromium substituted member of the layered double hydroxide group (LDHs) that occurs in nature [71, 72]. The ideal chemical structure of stichtite is $Mg_6Cr_2CO_3(OH)_{16}\cdot 4H_2O$. When compared to hydrotalcite, the aluminium(Al^{3+}) is substituted with chromium(Cr^{3+}) in a similar way as pyroaurite, which is an iron(Fe^{3+}) substituted LDH. Naturally occurring stichtite does exhibit varying amounts of partial substitution of Cr^{3+} in the cation layers for Al^{3+} or Fe^{3+} [73]. Stichtite is often described as a rare mineral as there are only 14 locations in the world in which the mineral is known to exist. One of these locations is Tasmania, Australia where there are abundant deposits. Unlike many other LDH minerals, little has been published in the literature on stichtite [34, 46, 71-74]. This lack of interest is likely due to the minerals perceived rarity. Stichtite is an interesting and potentially underutilised resource. Currently stichtite is valued only for its intense purple to pink colour (which depends on impurities present) resulting in its popularity as a semi-precious stone or in mineral collections.

Other substituted LDH's have previously been investigated for the removal of anions from water including reevesite, woodallite, iowaite as well as many others [6-10, 16, 18-22, 24, 26-32, 35, 43, 56, 60, 75-81]. Substitution of the layer cations of a LDH may change its affinity for various anions. For example, it has been reported that a manganese substituted LDH had an

unusually high affinity for phosphate anions [82]. In this chapter, we aim to summarise some of the previously published literature on stichtite and present the results of our own on-going investigations.

4.1.1. Discovery of Stichtite and Early Research (1891-1913)

Stichtite was first discovered in western Tasmania in 1891, however, it was mistakenly identified as kämmererite (a purple form of chlorite) by Stitt and Cullingsworth due to the remarkable similarity of the two minerals and the absence of chemical analysis. In 1910, Wesley the chief chemist at the Mount Lyell Mining and Railway Company conducted wet chemical analysis on a sample of stichtite and determined that the mineral was not a silicate, as expected, but a new uncatalogued mineral with the formula $(CrFe_2)O_3,6MgO,CO_2,13H_2O$. Stichtite was named after Robert Carl Sticht, the general manager of Mount Lyell Mining and Railway Company, in appreciation for his assistance in the preparation of the publication "catalogue of the minerals of Tasmania". It was in this publication by Petterd in which stichtite was first reported [71, 83]. Petterd was the first to identify the similarity of stichtite to pyroaurire an iron substituted LDH. Samples of stichtite were sent to the Mineralogic-petrological Institute in Zurich where Hezner carried out further chemical analysis and concluded the sample was a new mineral. In a paper published in 1912, Hezner suggested stichtite may be a chrome-brugnatellite with the formula: $2MgCO_3 5Mg(OH)_2 2Cr(OH)_3 4H_2O$. Himmelbauer [71] performed further investigations and found that the mineral had a hardness of 1 3/4 (between gypsum and rock salt) and a density of 2.161 (by the fluid method). Its

refractive index was found to be 1.542 (immersion method). Himmelbauer was among the first to report the similarity of stichtite to hydrotalcite and pyroaurire in 1913 [71].

4.1.2. Geological Origin of Stichtite

Lewis and Cairncross performed analysis of stichtite from various sources in an attempt to better understand the mechanisms of stichtite formation (see electron microprobe analysis section below) [73]. It was clear that serpentinite must be the source of Mg^{2+} as stichtite is only found in nature intergrown with serpentinites. Serpentinite is the name given to a rock that consists of one or more of the serpentine group of minerals, which is typically described by the formula $Mg_3Si_2O_5(OH)_4$. Magnesium may be substituted with Fe Ni, Al, Zn or Mn.

The trivalent cations found in stichtite such as Cr^{3+} and to a lesser extent Al^{3+} and Fe^{3+} most likely originate from chromite as it is present in most known cases [73]. No individual reaction could be proposed to adequately explain stichtite formation. It can be proposed that stichtite is a product of the breakdown of serpentinite and chromite by one of the two following equations:

2 serpentinite + chromite + $8H_2O$ + CO_2 → stichtite + 4 quartz + FeO (4.1)

3 serpentinite + chromite + $7H_2O$ + CO_2 → stichtite + talc + 4 quartz + FeO (4.2)

The difficulty with these reactions is the observed absence of quartz, talc or FeO in direct association with known stichtite deposits. This could be explained by dissolution and redeposition of silica by aqueous and carbonic fluids. FeO may be partially oxidised and form magnetite or removed in solution. The observation that stichtite commonly occurs as veins in serpentinite provides evidence to support this mechanism [73]. It was also suggested that stichtite may be formed from magnesite ($MgCO_3$) or brucite ($MgOH_2$). These two equations do not require the removal of silicates as it would have taken place during the original formation of the magnesite or brucite.

6 magnesite + chromite + $12H_2O$ → stichtite + $5CO_2$ + FeO (4.3)

6 brucite + chromite + $6H_2O$ + CO_2 → stichtite + FeO (4.4)

The presence of small amounts of magnesite associated with some stichtite deposits may provide evidence to support this mechanism. Though the exact mechanism of stichtite formation is still unclear, the absence of silicates associated with stichtite baring rocks and the overall rarity of the mineral suggests that a unique combination of conditions must exist for its formation.

4.1.3. Synthesis of Stichtite

As previously mentioned it is difficult to obtain pure stichtite from natural sources as the material is often intermixed with serpentinites as well as other LDHs including iowaite, pyroaurite and reevesite [71, 72]. It is therefore necessary to develop methods for the synthesis of pure samples of these

minerals to truly understand their properties and the complex relationship that exists between these LDHs [72]. Frost and Erickson [72] successfully use a variation of the co-precipitation method to prepare synthetic stichtite. This was achieved by preparing two solutions. Solution 1 contained NaOH and Na_2CO_3 (both 2M). Solution 2 contained Mg^{2+} (0.75M) as $Mg(NO_3)_2 \cdot 6H_2O$ and Cr^{3+} (0.25M) as $CrCl_3 \cdot 9H_2O$. Solution 2 was added to solution 1 at a rate of 40mL/min under a nitrogen atmosphere and with constant stirring. The resulting precipitate was collected then washed with boiled ultrapure water and dried. The material was characterised using vibrational spectroscopy and thermal analysis [34, 72]. The formula of the synthetic stichtite prepared by this method was found to be $Mg_{5.78}Cr_{2.09}CO_3(OH)_{16} \cdot 4H_2O$, which is very similar to the ideal formula of the naturally occurring mineral given earlier.

4.1.4. Vibrational Spectroscopy of Stichtite

To our knowledge, only a few papers have been published on the vibrational spectroscopy of stichtite. Frost and Erickson investigated samples of synthetic stichtite prepared by the co-precipitation method using IR, Raman and Near-IR spectroscopy [72, 84]. IR spectroscopy using a diamond ATR crystal was carried out on a sample of synthesised stichtite, prepared by the method described above, and numerous bands were identified [72]. A weak band observed at 1076 cm^{-1}, that was only observed with 50 times expansion, was attributed to the forbidden asymmetric stretching mode. The band observed at 1644cm^{-1} was attributed to the HOH water bending mode. The next two bands at 1457 and 1381cm^{-1} could be attributed to ν_3 CO_3

asymmetric stretching modes. Two bands at 744 and 685cm^{-1} were assigned to the ν_4 carbonate bending mode indicating that two carbonate species must exist in the interlayer. Bands at 909 and 861cm^{-1} may be attributed to MOH bending modes (where M is Cr or Mg). The hydroxyl stretching region, in the IR spectrum, was found to result from a complex combination of units. Some units proposed were Mg_3OH, Mg_2CrOH, $MgCr_2OH$ and Cr_3OH [72]. It would be expected for these units to be randomly distributed, however; this may not actually be the case. Three bands at 3618, 3529 and 3408cm^{-1} could be assigned to the Mg_3OH, Mg_2CrOH and Cr_3OHOH stretching bands respectively. Two remaining bands at 3220 and 2960cm^{-1} were assigned to water OH stretching [72].

Raman microprobe spectroscopy was also carried out on the same sample [72]. Two intense overlapping bands were observed at 1087 and 1067cm^{-1}. These bands were assigned to the ν_1 symmetric carbonate stretching mode. Again, two types of carbonate are observed and the band at 1087cm^{-1} is attributed to strongly hydrogen bonded carbonate. The ratio of the intensities of the two peaks was calculated to be 2.5/1. This corresponds well to the ratio of 2.3/1 obtained from the corresponding ν_4 bending mode peaks at 539 and 531cm^{-1}. The band at 453cm^{-1} was assigned to the CrO stretching mode, while the large number of bands between 200 and 366cm^{-1}could only be attributed to lattice modes [72].

Layered double hydroxides are well suited to be studied by near-IR spectroscopy (NIR), due to the presence of the hydroxyl surface and

interlayer water. Frost and Erickson [84] found that the three distinct spectral regions could be observed in the NIR spectra of stichtite. The high wavenumber region (6400 – 7400cm^{-1}) was attributed to the first overtone of the fundamental the hydroxyl stretching mode. The spectrum of stichtite was found to contain a broad profile with inflections at 7200 and 6800cm^{-1}. Bands were observed at 7246, 7151, 7069, 7017, 6890 and 6633cm^{-1}. These bands could only be attributed to the combination of OH stretching vibrations, observed in the mid-IR region, due to the complexity and distribution of the MOH bonds across the LDH [84].

The second spectral region (4800-5400cm^{-1}) contained the combination modes of the fundamental water vibrations. Bands were observed at 4460, 4411 and 4366cm^{-1}and attributed to OH combination bands. The third region (4000-4800cm^{-1}) was attributed to combination MOH stretching and deformation modes. NIR spectra of three different LDH materials (stichtite, iowaite and desautelsite) were compared and it was found that the minerals could be distinguished by their NIR spectra alone [84].

4.1.5. Thermal Decomposition of Stichtite

To the candidate's knowledge, thermal decomposition of natural stichtite has never been reported in the literature. Bouzaid and Frost appear to have carried out the only investigation reported, however this paper was about the thermal decomposition of synthetic stichtite [34]. Bouzaid and Frost used Thermogravimetry coupled with evolved gas mass spectrometry to determine the mechanism for the thermal decomposition of stichtite.

Decomposition was found to occur through a mechanism similar to most other LDH materials. The first step was removal of weakly adsorbed water at approximately 52°C, which was confirmed with evolved gas mass spectrometry, which showed the release of H_2O, OH and O in this temperature region. The theoretical mass loss determined from the ideal formula of stichtite was 11.0%. However, the mass loss in this temperature region was found to be considerably larger with a value of 24.9%. It was proposed that stichtite like other LDHs such as honessite and hydrohonessite may contain more than 6 water molecules per formula unit. Using the mass loss of 24.9% it was predicted that 9 moles of water must be present instead of 6 [34]. The first step of the decomposition mechanism (based on the ideal formula of $Mg_6Cr_2CO_3(OH)_{16}\cdot 4H_2O$) can be described by Equation 4.4 [34]:

$$\mathbf{Mg_6Cr_2CO_3(OH)_{16}\cdot 4H_2O \rightarrow Mg_6Cr_2CO_3(OH)_{16} + 4H_2O} \quad (4.4)$$

The next two steps in the thermal decomposition of stichtite appear to occur almost simultaneously at approximately 294°C. This region corresponds to the dehydroxylation and decarbonation of the LDH. By comparing the ion current curves it is clear that dehydroxylation occurred at a slightly lower temperature than decarbonation. The ion current curves clearly show the loss of H_2O, OH and CO_2 in this temperature region. Equations 4.5-4.8 describe the steps that occur in this temperature region during decomposition [34]:

$$\mathbf{Mg_6Cr_2CO_3(OH)_{16} \rightarrow (MgO)_6Cr_2CO_5 + 8H_2O} \quad (4.5)$$

$$\mathbf{(MgO)_6Cr_2CO_5 \rightarrow 6MgO + Cr_2O_3 + CO_2} \quad (4.6)$$

$$\mathbf{MgO + CO_2 \rightarrow MgCO_3} \quad (4.7)$$

$$\mathbf{Cr_2O_3 + CO_2 \rightarrow Cr_2CO_3} \quad (4.8)$$

Finally the ion current curves revealed the loss of CO_2 and O_2 at 545 and 675°C. These mass losses are described by the following equations [34]:

$$\mathbf{MgCO_3 \rightarrow MgO + CO_2} \quad (4.9)$$

$$\mathbf{Cr_2CO_3 \rightarrow Cr_2O_3 + CO_2} \quad (4.10)$$

4.1.6. Electron Microprobe Analysis of Stichtite

In an attempt to better understand the mineralogy and origin of stichtite, Lewis and Cairncross carried out electron probe microanalysis on samples of stichtite [73]. It was hoped that this technique would reduce the interference caused by the numerous impurities that may be present in samples of stichtite. Several difficulties were however encountered and overcome by Lewis and Cairncross before this technique could be successfully applied. As previously mentioned, stichtite is usually intergrown with serpentinite making it difficult to obtain pure samples. In some specimens, the stichtite and serpentinite were too tightly intergrown to be resolved even with probe microanalysis using a highly focused electron beam (1-2μm). A reasonable analysis was obtained by examining spots of the specimens with minimal intrusion of silicates using a rapid energy dispersive analysis technique [73]. A second difficulty that was discovered is that stichtite volatilises under the normal operating conditions of the electron microprobe used to perform the analyses. To counter this problem the beam current was reduced to 10nA (usually operated at 15kV and 15nA) [73].

The electron microprobe analysis was carried out on samples collected from the widest range of stichtite baring localities possible. The formulae calculated from all analyses corresponded well to the ideal formula of stichtite. The results obtained using electron microprobe analysis technique were much closer to the ideal formula than many results previously reported in the literature [73]. A small but consistent excess of divalent cations and a similar small deficiency of trivalent cations in the layers of the LDH suggest minor substitution of Cr^{3+} with Mg^{2+} or possible multivalency of ions of Mn or Ni present as impurities occurs in stichtite. Analysis revealed that the impurities often found in stichtite depends heavily on the location from which the samples are collected. For example, samples collected from Morocco or India contain more Fe^{3+} when compared to samples collected in Russia which contain higher levels of Al^{3+}. The purest stichtites were obtained from the Black Lake area in Quebec (Cr > 98 mol%) [73]. It appears that the composition of natural stichtites is variable with exact chemical composition likely depending on the geology of the locality in which it is found.

4.2. Preliminary Synthesis of Stichtite by the Co-Precipitation Method

Initial attempts at preparing synthetic stichtite proved to be unsuccessful. For the first attempt a similar method to that used for preparation of the Mg/Al LDH (described in chapter 2) was used in which aluminium(III) chloride was substituted with the required quantity of chromium(III) chloride as described below in (Table 4.1).

Table 4.1: Experimental conditions used during the first attempt to synthesis the Mg/Cr LDH.

Reagent	Theoretical Mass (g)	Mass Weighed (g)	Solution Volume (mL)
Mixed metal solution			
Magnesium chloride hexahydrate	38.1188 (0.3092mol)	38.1192 (0.3091mol)	250
Chromium chloride hexahydrate	16.6532 (0.08884mol)	16.6533 (0.08886mol)	
Caustic solution			
Sodium hydroxide	20.000	20.0128	250
Sodium carbonate	24.396	24.3986	
Total Mass of Product			
$Mg_6Cr_2(OH)_{16}(CO_3)\cdot 4H_2O$	---	80.2	---

The magnesium chloride hexahydrate (38.1192g, 0.3091mol) and chromium(III) chloride hexahydrate (16.6533g, 0.08886mol) was dissolved in deionised water (250mL). When the chromium(III) chloride was dissolved a very dark green solution was formed. Due to the colour of the solution, it was not possible to determine if all the metal salts had dissolved. The solution was therefore mixed as thoroughly as possible overnight. A new caustic solution was prepared by dissolving sodium hydroxide (20.0128g) and sodium carbonate (24.3986g) in deionised water (250mL).

The caustic solution (100mL) was added to the chromium containing mixed metal solution dropwise. Due to the intense dark colour of the mixed metal solution, the top of the meniscus was used (the same technique that is used for measuring potassium permanganate) for measuring the 100mL volume. It was difficult to observe if any change occurred when the caustic solution was first added due to the intense colour of the solution. When approximately half the caustic solution was added a fine light blue/grey

precipitate was observed. The mixture was left for approximately 24 hours with vigorous stirring. The precipitate was collected by vacuum filtration and dried for 48 hours in an oven at approximately 80°C. Powder XRD was carried out on a sample of the material which was found to be amorphous. The experiment was repeated using the same experimental conditions and solutions. This time the powder XRD indicated that the synthesis was successful, however, when the synthesis was carried out for a third time an amorphous light blue/grey product was again formed. The results for these experiments will not be presented here as the synthetic procedure did not appear to be reliable. Several variables were investigated before a more reliable procedure was found.

Stichtite was successfully prepared using a variation of the method described by Bouzaid and Frost [34]. This method has previously been summarised in the synthesis of stichtite section above. Stichtite was prepared using the same mixed metal solution described above with an increased concentration of sodium carbonate in the caustic solution was increased (Table 4.2). Magnesium chloride hexahydrate (38.12g, 0.3092mol) and chromium chloride hexahydrate (16.65g, 0.08887mol) were dissolved in ultrapure water (250mL) to prepare the mixed metal solution as before. A caustic solution consisting of sodium hydroxide (20.02g) and sodium carbonate (53.00g) dissolved in ultrapure water (250mL) was then prepared. Equal volumes of the caustic and mixed metal solutions (100mL) were combined dropwise by delivering the caustic solution from a burette into a beaker containing the mixed metal solution with constant stirring. As

soon as the two solutions were combined, a light blue precipitate began to form. The mixture was allowed to stir for approximately two hours before it was separated by vacuum filtration. The dark blue/purple solids where dried in an oven set to approximately 40°C. The original method proposed by Bouzaid and Frost [34] was not replicated as no powder XRD characterisation of the samples prepared by this method appear to have been reported in the literature.

Table 4.2: Experimental conditions used during the successful attempt to synthesis the Mg/Cr LDH.

Reagent	Theoretical Mass (g)	Mass Weighed (g)	Solution Volume (mL)
Mixed metal solution			
Magnesium chloride hexahydrate	38.1188 (0.3092mol)	38.1188 (0.3092mol)	250
Chromium chloride hexahydrate	16.6532 (0.08886)	16.6541 (0.08887)	
Caustic solution			
Sodium hydroxide	20.000	20.0202	250
Sodium carbonate	52.995	52.9945	

To the author's knowledge, this is the first time synthetic stichtite has been prepared from a mixed metal solution containing only chloride salts as Bouzaid and Frost [34] used magnesium nitrate as a source of the divalent cation. This difference may prove useful if nitrate adsorption by stichtite is to be investigated.

4.3. Characterisation of Synthetic Stichtite by Powder X-ray Diffraction

X-ray diffraction patterns were collected using a Philips X'pert wide angle X-Ray diffractometer, with Cu Kα radiation (1.54052 Å). Crystallographic

work on samples of natural stichtite were carried out by Frondel [85] in 1941 and was recently reinterpreted by Bookin et. al. [46] and Mills et. al [74]. It is important to note that these experiments have been carried out using natural samples of the mineral obtained from varying sources. As previously mentioned stichtite is rarely found in high purity in nature meaning that natural samples will contain different impurities and likely exhibit different crystallinity to synthetically prepared samples. These factors may be evident in the diffraction patterns of the materials

The powder XRD pattern shown in Figure. 4.1 revealed a characteristic LDH structure that corresponded well to the accepted reference pattern of stichtite (00-001-0993). Peaks in the XRD pattern were very broad and of low intensity indicating poor crystallinity or distortion of the LDH structure. It has been previously established that natural stichtite has low crystallinity and is often amorphous in nature. It is therefore not surprising that synthetic stichtite prepared with relatively short time for crystallite growth would exhibit similar properties [71]. Other more crystalline phases observed in the sample were attributed to impurities. These included: sodium chloride, sodium carbonate and sodium carbonate hydrate. All these impurities were expected by-products of the method of synthesis that if desired, could be removed through simple repeated washing with dilute sodium carbonate solution and deionised water. As the preliminary samples were prepared to test the suitability of the synthetic method proposed and not required for any future experiments, it was decided to by-pass the washing step as it was un-necessary. Finally, the d_{003} spacing of the sample was also investigated and

found to be 8.41Å which is within the acceptable region for a LDH structure.

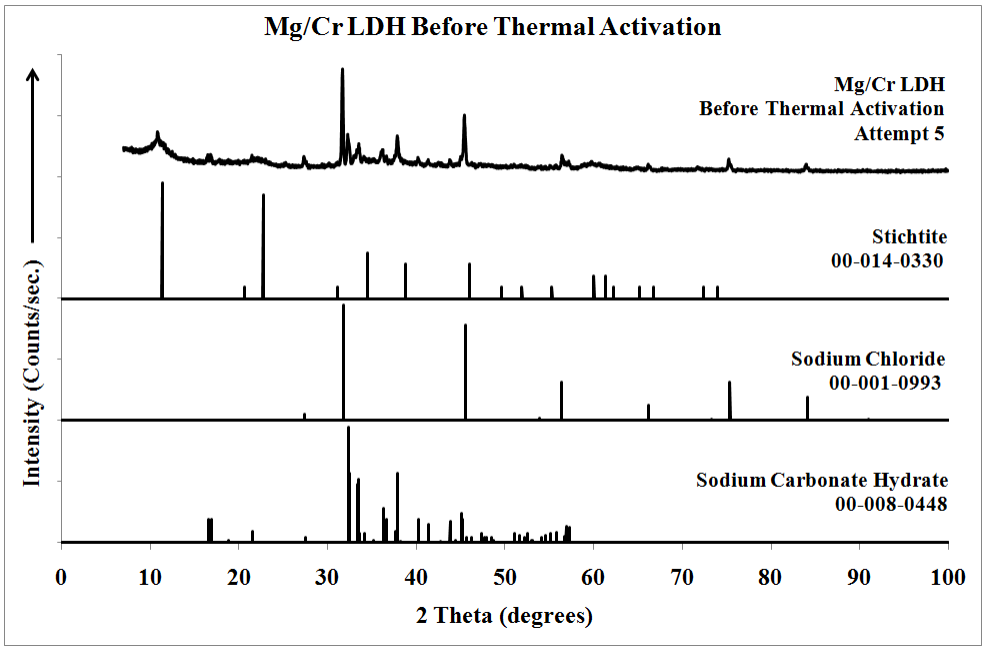

Figure. 4.1: Powder XRD of synthetic stichtite

4.4. Characterisation of Synthetic Stichtite by Thermal Analysis

Thermogravimetric analysis was performed using a TA® Instrument incorporated high resolution thermogravimetric analyser (series Q500) under a flowing nitrogen atmosphere (40mL/min). The samples were placed in an open platinum pan and heated from room temperature at a rate of 2.5°C/min to a maximum temperature of 1000°C. TG and DTG curves were obtained for all samples. Evolved gas mass spectrometry was used for a sample of the synthetic stichtite by coupling the Q500 thermogravimetric analyser to a Balzers (Pfeiffer) mass spectrometer. Only selected gases were investigated including CO_2 (m/Z = 44), C (m/Z = 12), O (m/Z = 16) OH

(m/Z = 17) and H_2O (m/Z = 18). The mass spectrometer was unfortunately only available for one sample.

TG results will be compared with those obtained by Bouzaid and Frost in 2007 [34] as they appear to have carried out the only other investigation reported in literature on the thermal decomposition of synthetic stichtite. To our knowledge, no studies have ever been reported on the thermal decomposition of natural stichtite.

Three mass losses were observed during the thermal decomposition of synthetic stichtite (Figure. 4.2). The first mass loss occurred at 51°C and accounted for 18.61% of the total mass lost. The corresponding peak in the DTG curve appears to have a small shoulder on the right side suggesting that two decomposition reactions are occurring almost simultaneously. It is difficult to identify this mass loss without the results of the evolved gas analysis (discussed later in this section), which identifies that H_2O, OH and small amounts of C are lost in this temperature region. This indicated the mass loss is likely due to the removal of adsorbed water. The shoulder on the peak in the DTG curve as well as the absence of a higher temperature feature around 100-200°C may indicate that removal of interlayer water is also occurring. However, if this is the case, the temperature is lower than expected for removal of interlayer water, which is usually over 100°C. The presence of carbon at this temperature is also difficult to explain, as the temperature is too low for removal of interlayer carbonate anions to occur.

The carbon is most likely due to the decomposition of some impurity present in the sample.

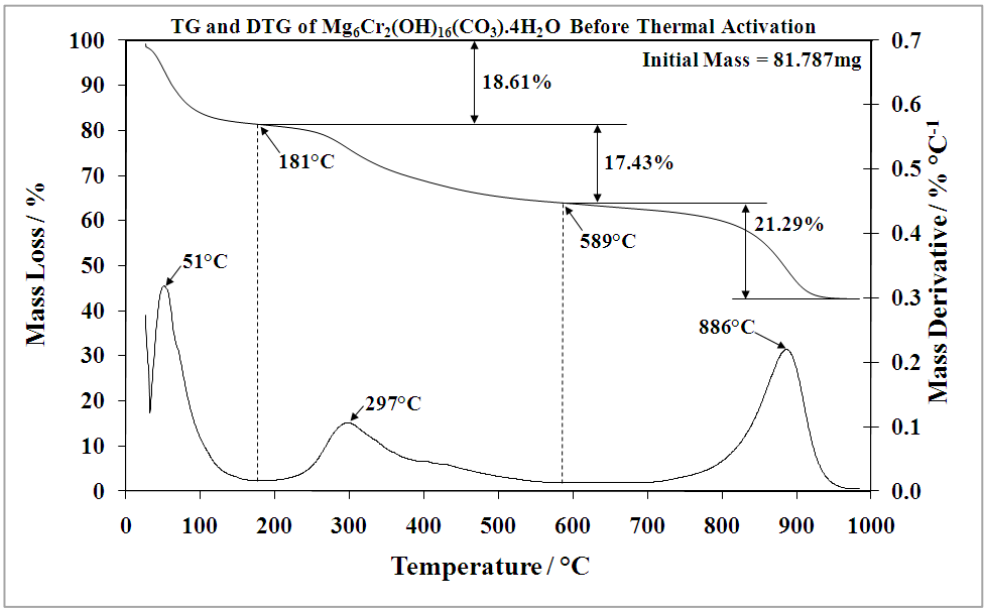

Figure. 4.2: Thermogravametric analysis of synthetic stichtite prepared by the co-precipitation method

The second mass loss occurred at 297°C accounting for 17.43% mass loss. Again, the DTG curve shows a shoulder on the right side of the corresponding peak. It was also difficult to assign this mass loss without looking at the results of the evolved gas mass spectrometry. In this sample H_2O, OH, and O are lost at around 300°C along with small amounts of CO_2 and C. The majority of CO_2 and C loss as well as the loss of O, appears to occur at higher temperatures of around 400°C which corresponds well to the shoulder on the peak seen in the DTG curve. This mass loss can be attributed to dehydroxylation and decarbonation as this is the only mass loss that occurs in the expected temperature region. Removal of interlayer water

may also be occurring at this point, however, it is not possible to confirm this using the available data.

The final mass loss occurred at 886°C. This was the largest mass loss observed accounting for 21.29% of total mass lost. The largest mass loss during thermal decomposition is usually attributed to dehydroxylation and removal of interlayer anions, however, the temperature of this feature is unusually high for the decomposition of a typical LDH. This feature must therefore be attributed to the presence of an impurity that has not yet been identified.

Evolved gas mass spectrometry was performed to provide additional information on the composition of the LDH and results are presented in Figure. 4.3. The following gases were observed during the decomposition of the LDH: OH (m/Z=17), H_2O (m/Z=18), O (m/Z=16), C (m/Z=12) and CO_2 (m/Z=44). Water and hydroxide lost from the sample at 63°C is attributed to the loss of interlayer water. A small shoulder on this peak is observed at lower tempratures and can be attributed to the removal of weakly adsorbed water. A second and final loss of water is observed at 312°C and is attributed to dehydroxylation. No water is lost beyond 500°C. Carbon dioxide is lost over a broad region around 383°C, with two distinct peaks at 325 and 383°C. This may indicate at least two distinct forms of carbon dioxide. Mass losses above 600°C can be attributed to the loss of carbon dioxide that is likely resulting from the decomposition of impurities in the sample.

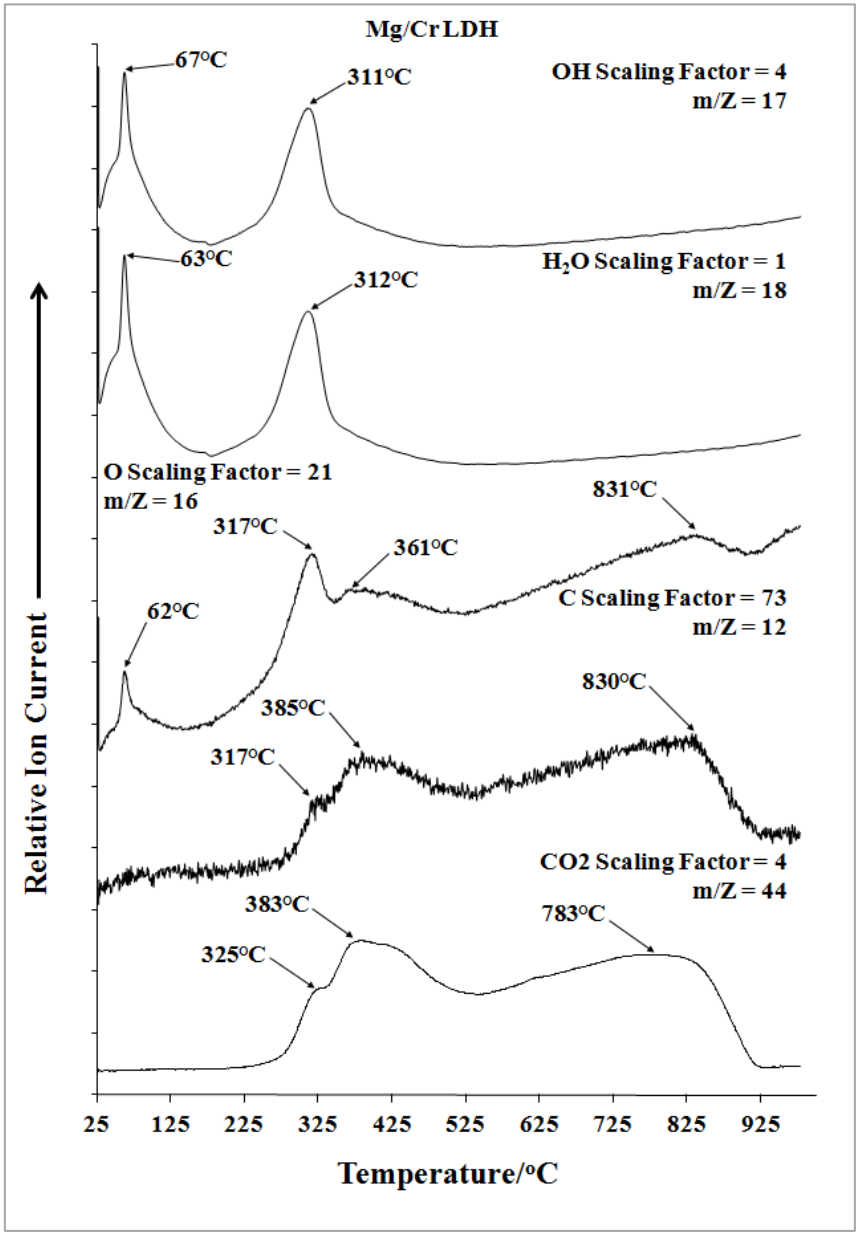

Figure. 4.3: Evolved gas analysis of synthetic stichtite prepared by the co-precipitation method

Thermogravimetric analysis was repeated using a sample prepared by almost the same method (described below) as the previous sample (Figure. 4.4). This time it was possible to separate some of the features seen in the previous TG pattern. This time four identifiable mass loss steps in the region between 50 and 1000°C were observed. The first mass loss occurred at 57

with a shoulder at 73°C. This feature accounted for 10.97% of the total mass lost. The two peaks in this region suggest that two types of water are being removed. This feature can be attributed to the removal of water weakly adsorbed to the surface of the LDH and possibly interlayer water as well. Again, this mass occurs at a temperature lower than would be expected for the removal of interlayer water.

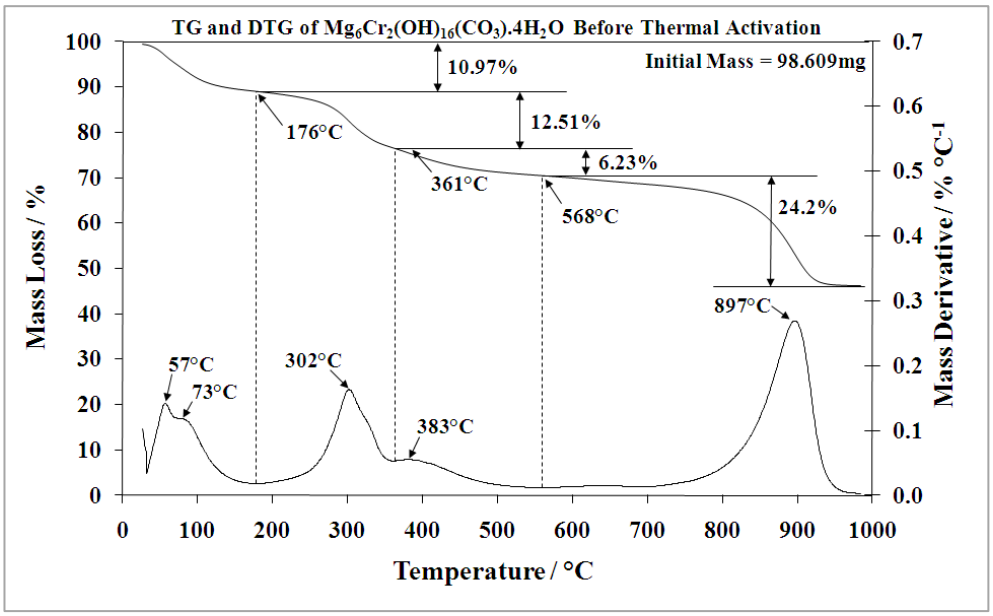

Figure. 4.4: Thermogravametric analysis of synthetic stichtite prepared by the co-precipitation method with 2 hours stirring after addition of the caustic solution

Unlike the previous TG pattern it was possible to separate the next mass loss into two and identify the temperatures at which they occur. The second mass loss occurring at 302°C accounted for 12.51% of the total mass loss. Mass losses in this region can usually be attributed to loss of interlayer anions and dehydroxylation. Evolved gas analysis from the previous sample suggests that dehydroxylation and possibly removal of interlayer water occurs at 302°C. If this is the case, the mass loss observed at 383°C, that accounts for

6.23% of the total mass loss, must correspond to decarbonation of the LDH. The final and largest mass loss occurred at 897°C and accounted for 24.2%. This was again attributed to the presence of an impurity and not investigated further due to time constraints.

Our results only differ slightly from those observed by Bouzaid and Frost [34]. The most obvious difference is the absence of features above 700°C, which have already been attributed to the presence of impurities.

4.5. Effect of Stirring Time on the Product

The synthesis was repeated using a method similar to the one described above in an attempt to determine the effect of stirring time on the quality of the product. It was hypothesised that this variable would have little impact on the quality of the final product, however, after several failed attempts to prepare synthetic stichtite it was decided to investigate this variable to eliminate it from further work. Approximately one third of the mixture was removed 2 hours after completion of the addition of caustic solution. A second third was removed after 24 hours and the remaining mixture was removed after 48 hours. Again, the LDH was separated by vacuum filtration before drying in an oven. All three samples were characterised by powder XRD. The 2 and 24 hour samples were also characterised by thermal analysis (described above).

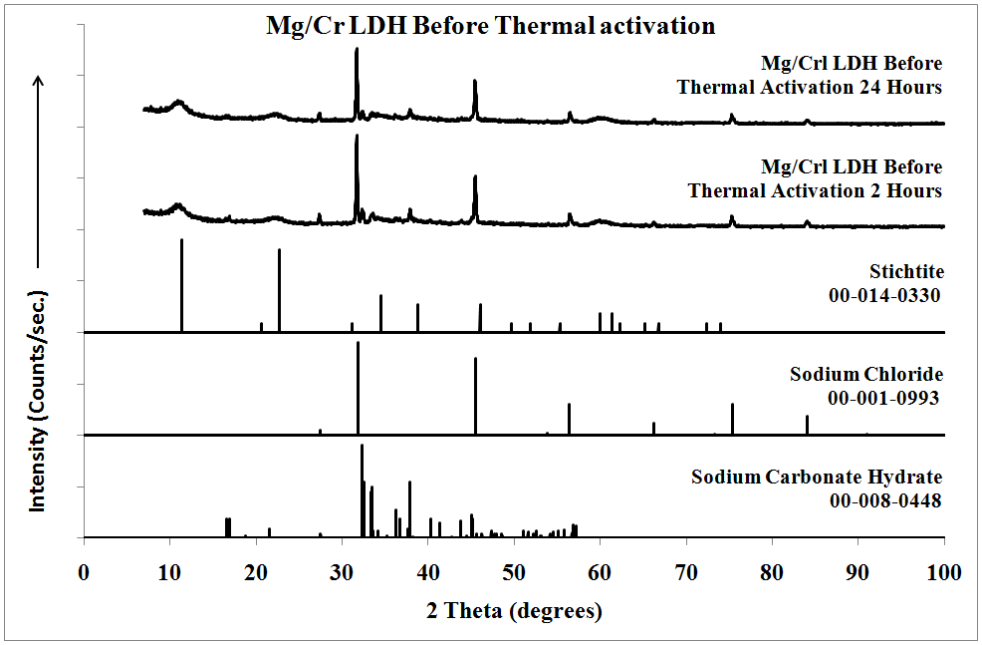

Figure. 4.5: Comparison of powder XRD of synthetic stichtite with 2 and 24 hours stirring after addition of the caustic solution

Powder XRD (shown in Figure. 4.5 and 4.6) revealed no significant difference between the 2, 24 and 48 hour samples. A slight difference in peaks in the region between 30 and 40 2θ° of the 48 hour sample when compared to the others was observed. This difference was attributed to the presence of sodium carbonate instead of sodium carbonate hydrate. This is not unexpected as the 48 hour sample was dried for longer than the other two. The d_{003} spacing for the samples are 8.04, 7.94 and 7.96Å for the 2, 24 and 48 hour samples respectively. No significant change in the d_{003} was observed as a result of changes in stirring time. This experiment is not however conclusive as powder XRD provides the average interlayer spacing. To conclusively determine whether or not stirring time affects interlayer spacing, transmission electron microscopy (TEM) must be used to examine the layers more closely.

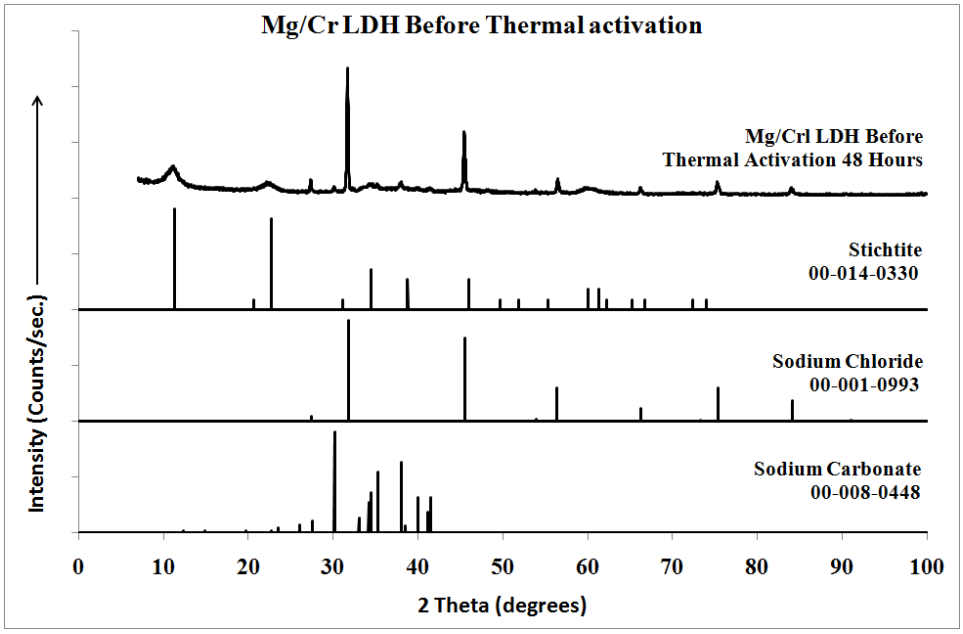

Figure. 4.6: Powder XRD of synthetic stichtite with 48 hours stirring after addition of the caustic solution

As previously mentioned, no significant change in the thermal analysis results were observed between the 2 and 24 hour samples. From these results, it is possible to conclude that synthetic stichtite can be prepared to the same quality using a mixing time as short as 2 hours rather than waiting 24 hours. It is therefore possible to eliminate this as a variable in future experiments.

4.6. Conclusions

Stichtite has been successfully prepared from magnesium chloride hexahydrate and chromium chloride hexahydrate using the co-precipitation method. The first attempt at synthesis resulted in an amorphous blue/grey precipitate that could not be identified by powder XRD. The synthesis was successfully achieved by preparing fresh caustic solution with a higher concentration of sodium carbonate (2 mol/L). The reason for the change in

experimental conditions is not yet understood. Powder XRD and thermal analysis show that the synthesised stichtite contains impurities. Visual inspection showed a lighter blue/grey coloured material in some samples. This suggests that some of the unidentified blue/grey precipitate may have still formed during synthesis. The low crystalinity may also be an indicator that incomplete synthesis of stichtite has occurred. It is clear that the blue/grey precipitate must be identified so that it can be removed from the sample.

The powder XRD pattern of the synthesised stichtite corresponded to the accepted reference pattern of stichtite (00-001-0993). The material did however contain numerous impurities including sodium chloride and sodium carbonate hydrate. No attempt was made to remove any impurities from the products of this synthesis as there was not sufficient time to investigate any applications of the synthetic stichtite. Furthermore it would be difficult to remove impurities that could not be identified by the characterisation techniques used. The material also appeared to exhibit poor crystalinity, showing only broad peaks of low intensity that corresponded to the reference pattern. The d_{003} spacing was found to be 8.41Å, which is acceptable for a LDH structure. Powder XRD has shown that the product produced by the current co-precipitation synthesis is not of a sufficient quality to investigate new applications for the mineral stichtite. Better control of the pH during co-precipitation and ageing of the LDH in its mother liquor at elevated temperatures may help optimise the quality and yield of the product.

Thermal analysis showed that the decomposition of the synthesised stichtite could be adequately described by a mechanism previously reported in literature, [34] although, slight differences were observed in the temperatures at which they occurred. The thermal decomposition of stichtite appears to occur through four steps. Firstly, removal of adsorbed water occurs at approximately 60-70°C. This is followed by the removal of interlayer water around 300°C. Dehydroxylation also appears to occur around 300°C with decarbonation occurring at a slightly higher temperature, (350-400°C). This mechanism confirmed by the results of evolved gas mass spectrometry which identified the decomposition steps based on the gases evolved. Considerable work is still needed before useful applications for the mineral stichtite can be found. This work has however reviewed previously published literature (which does not appear to have been done since 1914) and confirmed a number of findings. This project will provide a sound footing for future work on stichtite.

Chapter 5:
Overall Conclusions.

Chapter 5: Overall Conclusions

Selected Mg, Zn and Cr layered double hydroxides were successfully prepared using variations of the co-precipitation method. All synthesised materials were characterised using powder X-ray diffraction and thermogravimetric analysis.

Thermal activation and the reformation effect were investigated using a Mg/Al layered double hydroxide with a molar ratio of 3:1. The characteristic powder XRD pattern of the LDH was destroyed after thermal activation at 380°C. The powder XRD pattern of the thermally activated LDH appeared to contain a number of Mg and Al oxides. Samples of the thermally activated LDH were treated with sulfate, nitrate and fluoride solutions. In all three cases a LDH structure similar to that of the original material was re-formed. The observed $d_{(003)}$ spacing of all samples was almost similar with the only increase occurring in the sample treated with nitrate solution. This may indicate that the sulfate and fluoride anions were adsorbed onto the surface rather than intercalated into the interlayer of the LDH. Thermogravametric analysis revealed that all samples investigated appeared to decompose through a similar mechanism involving four steps. Firstly, weakly adsorbed surface water was removed. Next, interlayer water is removed. The final steps are dehydroxylation and the removal of the interlayer anions, which appear to occur almost simultaneously.

A Zn/Al LDH with a molar ratio of 3:1 was investigated as a potential adsorbent for the removal of iodine species from water. To the candidate's

knowledge, this is the first time iodine removal has been attempted using a Zn/Al LDH. Successful anion sorption was achieved using batch processes with relatively short mixing times. No attempt was made to prevent competitive adsorption of carbonate from the water or atmosphere. Removal of iodide from a solution was 36.8%, however, a 99.5% removal of iodine (prepared by the reaction of potassium iodate and potassium iodide under acidic conditions) was observed under similar experimental conditions. Analysis of the mass losses observed during thermal analysis combined with the results of the evolved gas mass spectrometry indicates that the Zn/Al LDH treated with iodide (I^-) solution does not appear to release any of the iodine species investigated during thermal decomposition at temperatures below 1000°C. However, under the same experimental conditions a sample of the Zn/Al LDH treated with iodine solution (I_2) appeared to evolve a gas with m/z = 127, which may correspond to elemental iodine. The candidate is unable to provide a mechanism to explain the thermal decomposition of these samples at this time. Zn/Al LDHs show promise for the removal of harmful iodine species from water, however, more research is still required.

Attempts have been made to prepare a synthetic equivalent to the naturally occurring mineral stichtite (a Mg/Cr LDH with a cationic ratio of 3:1). Stichtite was successfully prepared using the co-precipitation method from magnesium(II) chloride hexahydrate and chromium(III) chloride hexahydrate. Samples were characterised by powder XRD and thermogravametric analysis coupled with evolved gas mass spectrometry.

Unfortunately, due to the unexpected complexity of developing a method for synthesis of the Mg/Cr no new applications for the mineral stichtite can be proposed at this time.

Chapter Six:

References

6. References

1. Lin, Y.-H., et al., *Thermogravimetric analysis of hydrotalcites based on the takovite formula $Ni_xZn_{6-x}Al_2(OH)_{16}(CO_3).4H_2O$.* J. Therm. Anal. Calorim., 2005. **81**: p. 83-89.
2. Rives, V. and Editor, *Layered Double Hydroxides: Present and Future*2001, New York: Nova Science Pub Inc 439 pp.
3. Rives, V., *Characterisation of layered double hydroxides and their decomposition products* Materials Chemistry and Physics, 2002. **75**: p. 19-25.
4. Tong, D.S., et al., *Structure and catalytic properties of Sn-containing layered double hydroxides synthesized in the presence of dodecylsulfate and dodecylamine.* Applied Clay Science, 2010. **48**: p. 569-574.
5. Theo Kloprogge, J. and R.L. Frost, *Infrared emission spectroscopic study of the thermal transformation of Mg-, Ni- and Co-hydrotalcite catalysts.* Appl. Catal., A, 1999. **184**(1): p. 61-71.
6. Theo Kloprogge, J. and R.L. Frost, *Infrared emission spectroscopic study of the dehydroxylation of synthetic Mg/Al and Mg/Zn/Al-hydrotalcites.* Physical Chemistry Chemical Physics 1999. **1**(7): p. 1641-1647.
7. Tao, Q., et al., *Synthesis and infrared spectroscopic characterization of selected layered double hydroxides containing divalent Ni and Co.* Mater. Chem. Phys., 2008. **112**(3): p. 869-875.
8. Spratt, H.J., S.J. Palmer, and R.L. Frost, *Thermal decomposition of synthesised layered double hydroxides based upon Mg/(Fe,Cr) and carbonate.* Thermochim. Acta, 2008. **479**(1-2): p. 1-6.
9. Rives, V., *Layered double hydroxides with the hydrotalcite-type structure containing Cu2+, Ni2+ and Al3+*. The Journal of the Royal Society of Chemistry 1999. **10**: p. 489-495.
10. Lin, Y.-H., et al., *Thermogravimetric analysis of hydrotalcites based on the takovite formula NixZn6-xAl2(OH)16(CO3)·4H2O.* J. Therm. Anal. Calorim., 2005. **81**(1): p. 83-89.
11. Lakshmi Reddy, S., et al., *Optical absorption, infrared, Raman, and EPR spectral studies on natural iowaite mineral.* Transition Met. Chem. (Dordrecht, Neth.), 2010. **35**(3): p. 331-336.
12. Kloprogge, J.T., et al., *Intercalation of iron hexacyano complexes in Zn,Al hydrotalcite. Part 2. A mid-infrared and Raman spectroscopic study.* J. Solid State Chem., 2004. **177**(4-5): p. 1382-1387.
13. Kloprogge, J.T., L. Hickey, and R.L. Frost, *The effect of varying synthesis conditions on zinc chromium hydrotalcite: a spectroscopic study.* Mater. Chem. Phys., 2005. **89**(1): p. 99-109.
14. Kloprogge, J.T., L. Hickey, and R.L. Frost, *The effects of synthesis pH and hydrothermal treatment on the formation of zinc aluminum hydrotalcites.* J. Solid State Chem., 2004. **177**(11): p. 4047-4057.
15. Kloprogge, J.T., L. Hickey, and R.L. Frost, *FT-Raman and FT-IR spectroscopic study of synthetic Mg/Zn/Al-hydrotalcites.* J. Raman Spectrosc., 2004. **35**(11): p. 967-974.

16. Kloprogge, J.T. and R.L. Frost, *Fourier Transform Infrared and Raman Spectroscopic Study of the Local Structure of Mg-, Ni-, and Co-Hydrotalcites.* J. Solid State Chem., 1999. **146**(2): p. 506-515.
17. Johnson, T.E., et al., *Structured water in hydrotalcites of formula MgxZn6-xAl2(OH)16(CO3)·4H2O: a Raman microscopic study.* J. Raman Spectrosc., 2002. **33**(8): p. 604-609.
18. Grand, L.-M., S.J. Palmer, and R.L. Frost, *Synthesis and thermal stability of hydrotalcites based upon gallium.* J. Therm. Anal. Calorim., 2010. **101**(1): p. 195-198.
19. Grand, L.-M., S.J. Palmer, and R.L. Frost, *Synthesis and thermal stability of hydrotalcites containing gallium.* J. Therm. Anal. Calorim., 2009.
20. Grand, L.-M., S.J. Palmer, and R.L. Frost, *Synthesis and thermal stability of hydrotalcites containing manganese.* J. Therm. Anal. Calorim., 2009.
21. Frost, R.L., et al., *Thermal decomposition of the natural hydrotalcites carrboydite and hydrohonessite.* Thermochim. Acta, 2003. **407**(1-2): p. 1-9.
22. Frost, R.L., et al., *Infrared spectroscopic study of natural hydrotalcites carrboydite and hydrohonessite.* Spectrochim. Acta, Part A, 2003. **59A**(14): p. 3313-3319.
23. Frost, R.L., et al., *Thermo-Raman spectroscopy of selected layered double hydroxides of formula Cu6Al2(OH)16CO3 and Zn6Al2(OH)16CO3.* J. Raman Spectrosc., 2009. **40**(6): p. 645-649.
24. Frost, R.L. and B.J. Reddy, *Thermo-Raman spectroscopic study of the natural layered double hydroxide manasseite.* Spectrochim. Acta, Part A, 2006. **65A**(3-4): p. 553-559.
25. Frost, R.L., S.J. Palmer, and L.-M. Grand, *Synthesis and thermal analysis of indium-based hydrotalcites of formula Mg6In2(CO3)(OH)16·4H2O.* J. Therm. Anal. Calorim., 2010. **101**(3): p. 859-863.
26. Frost, R.L., S.J. Palmer, and L.-M. Grand, *Raman spectroscopy of gallium-based hydrotalcites of formula Mg6Ga2(CO3)(OH)16· 4H2O.* J. Raman Spectrosc., 2010. **41**(7): p. 791-796.
27. Frost, R.L. and K.L. Erickson, *Decomposition of the synthetic hydrotalcites mountkeithite and honessite-a high resolution thermogravimetric analysis and infrared emission spectroscopic study.* Thermochim. Acta, 2004. **421**(1-2): p. 51-58.
28. Frost, R.L. and K.L. Erickson, *Thermal decomposition of natural iowaite.* J. Therm. Anal. Calorim., 2004. **78**(2): p. 367-373.
29. Frost, R.L., et al., *Thermal decomposition of the syenthetic hydrotalcite iowaite.* J. Therm. Anal. Calorim., 2006 **86**: p. 437-441.
30. Frost, R.L., J.M. Bouzaid, and W.N. Martens, *Thermal decomposition of the composite hydrotalcites of iowaite and woodallite.* J. Therm. Anal. Calorim., 2007. **89**(2): p. 511-519.
31. Frost, R.L., K.H. Bakon, and S.J. Palmer, *Raman spectroscopic study of synthetic reevesite and cobalt substituted reevesite (Ni,Co)6Fe2(OH)16(CO3)·4H2O.* J. Raman Spectrosc., 2010. **41**(1): p. 78-83.

32. Frost, R., et al., *Thermal decomposition of the syenthetic hydrotalcite woodallite* J. Therm. Anal. Calorim., 2006. **86**(2): p. 437-441.
33. Das, D.P., J. Das, and K. Parida, *Physicochemical characterization and adsorption behavior of calcined Zn/Al hydrotalcite-like compound (HTlc) towards removal of fluoride from aqueous solution.* Journal of Colloid and Interface Science, 2002. **261**: p. 213-220.
34. Bouzaid, J. and R.L. Frost, *Thermal decomposition of stichtite.* J. Therm. Anal. Calorim., 2007. **89**(1): p. 133-135.
35. Bakon, K.H., S.J. Palmer, and R.L. Frost, *Thermal analysis of synthetic reevesite and cobalt substituted reevesite (Ni,Co)6Fe2(OH)16(CO3) · 4H2O.* J. Therm. Anal. Calorim., 2010. **100**(1): p. 125-131.
36. Frost, R.L., S.J. Palmer, and H.J. Spratt, *Thermal decomposition of hydrotalcites with variable cationic ratios.* J. Therm. Anal. Calorim., 2009. **95(1)**: p. 123-129.
37. Miyata, S., *Anion Exchange Properties of Hydrotalcite-like Compounds* Clays and Clay Minerals, 1983. **31**(4): p. 305-311.
38. Palmer Sara, J., A. Soisonard, and L. Frost Ray, *Determination of the mechanism(s) for the inclusion of arsenate, vanadate, or molybdate anions into hydrotalcites with variable cationic ratio.* J Colloid Interface Sci, 2009. **329**(2): p. 404-9.
39. Erickson, K.L., T.E. Bostrom, and R.L. Frost, *A study of structural memory effects in synthetic hydrotalcites using environmental SEM.* Mater. Lett., 2004. **59**(2-3): p. 226-229.
40. Lv, L., et al., *Factors influencing the removal of fluoride from aqueous solution by calcined Mg-Al-CO3 layered double hydroxides.* J. Hazard. Mater., 2006. **133**(1-3): p. 119-128.
41. Wang, H., et al., *Defluoridation of drinking water by Mg/Al hydrotalcite-like compounds and their calcined products.* Applied clay science, 2007. **35**(1-2): p. 59-66.
42. Othman, M.R., et al., *Synthetic hydrotalcites from different routes and their application as catalysts and gas adsorbents: a review.* Applied Organometallic Chemistry, 2009. **23**(9): p. 335-346.
43. Olfs, H.W., et al., *Comparison of different synthesis routes for Mg-Al layered double hydroxides (LDH): Characterization of the structural phases and anion exchange properties.* Applied clay science, 2009. **43**(3-4): p. 459-464.
44. Duan, X. and D.G. Evans, *Layered Double Hydroxides*2006: Springer.
45. Mills, S.J., et al., *The crystal structure of stichtite, re-examination of barbertonite, and the nature of polytypism in MgCr hydrotalcites.* Am. Mineral., 2011. **96**: p. 179-187.
46. Bookin, Cherkashin, and Drits, *Reinterpretation of the x-ray diffraction Patterns of Stichtite and Reevesite.* Clays Clay Min., 1993. **41**(5): p. 631-634.
47. Willard, H.H., et al., eds. *Instrumental methods of analysis*. seventh edition ed., ed. J. Carey1988, Wadsworth inc Belmont California. 895.

48. Brown, M.E., *Introduction to thermal analysis techniques and applications* 1988, Chapman and Hall New York
49. Lin, Y.-H., et al., *Thermogravimetric analysis of hydrotalcites based on the takovite formula* $Ni_xZn_{6-x}Al_2(OH)_{16}(CO_3).4H_20$. journal of thermal analysis and calorimetry, 2005. **81**: p. 83-89.
50. Organization, W.H., *Guidelines for Drinking-water Quality*. Third ed, ed. W.H. Organization. Vol. 1. 2008, Geneva: WHO Press, World Health Organization, 20 Avenue Appia, 1211 Geneva 27, Switzerland.
51. Fawell, J., et al., *Fluoride in Drinking-water*2006: Published on behalf of the World Health Organization by IWA Publishing, Alliance House, 12 Caxton Street, London SW1H 0QS, UK.
52. Frost, R.L. and A.W. Musumeci, *Nitrate absorption through hydrotalcite reformation.* J. Colloid Interface Sci., 2006. **302**(1): p. 203-206.
53. Das, J., et al., *Adsorption of phosphate by layered double hydroxides in aqueous solutions.* Applied clay science, 2006. **32**(3-4): p. 252-260.
54. Cordell, D., J.-O. Drangert, and S. White, *The story of phospherous: Global food security and food for thought.* Global Environ. Change 2009. **19**(2): p. 292-305.
55. Dawson, C.J. and J. Hilton, *Fertiliser availability in a resource-limited world: Production and recycling of nitrogen and phosphorus.* Food Policy, 2011. **36**(Supplement 1): p. S14-S22.
56. Seida, Y. and Y. Nakano, *Removal of phosphate by layered double hydroxides containing iron.* Water Res., 2002. **36**(5): p. 1306-1312.
57. Triantafyllidis, K.S., et al., *Iron-modified hydrotalcite-like materials as highly efficient phosphate sorbents.* journal of colloid and interface science, 2010. **342**(2): p. 427-436.
58. Węgrzyn, A., et al., *The influence of mixed anionic composition of Mg-Al hydrotalcites on the thermal decomposition mechanism based on in situ study.* J. Therm. Anal. Calorim., 2010. **99**(2): p. 443-457.
59. Kloprogge, J.T. and R.L. Frost, *Introduction to syntheses and uses of hydrotalcites.* Tijdschr. Klei, Glas Keram., 2000. **21**(3): p. 7-11, 27.
60. Chitrakar, R., et al., *A New Method for Synthesis of Mg-Al, Mg-Fe, and Zn-Al Layered Double Hydroxides and Their Uptake Properties of Bromide Ion.* Ind. Eng. Chem. Res., 2008. **47**(14): p. 4905-4908.
61. Ay, A.N., B. Zumreoglu-Karan, and L. Mafra, *A simple mechanochemical route to layered double hydroxides: synthesis of hydrotalcite-like Mg-Al-NO3-LDH by manual grinding in a mortar.* Journal of Inorganic and General Chemistry 2009(635): p. 1470-1475.
62. Theiss, F., et al., *Sulfate intercalated layered double hydroxides prepared by the reformation effect.* Journal of thermal analysis and calorimetry, 2011: p. 1-6.
63. Lopez, T., et al., *DTA and TGA characterisation of sol-gel hydrotalcites.* Materials Letters 1997. **30**: p. 279-282.
64. Liang, L. and L. Li, *Adsorption behavior of calcined layered double hydroxides towards removal of iodide contaminants.* J. Radioanal. Nucl. Chem., 2006. **273**(1): p. 221-226.

65. Fetter, G., et al., *Sorption of ^{131}I by hydrotalcites.* J. Radioanal. Nucl. Chem., 1997. **221**: p. 63-66.
66. Kulyukhin, S.A., et al., *Sorption of radioiodine from aqueous solutions on layered double magneisum aluminum hydroxides at 300 K.* Radiochemistry 2007. **49**(5): p. 499-503.
67. Lv, L., et al., *Removal of chloride ion from aqueous solution by ZnAl-NO3 layered double hydroxides as anion-exchanger.* J. Hazard. Mater., 2009. **161**(2-3): p. 1444-1449.
68. Frost, R.L., W.N. Martens, and K.L. Erickson, *Thermal decomposition of the hydrotalcite.* J. Therm. Anal. Calorim., 2005. **82**: p. 603-608.
69. Theiss, F.L., et al., *Zinc Aluminium Layered Double Hydroxides for the Removal of Iodine and Iodide from Aqueous Solutions.* Desalination and Water Treatment, 2011. **Accepted for Publication 14 September 2011**
70. Harris, D.C., *Quantitative chemical analysis*. seventh ed2007, NY 10010: W. H Freeman and company 14 Madison avenue Naw York.
71. Twelvetrees, W.H., *Stichtite A New Tasmanian Mineral*, 1914, Tasmania Department of Mines: Hobart.
72. Frost, R.L. and K.L. Erickson, *Vibrational spectroscopy of stichtite.* Spectrochim Acta A Mol Biomol Spectrosc, 2004. **60**(13): p. 3001-3005.
73. Ashwal, L.D. and B. Cairncross, *Mineralogy and origin of stichtite in chromite-bearing serpentinites.* Contributions to Mineralogy and Petrology, 1997. **127**(1): p. 75-86.
74. Mills, S.J., et al., *The crystal structure of stichtite, re-examination of barbertonite, and the nature of polytypism in MgCr hydrotalcites.* Am. Mineral., 2011. **96**(1): p. 179-187.
75. Badreddine, M., et al., *Ion exchange of different phosphate ions into the zinc-aluminium-chloride layered double hydroxide.* Mater. Lett., 1999. **38**(6): p. 391-395.
76. Chitrakar, R., et al., *Fe-Al layered double hydroxides in bromate reduction: Synthesis and reactivity.* J. Colloid Interface Sci., 2011. **354**(2): p. 798-803.
77. Fogg, A.M., et al., *A novel family of layered double hydroxides-[MAl4(OH)12](NO3)2·xH2O (M = Co, Ni, Cu, Zn).* J. Mater. Chem., 2004. **14**(15): p. 2369-2371.
78. Frost, R.L., M.O. Adebajo, and K.L. Erickson, *Raman spectroscopy of synthetic and natural iowaite.* Spectrochim. Acta, Part A, 2005. **61A**(4): p. 613-620.
79. Frost, R.L., S.J. Palmer, and L.-M. Grand, *Synthesis and thermal analysis of indium-based hydrotalcites of formula $Mg_6In_2(CO_3)(OH)_{16}.4H_2O$.* J. Therm. Anal. Calorim., 2010. **101**(3): p. 859-863.
80. Kloprogge, J.T., et al., *Characterization of Intercalated Ni/Al Hydrotalcites Prepared by the Partial Decomposition of Urea.* Cryst. Growth Des., 2006. **6**(6): p. 1533-1536.
81. Palmer, S.J., R.L. Frost, and H.J. Spratt, *Synthesis and Raman spectroscopic study of Mg/Al,Fe hydrotalcites with variable cationic ratios.* J. Raman Spectrosc., 2009. **40**(9): p. 1138-1143.

82. Chitrakar, R., et al., *Adsorption of phosphate from seawater on calcined MgMn-layered double hydroxides.* journal of colloid and interface science, 2005. **290**(1): p. 45-51.
83. Petterd, W.F., *Catalogue of the minerals of Tasmania / by W.F. Petterd*, ed. M. Tasmania. Dept. of1910, [Hobart] :: Mines Department.
84. Frost, R.L. and K.L. Erickson, *Near-infrared spectroscopy of stitchtite, iowaite, desautelsite and arsenate exchanged takovite and hydrotalcite.* Spectrochimica Acta Part A: Molecular and Biomolecular Spectroscopy, 2005. **61**(1-2): p. 51-56.
85. Frondel, C., *Constitution and Polymorphism of the Pyroaurite and Sjögerenite Groups.* The American Mineralogist, 1941. **26**(5): p. 295-315.

Chapter Seven:

Appendices

Appendix 1: Figures

Enlargements of all figures contained in this thesis are presented in Appendix 1 for the reader's convenience.

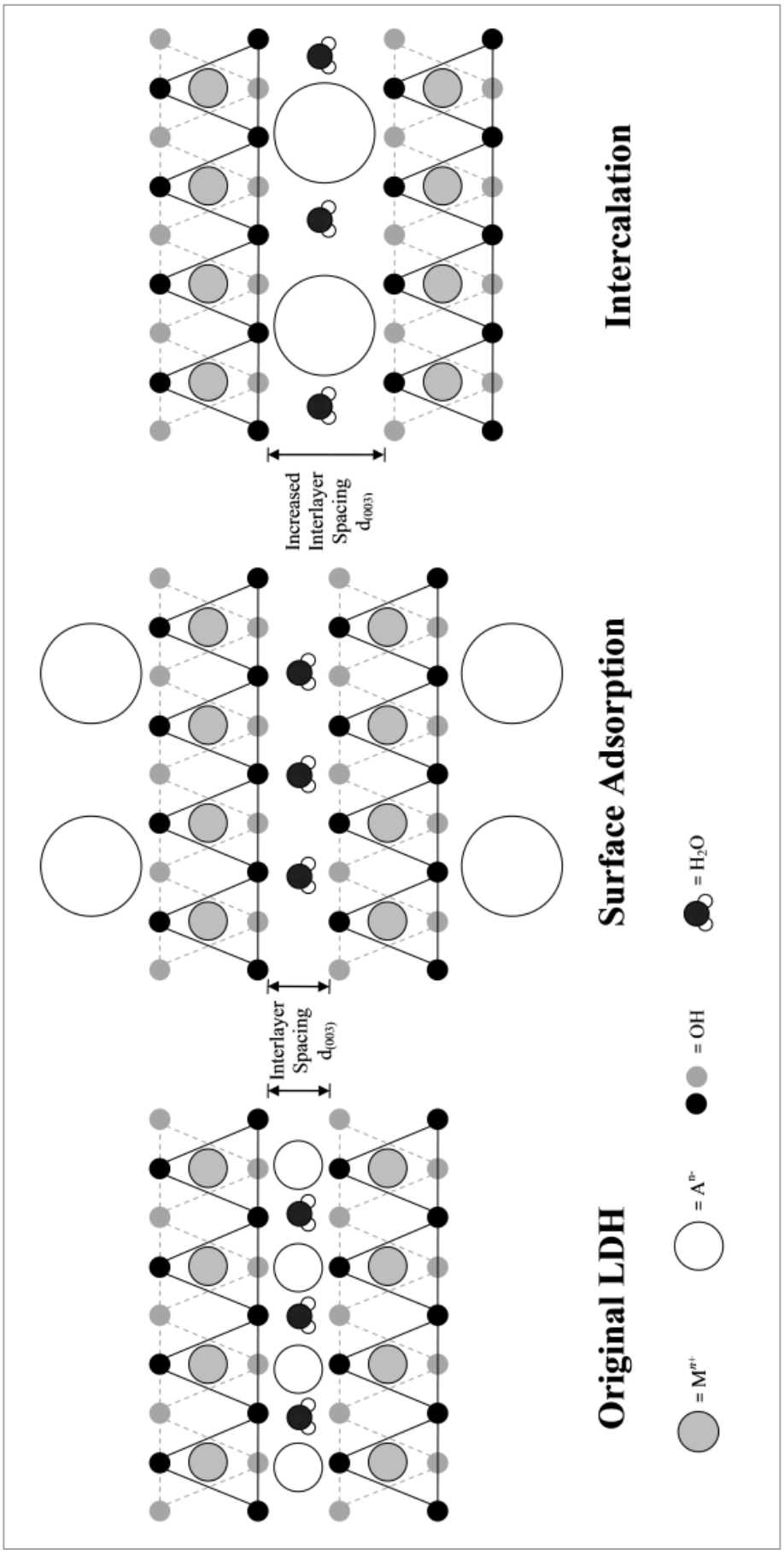

Figure. 1.1: Intercalation of anions in a LDH material.

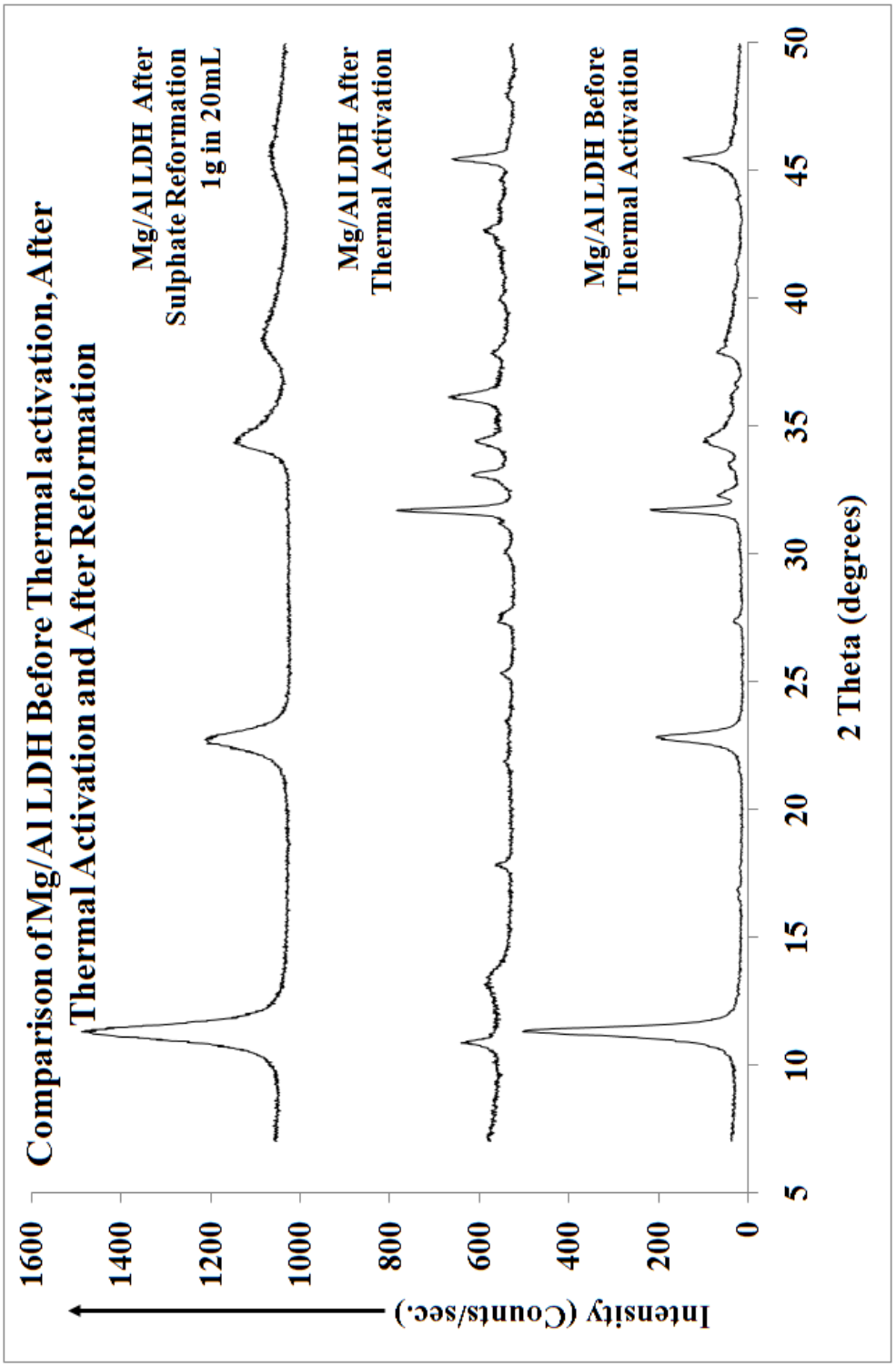

Figure. 1.2: Powder XRD pattern of Mg/Al LDH before thermal activation (Bottom), after thermal activation (middle) and reformation after treatment of 1g of Mg/Al LDH in 20mL of sodium sulfate solution (top).

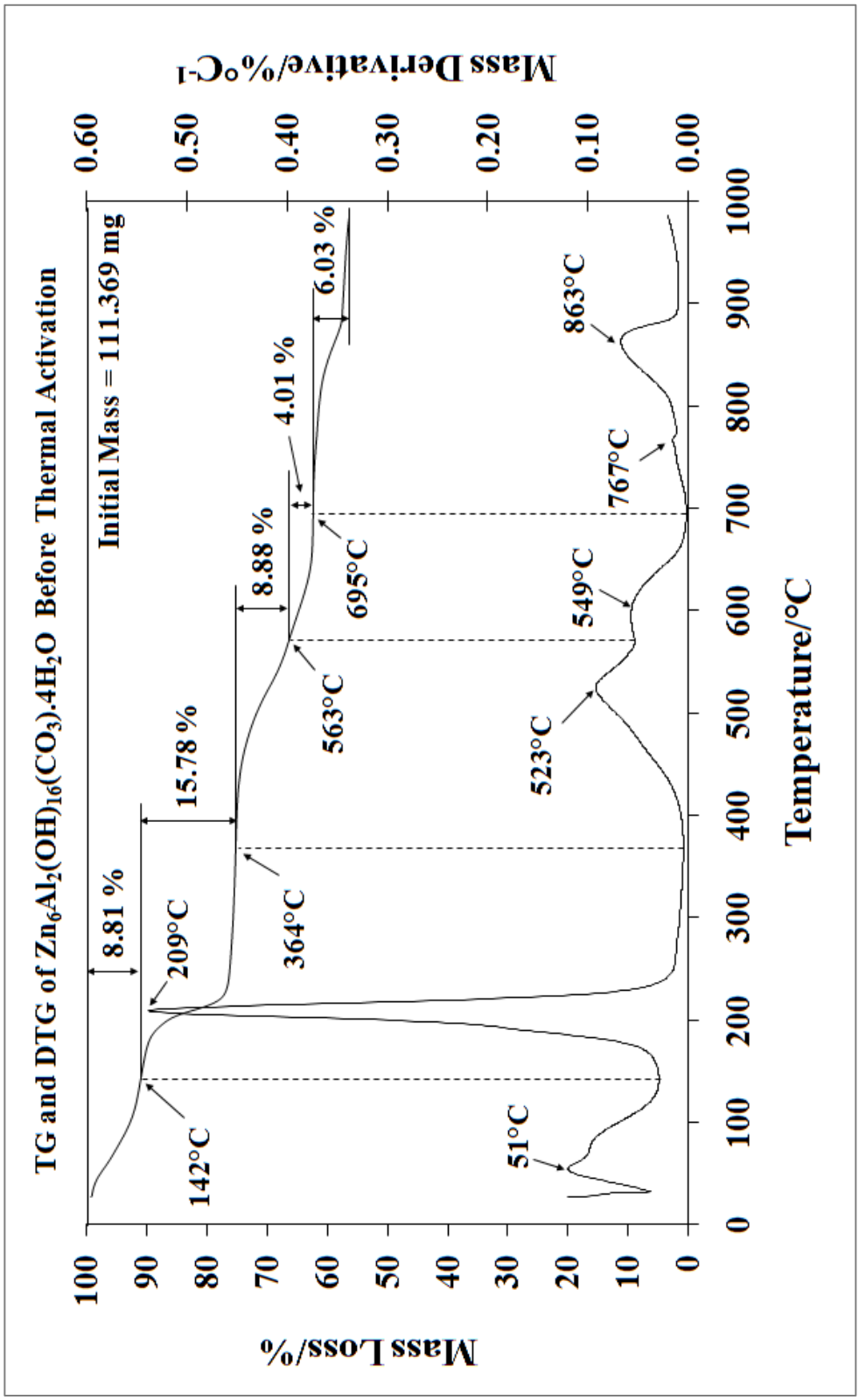

Figure. 1.3:TG and DTG curve for the thermal decomposition of a Zn/Al LDH.

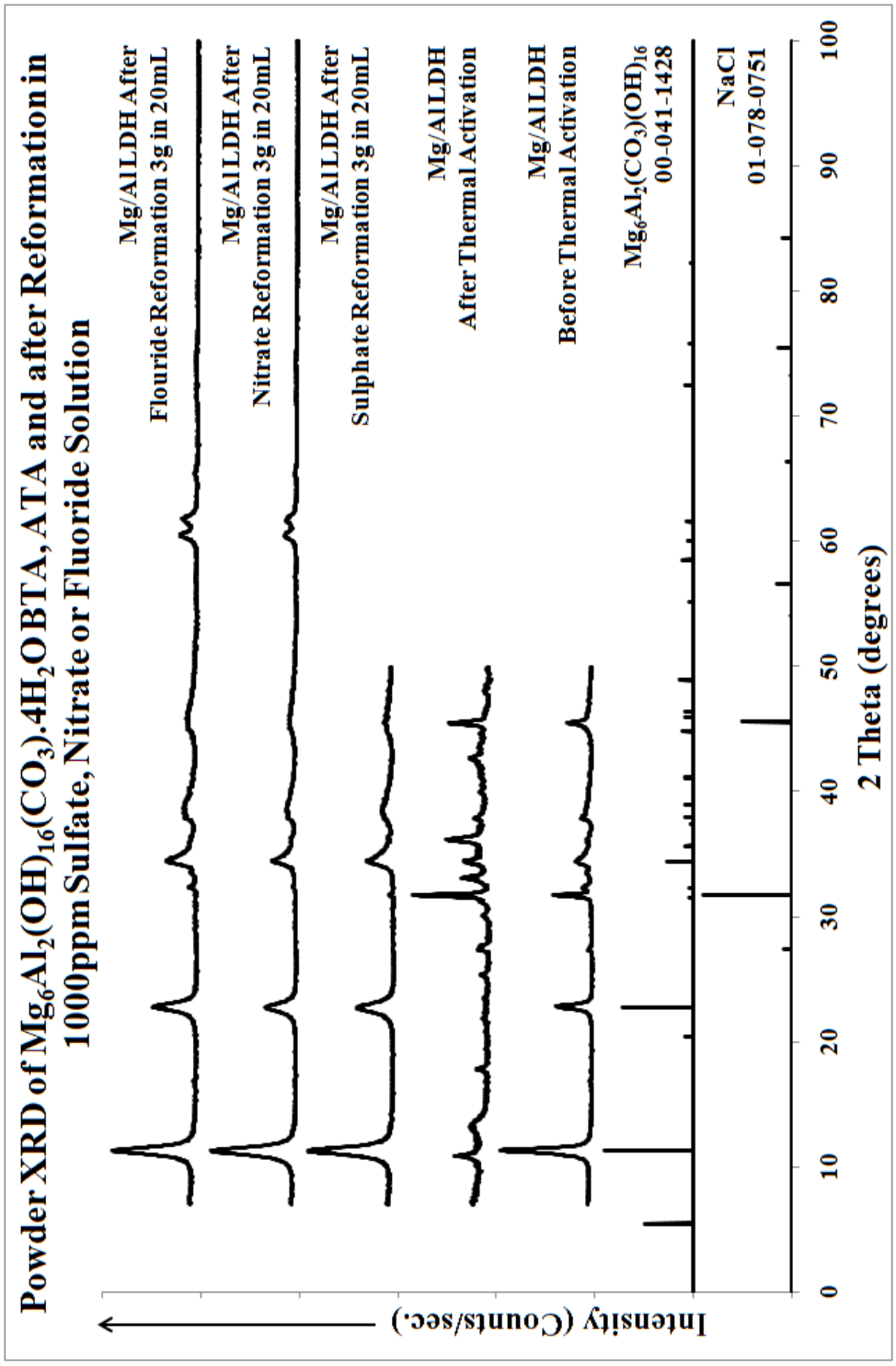

Figure. 2.1: XRD pattern of Mg/Al LDH before thermal activation, after treatment of 3g of Mg/Al LDH in 20cm3 of sodium sulfate, nitrate or fluoride solutions and references.

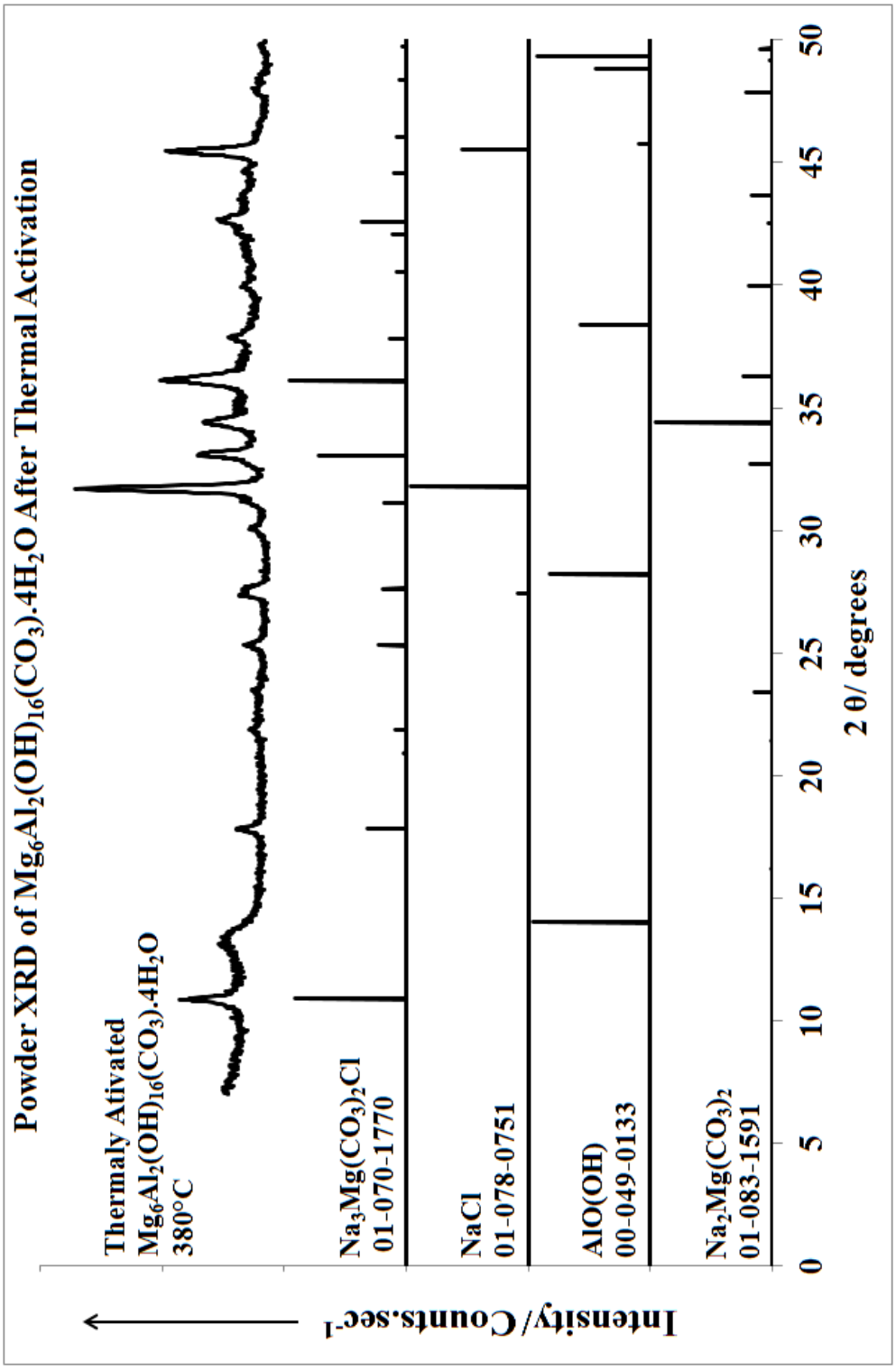

Figure. 2.2: XRD pattern of Mg/Al LDH after thermal activation with references of possible phases.

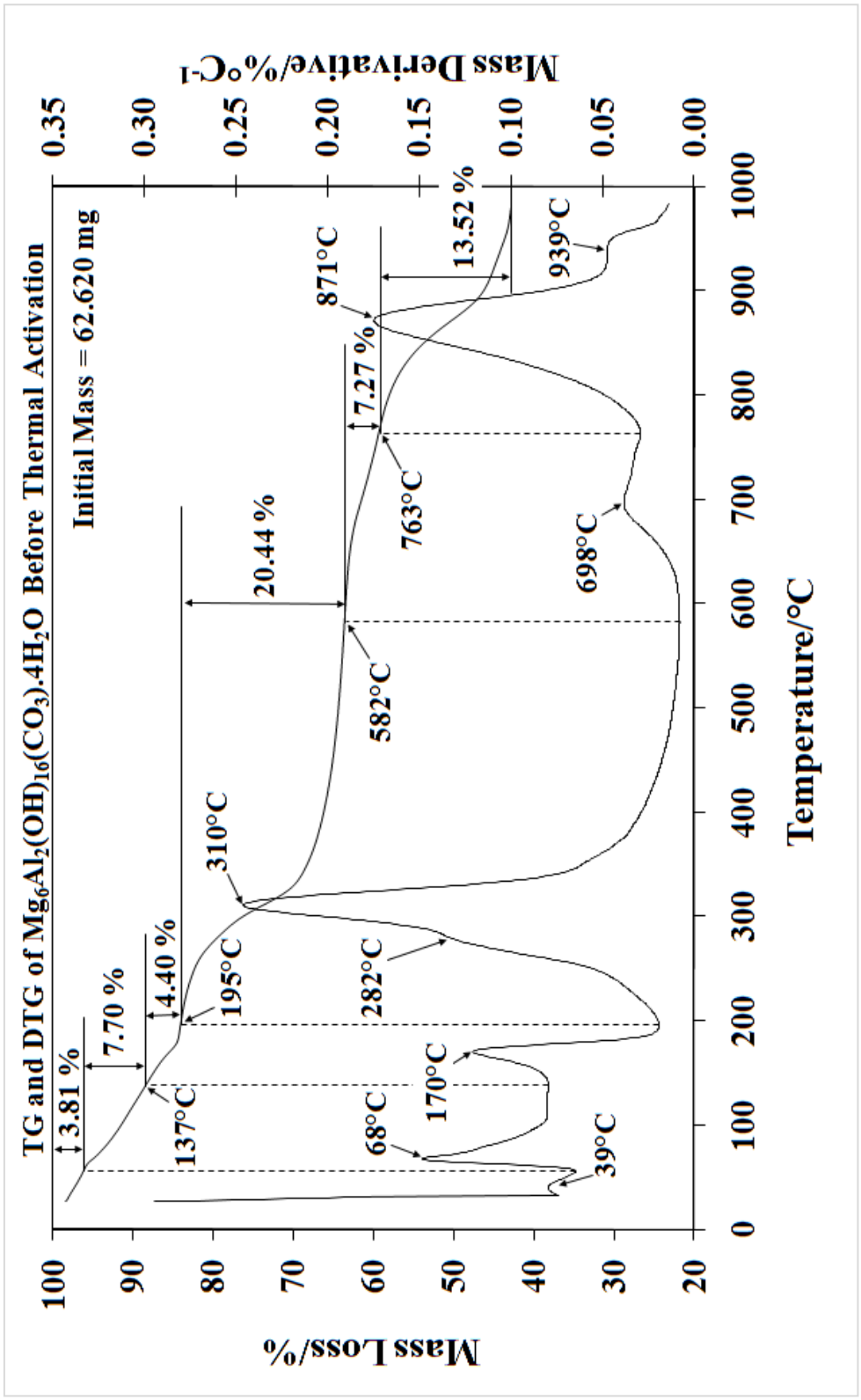

Figure. 2.3: TG and DTG curves of Mg/Al LDH before thermal activation or absorption experiments.

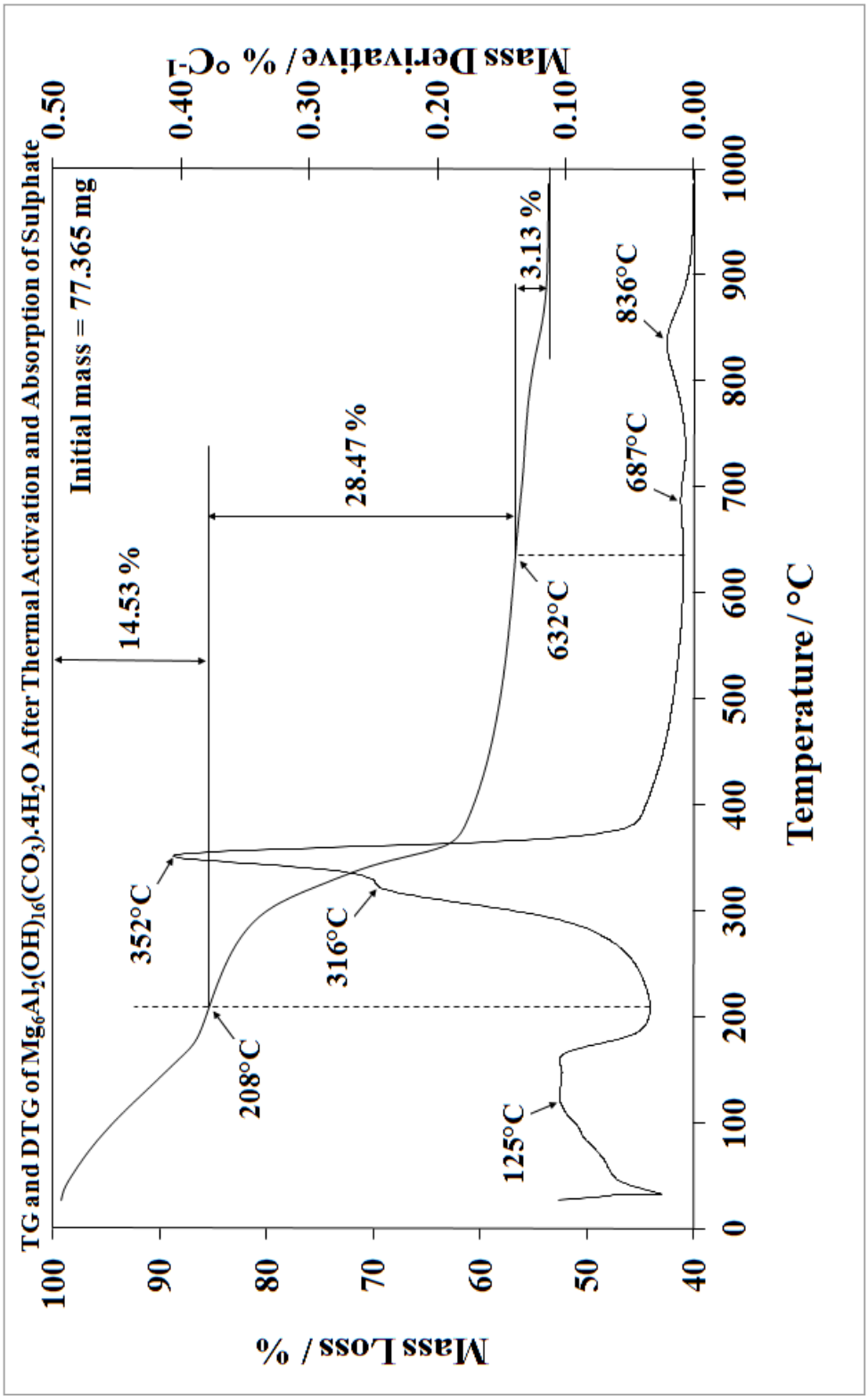

Figure. 2.4: TG and DTG curves of Mg/Al LDH After thermal activation and reformation by treatment of 3g of Mg/Al LDH with 1000ppm sodium sulfate solution (20mL).

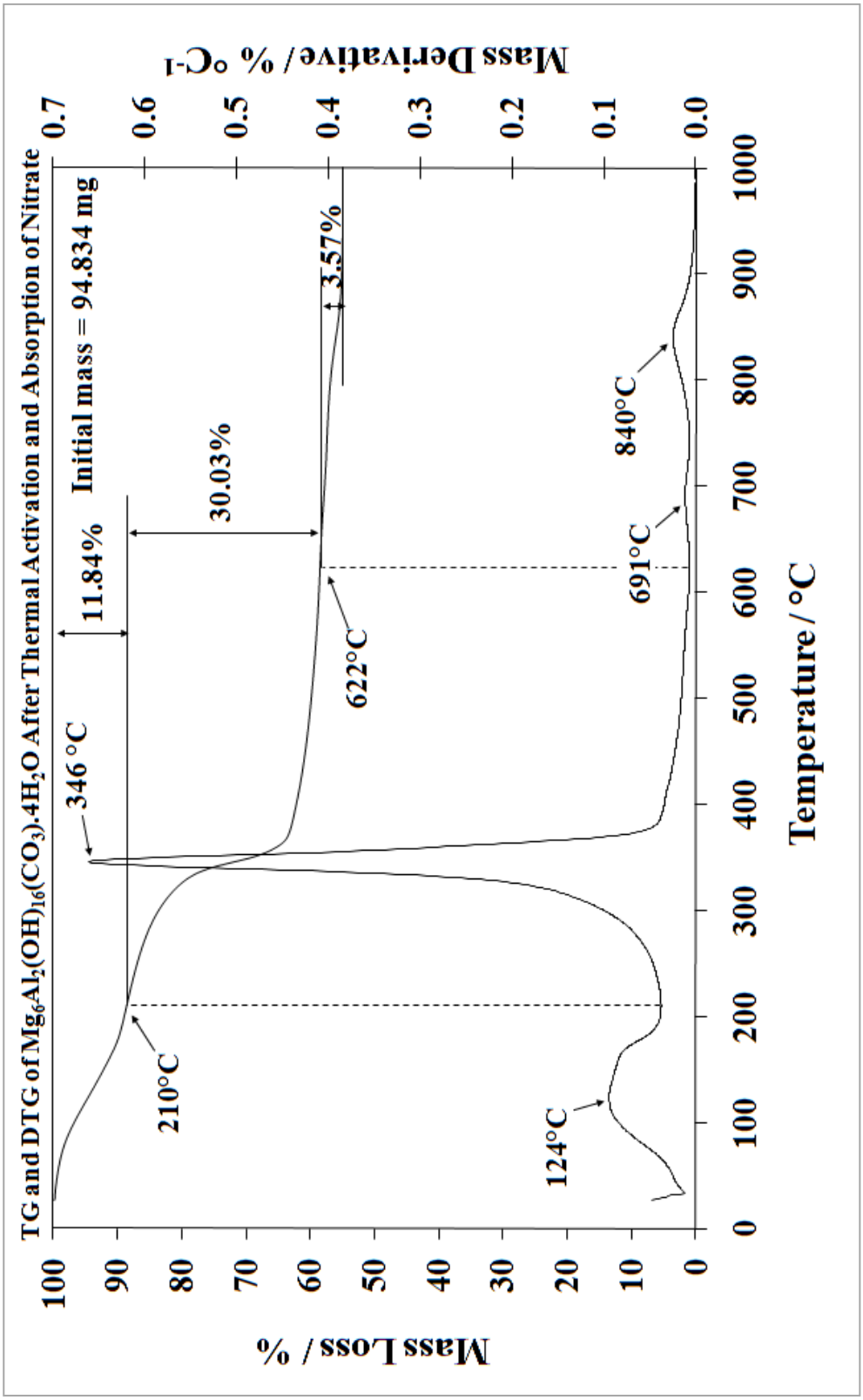

Figure. 2.5: TG and DTG of Mg/Al LDH, after thermal activation and reformation with the adsorption of nitrate solution (20mL, 1000ppm).

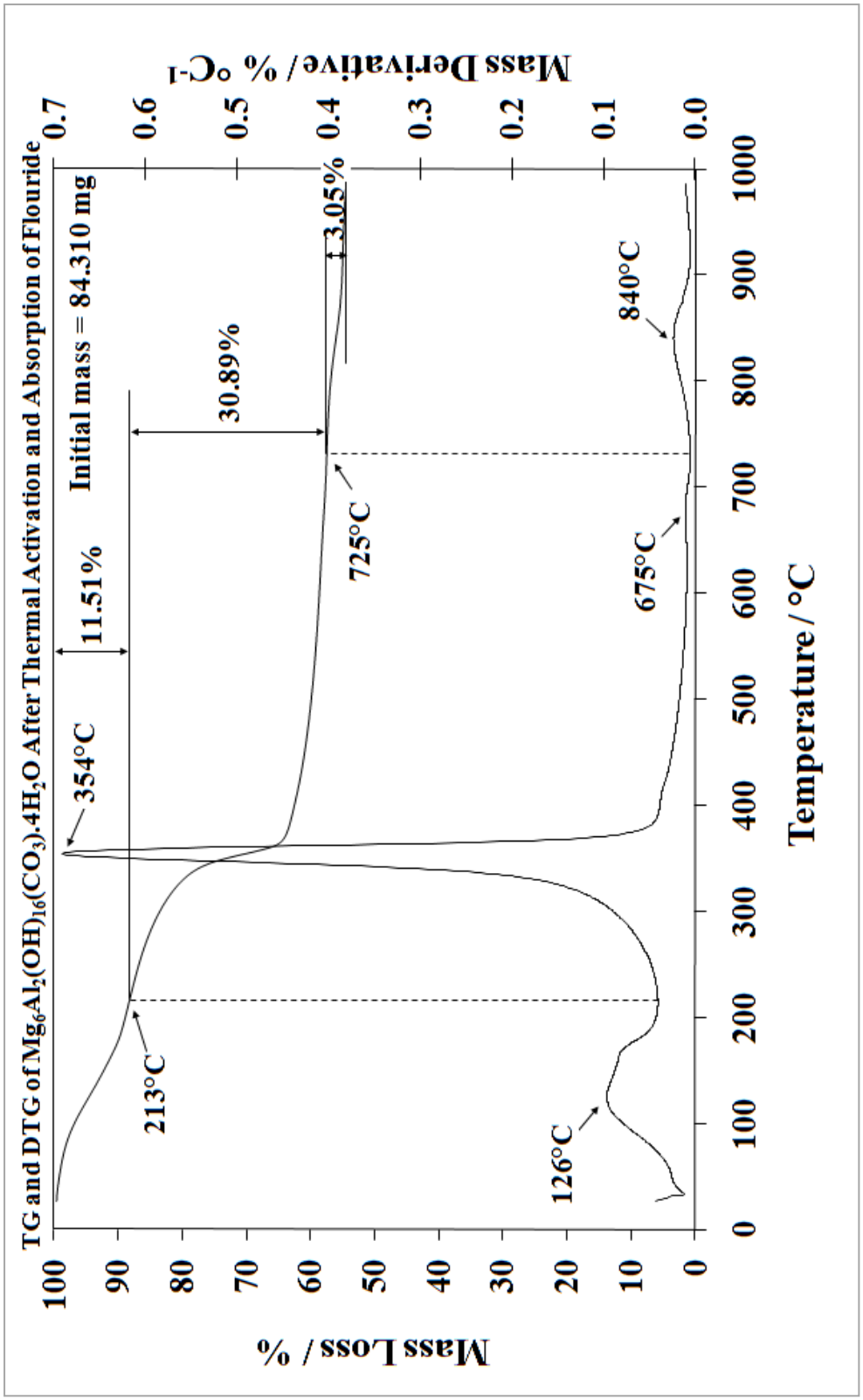

Figure. 2.6: TG and DTG of Mg/Al LDH, after thermal activation and reformation with the adsorption of fluoride solution (20mL, 1000ppm).

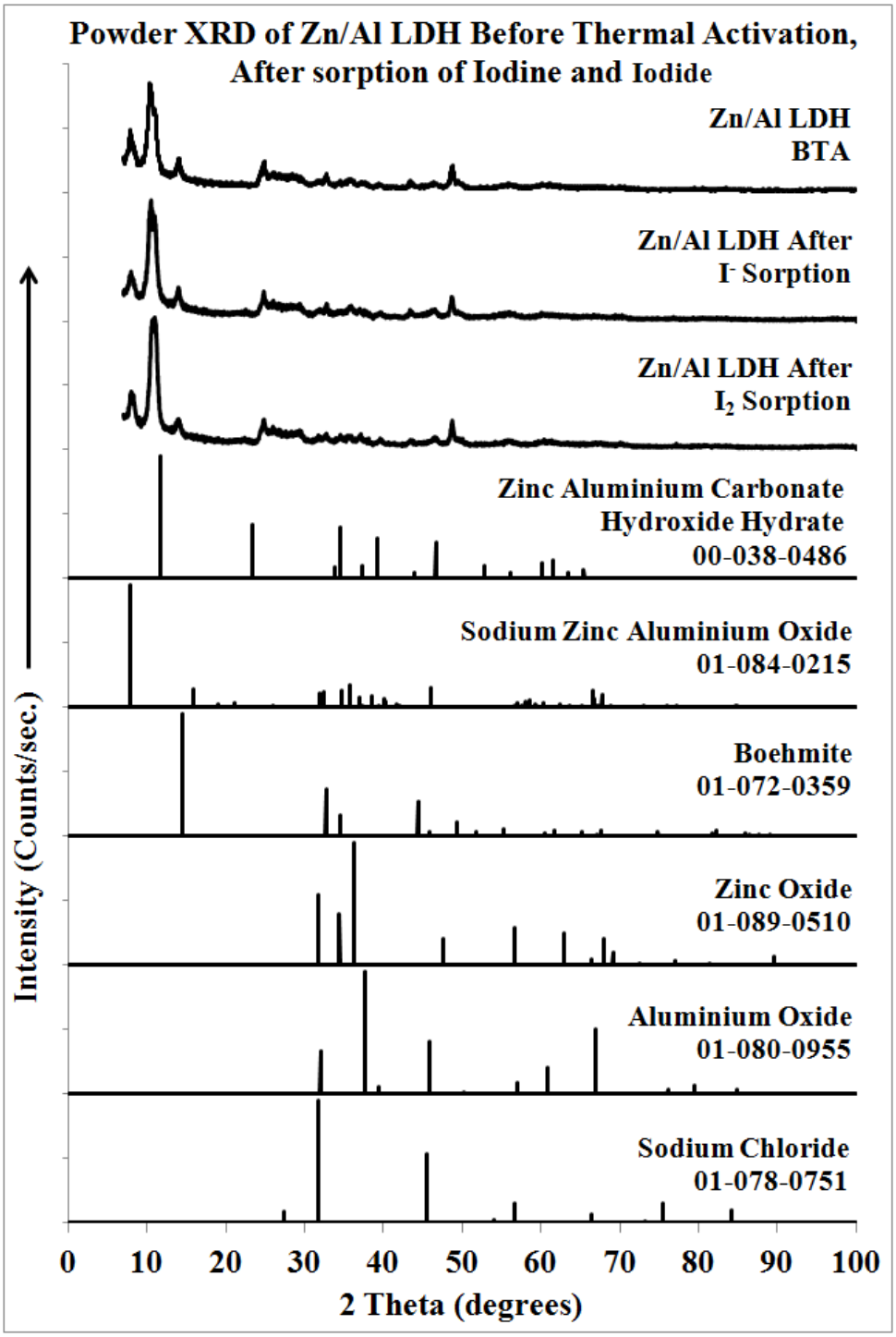

Figure. 3.1: Powder XRD pattern of Zn/Al LDH before thermal activation and after reformation in iodide or iodine solution with references.

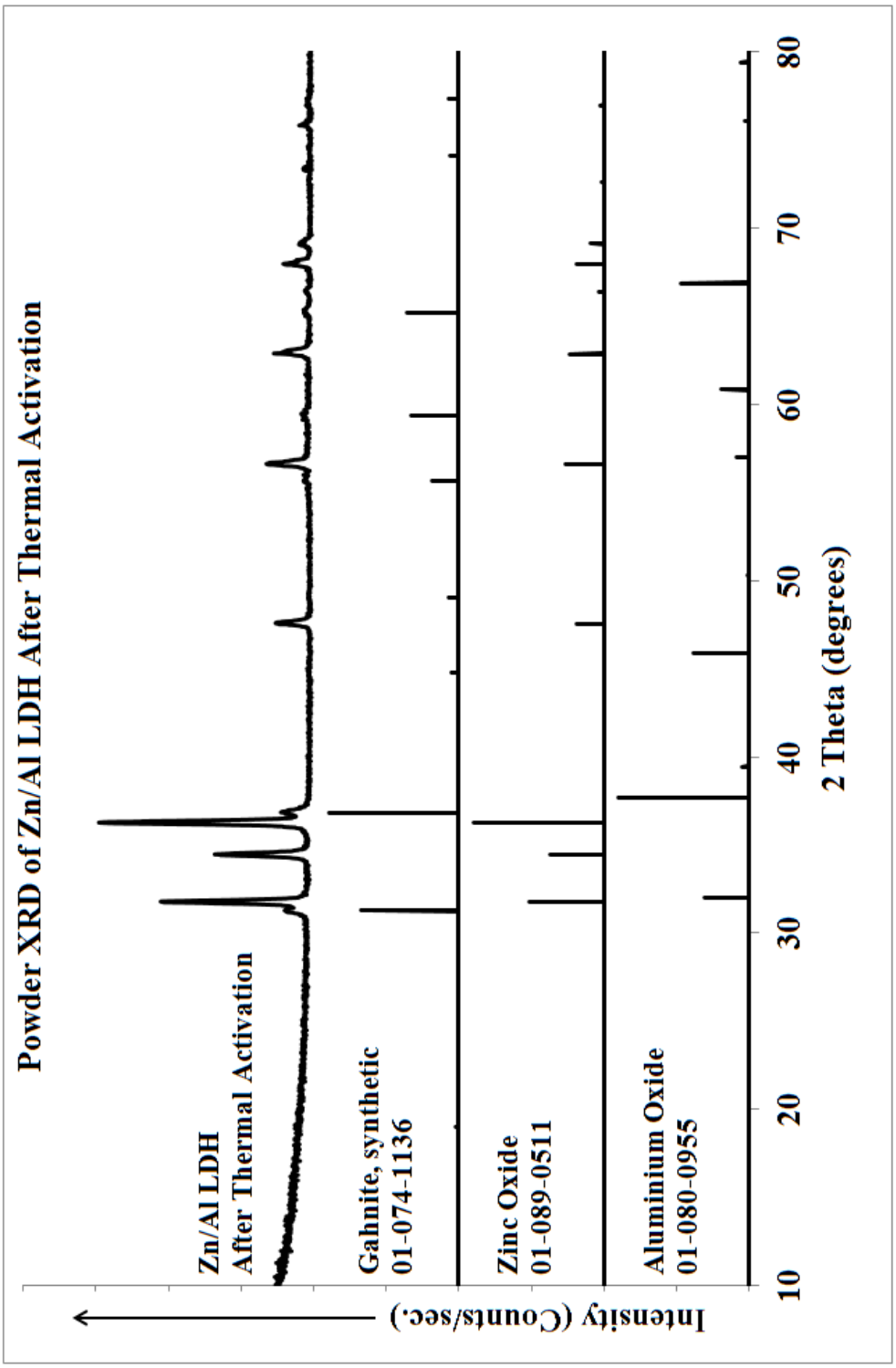

Figure. 3.2: Powder XRD pattern of Zn/Al LDH after thermal activation with references.

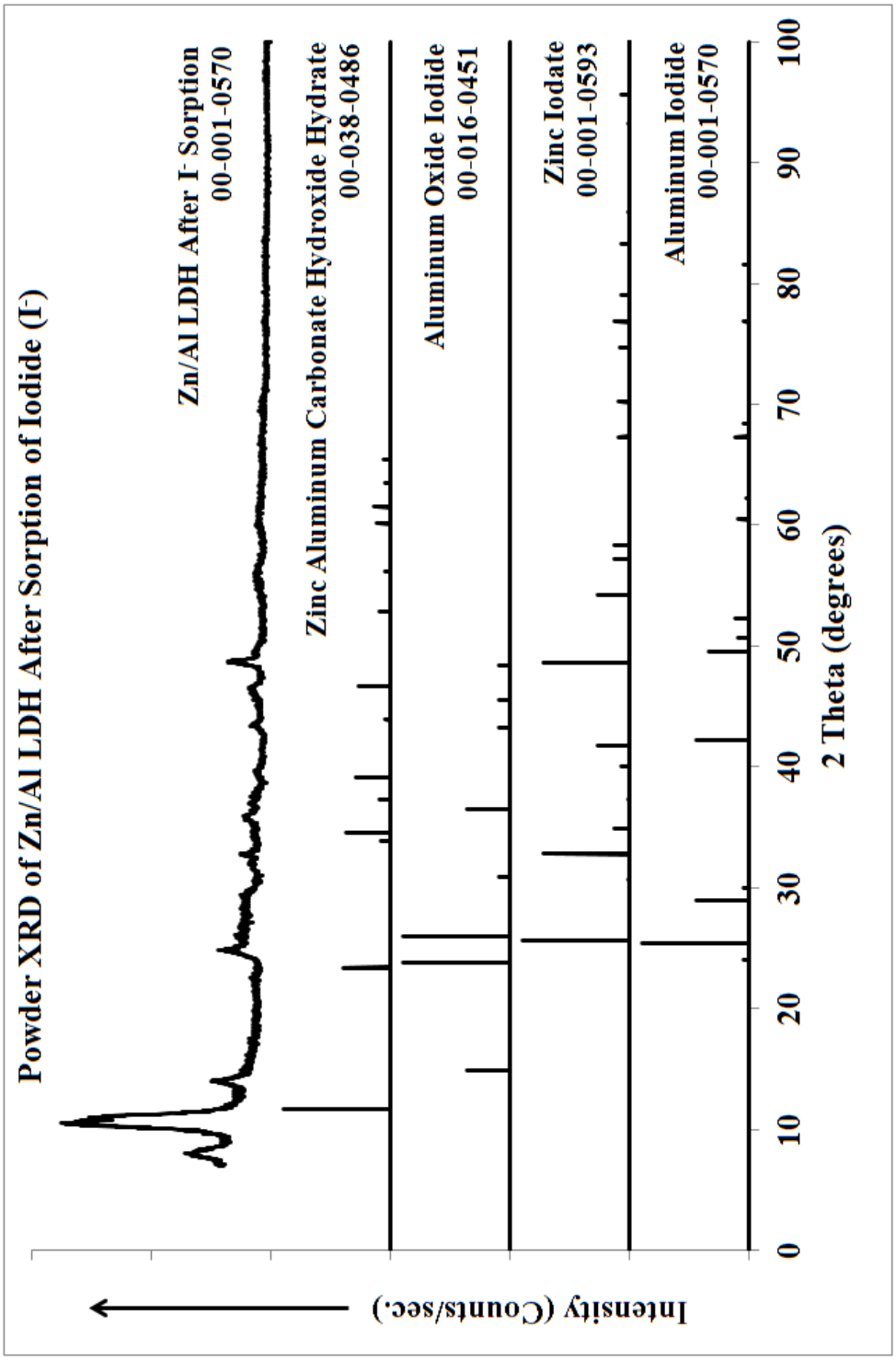

Figure. 3.3: Powder XRD pattern of Zn/Al LDH treatment with iodide solutions with references.

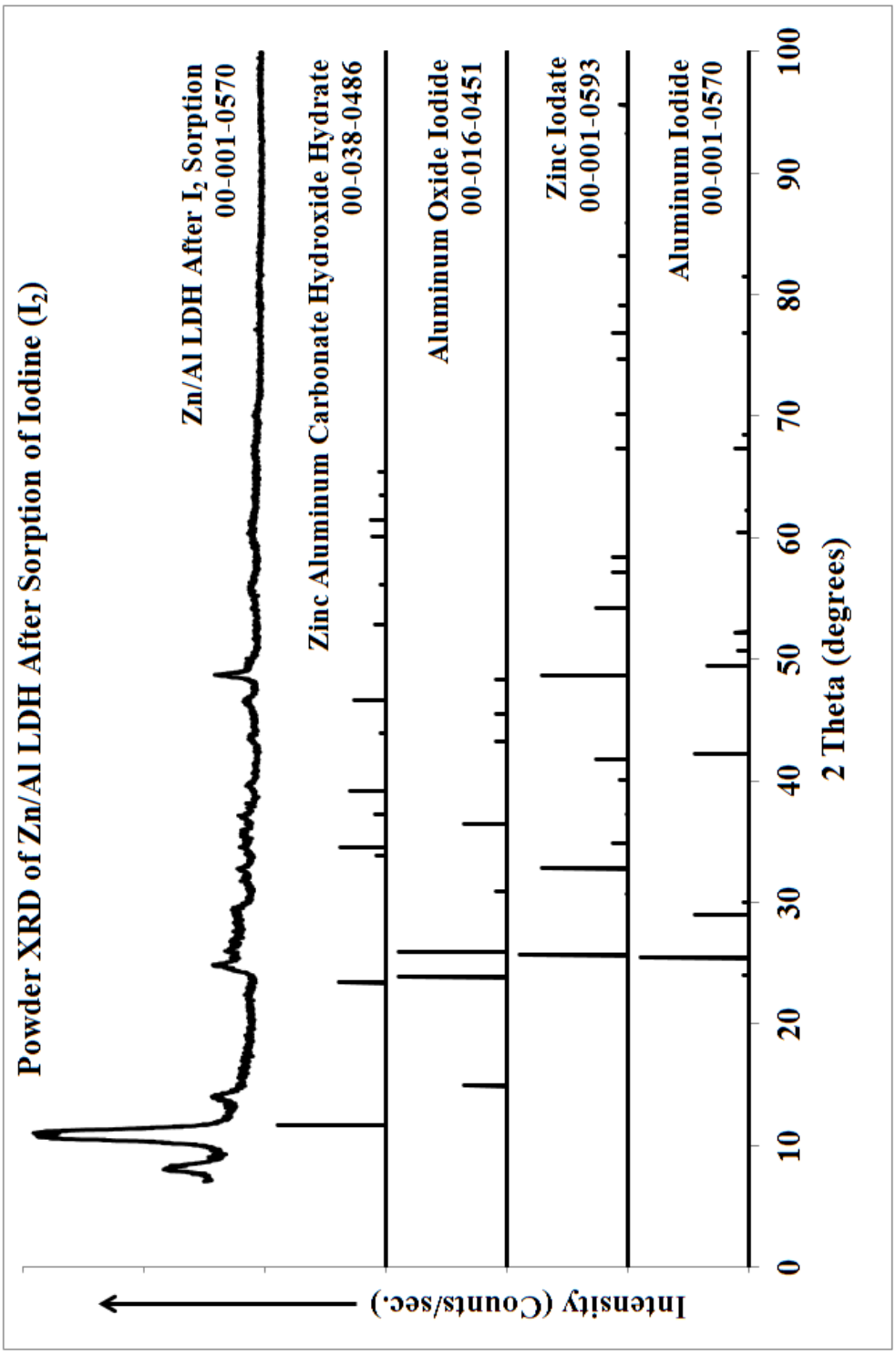

Figure. 3.4: Powder XRD pattern of Zn/Al LDH treatment with iodine solutions with references.

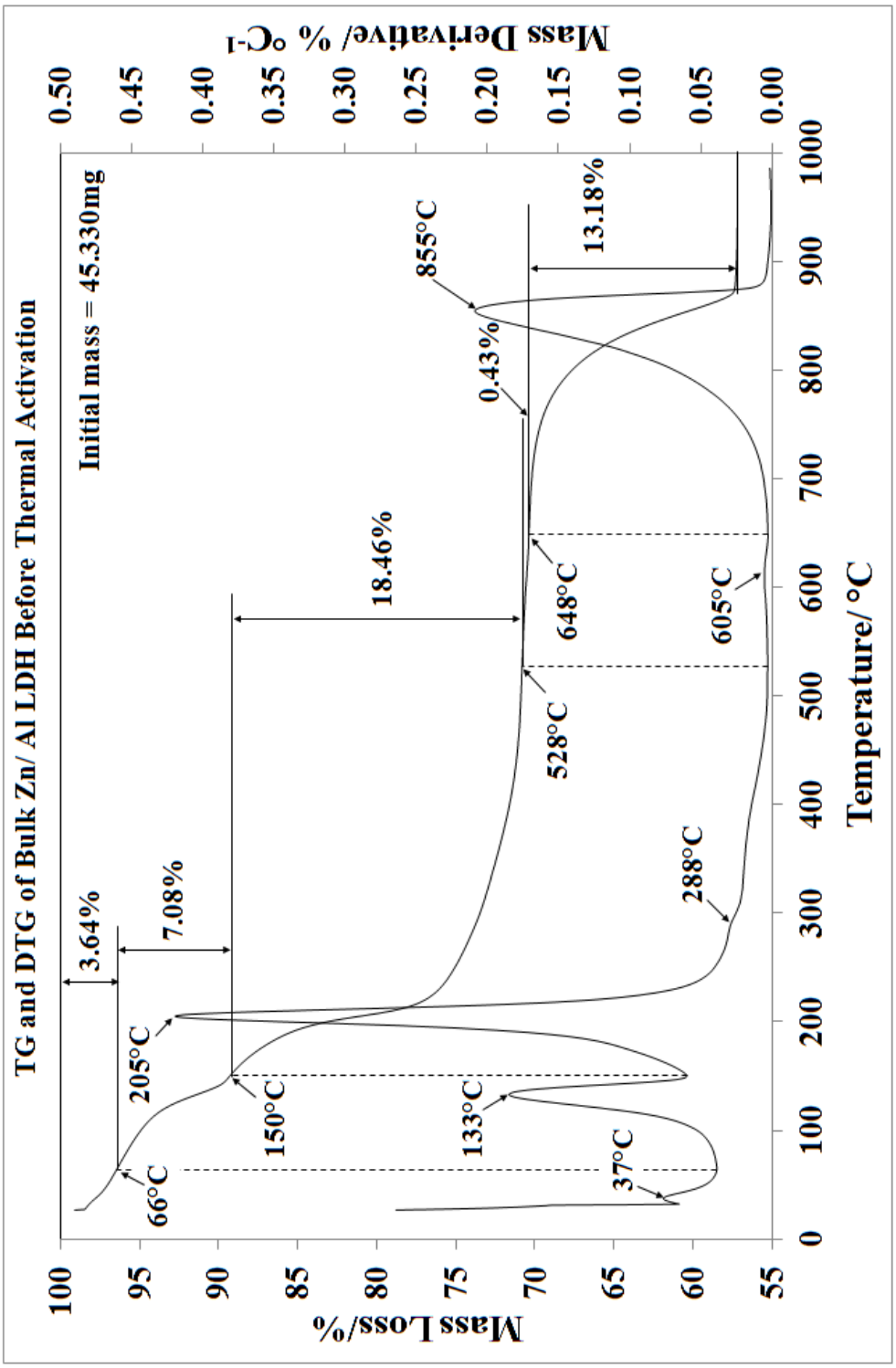

Figure. 3.5: TG and DTG of Bulk Zn/Al LDH before thermal activation

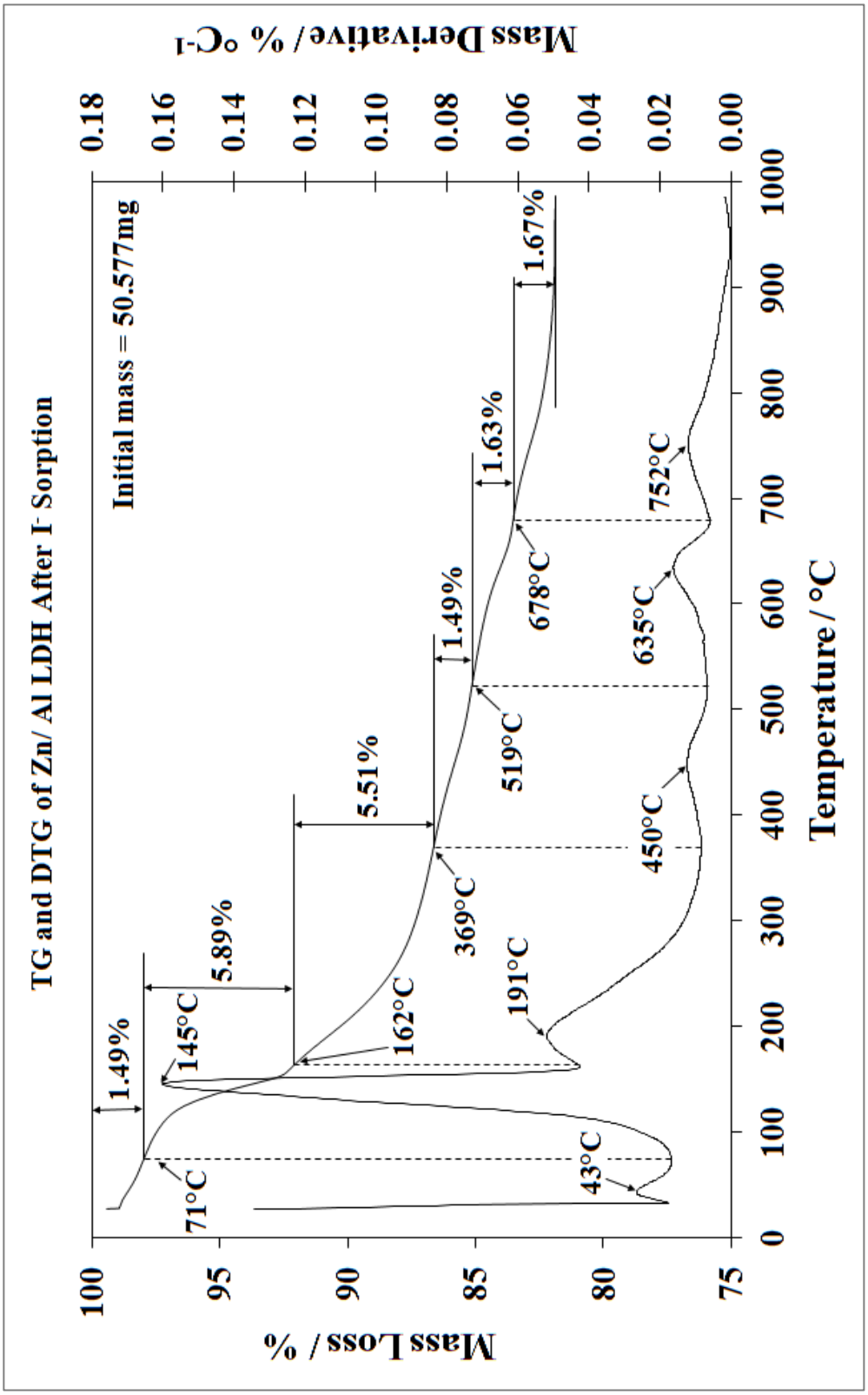

Figure. 3.6: TG and DTG of Bulk Zn/Al LDH after reformation in iodide solution

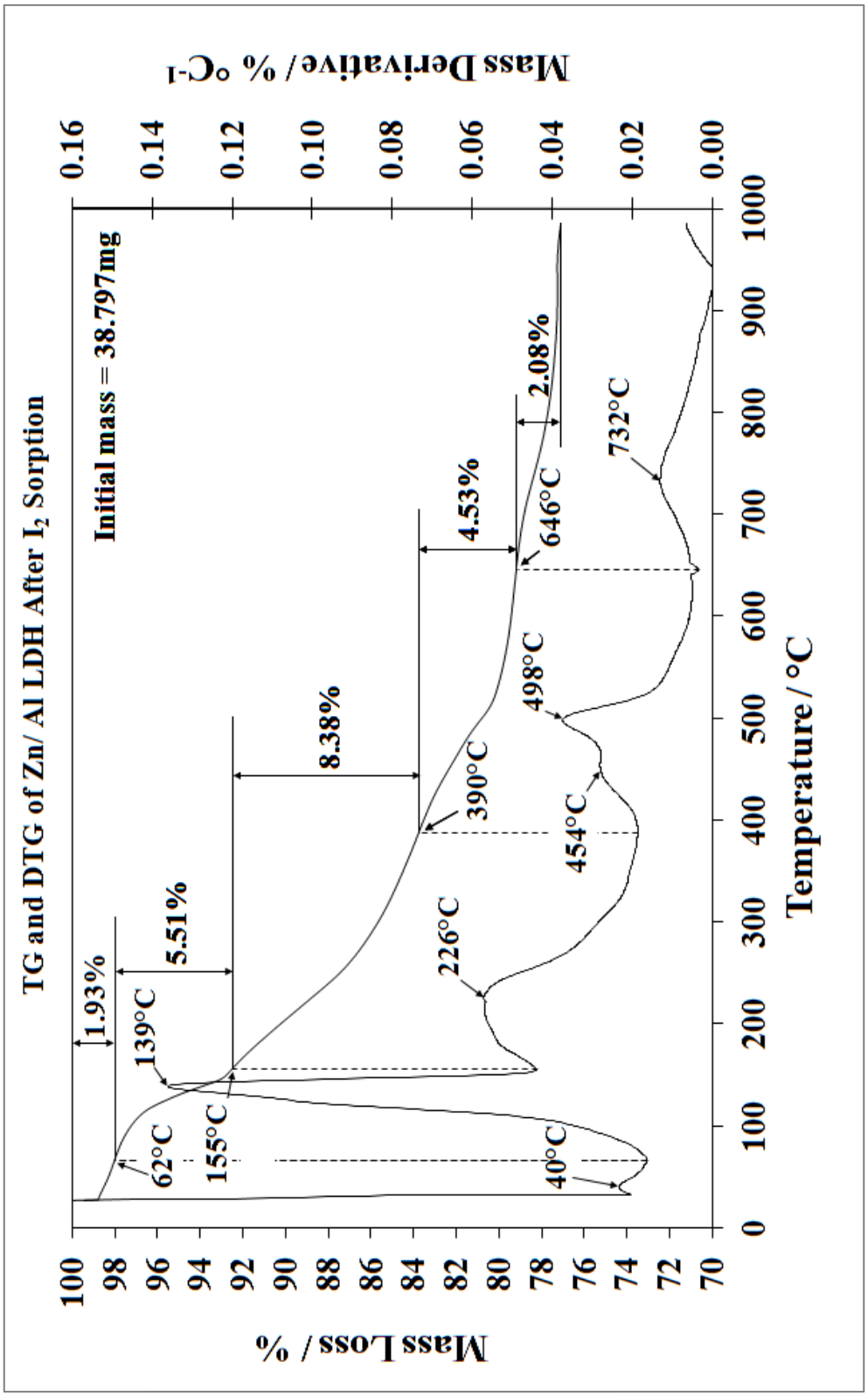

Figure. 3.7: TG and DTG of Bulk Zn/Al LDH after reformation in iodine solution

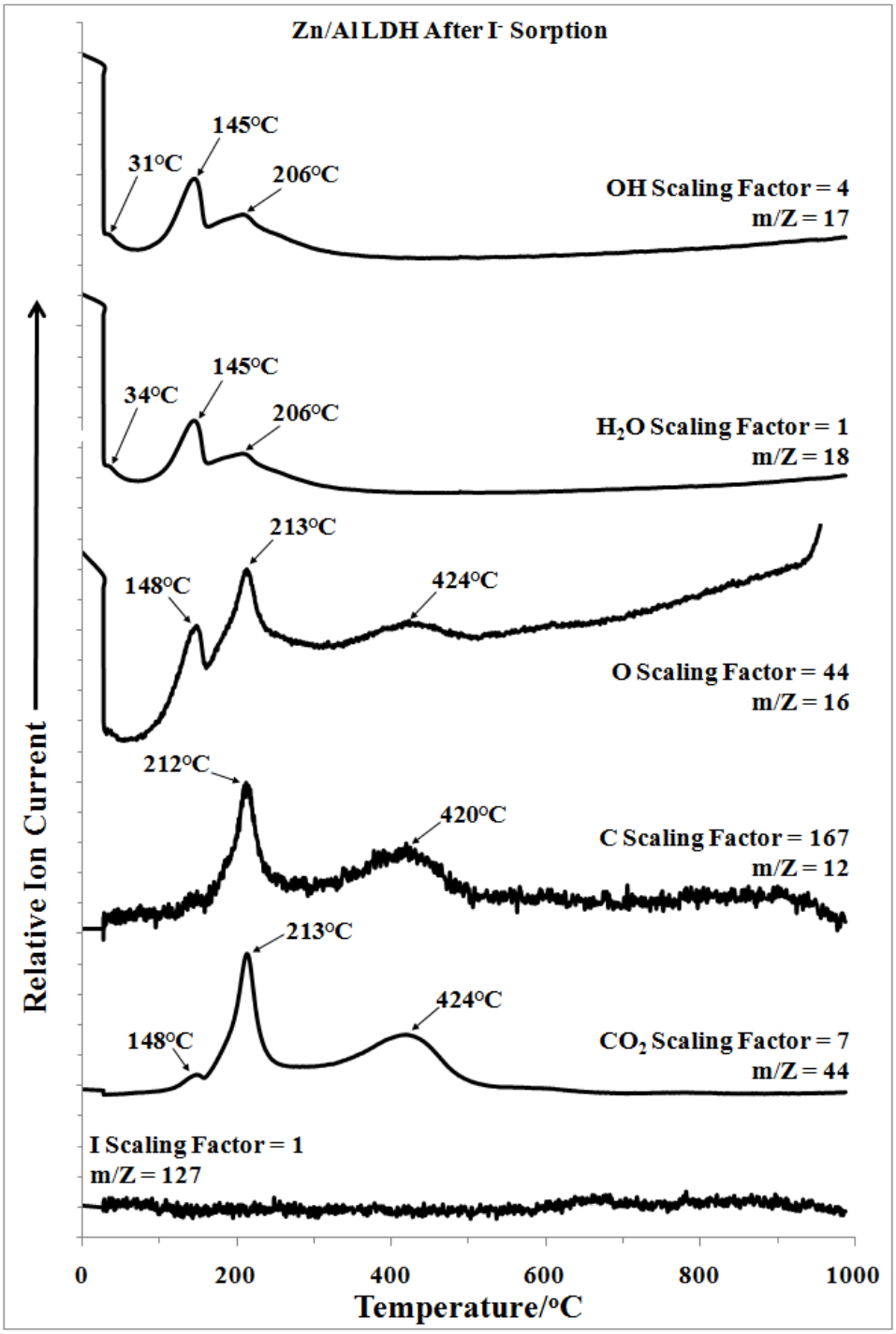

Figure. 3.8: Evolved gas mass spectrometry of selected ions evolved during the thermal decomposition of Zn/Al LDH treated with iodide solution.

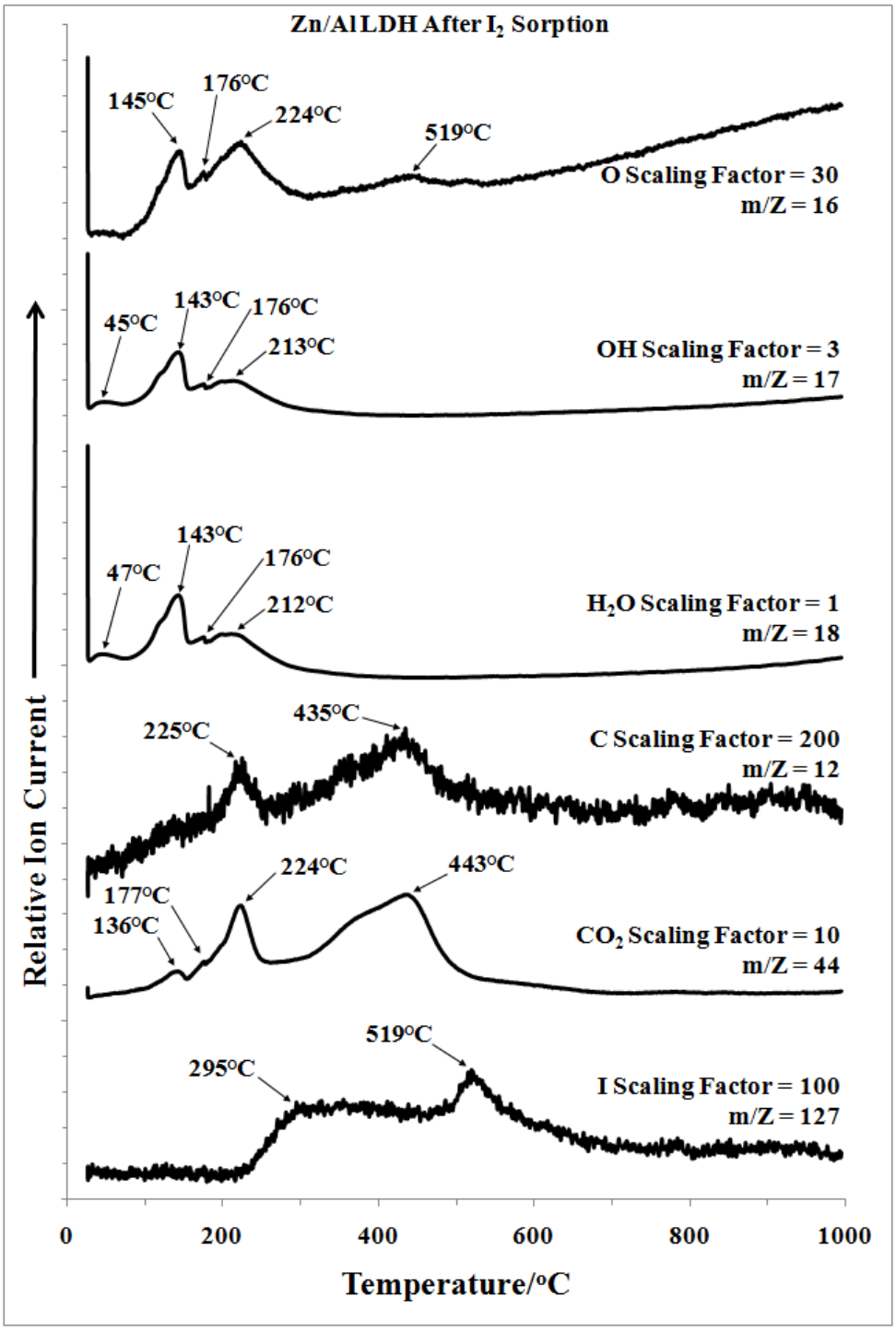

Figure. 3.9: Evolved gas mass spectrometry of selected ions evolved during the thermal decomposition of Zn/Al LDH treated with iodine solution.

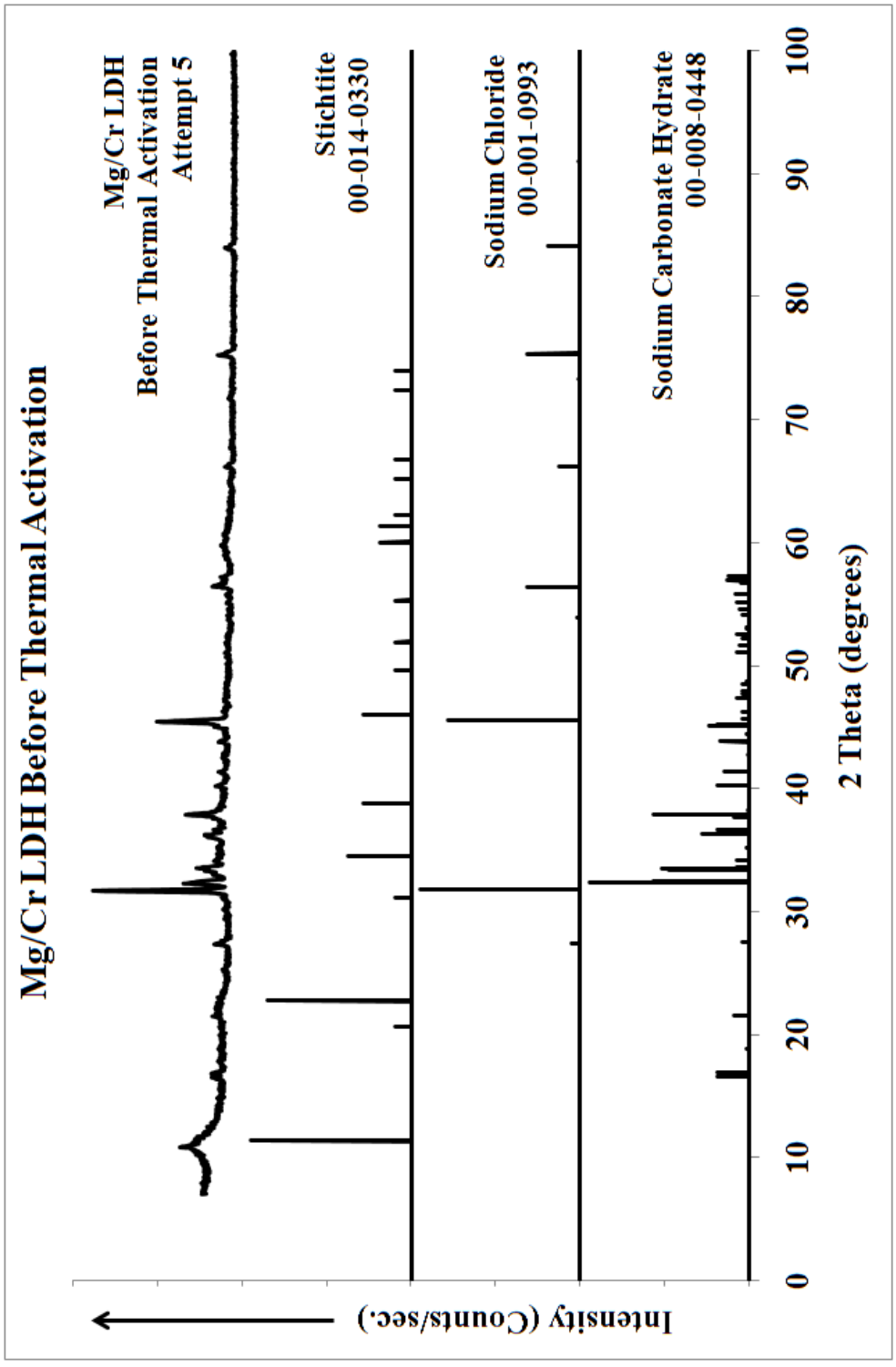

Figure. 4.1: Powder XRD of synthetic stichtite

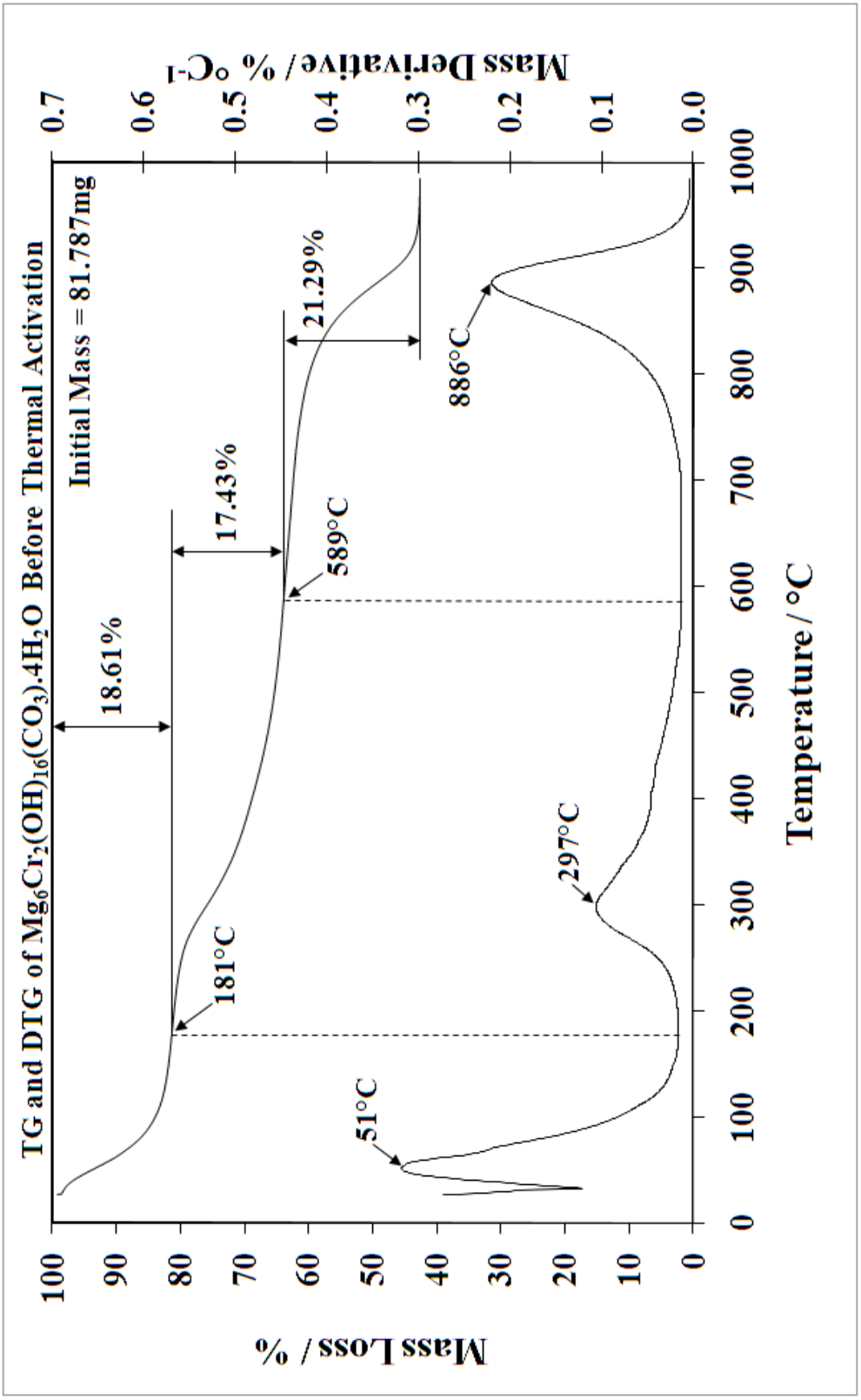

Figure. 4.2: Thermogravametric analysis of synthetic stichtite prepared by the co-precipitation method

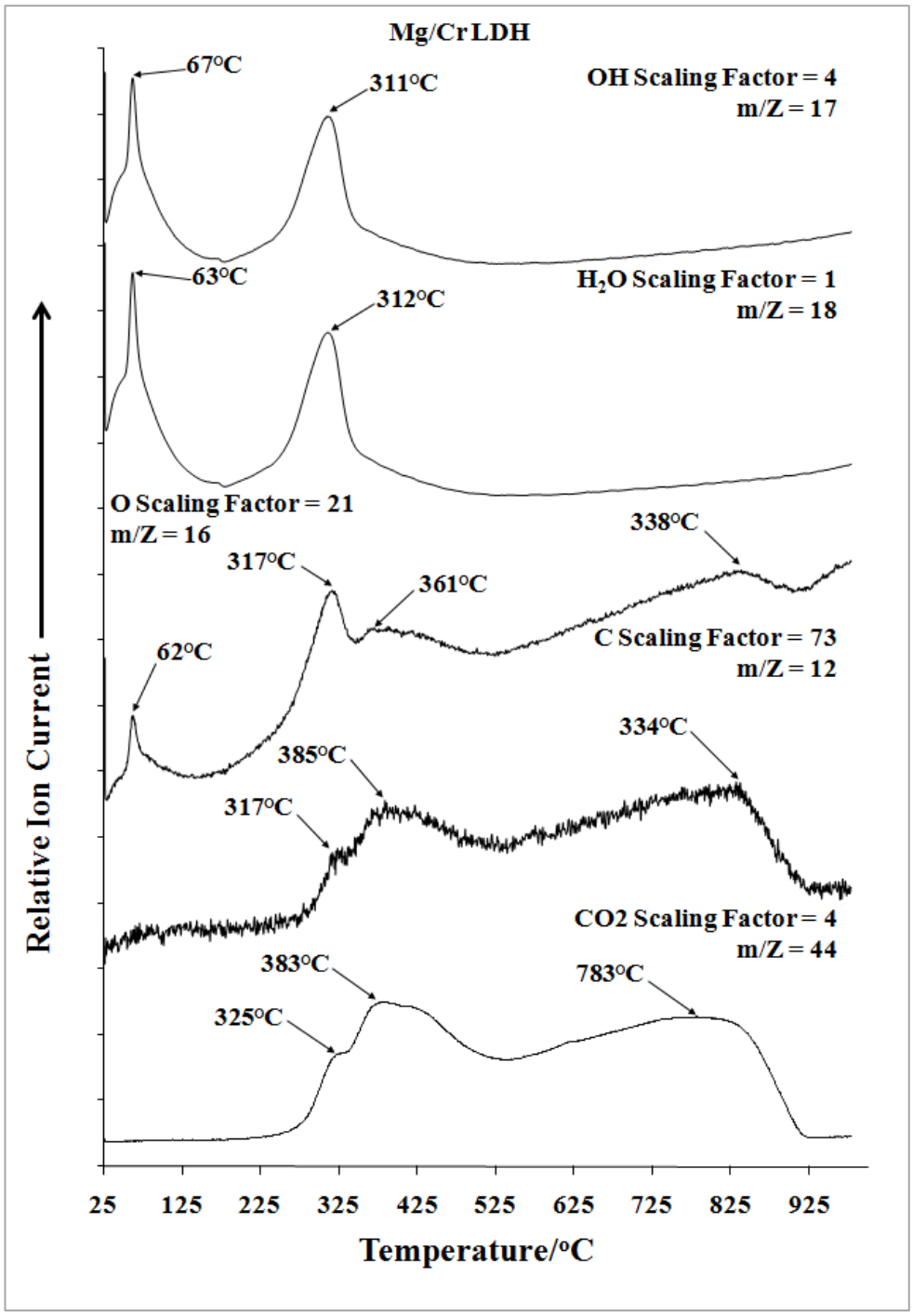

Figure. 4.3: Evolved gas analysis of synthetic stichtite prepared by the co-precipitation method

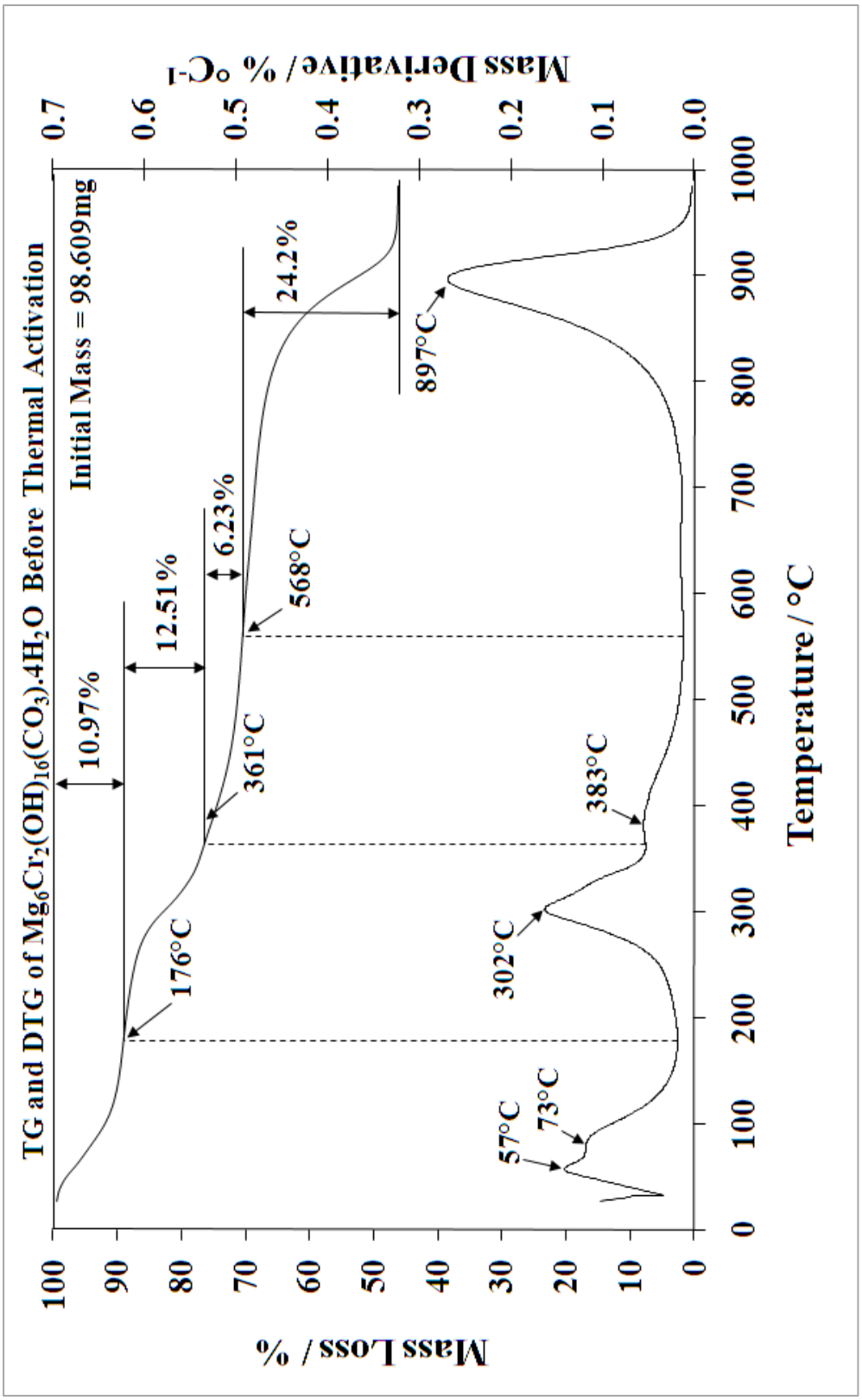

Figure. 4.4: Thermogravametric analysis of synthetic stichtite prepared by the co-precipitation method with 2 hours stirring after addition of the caustic solution

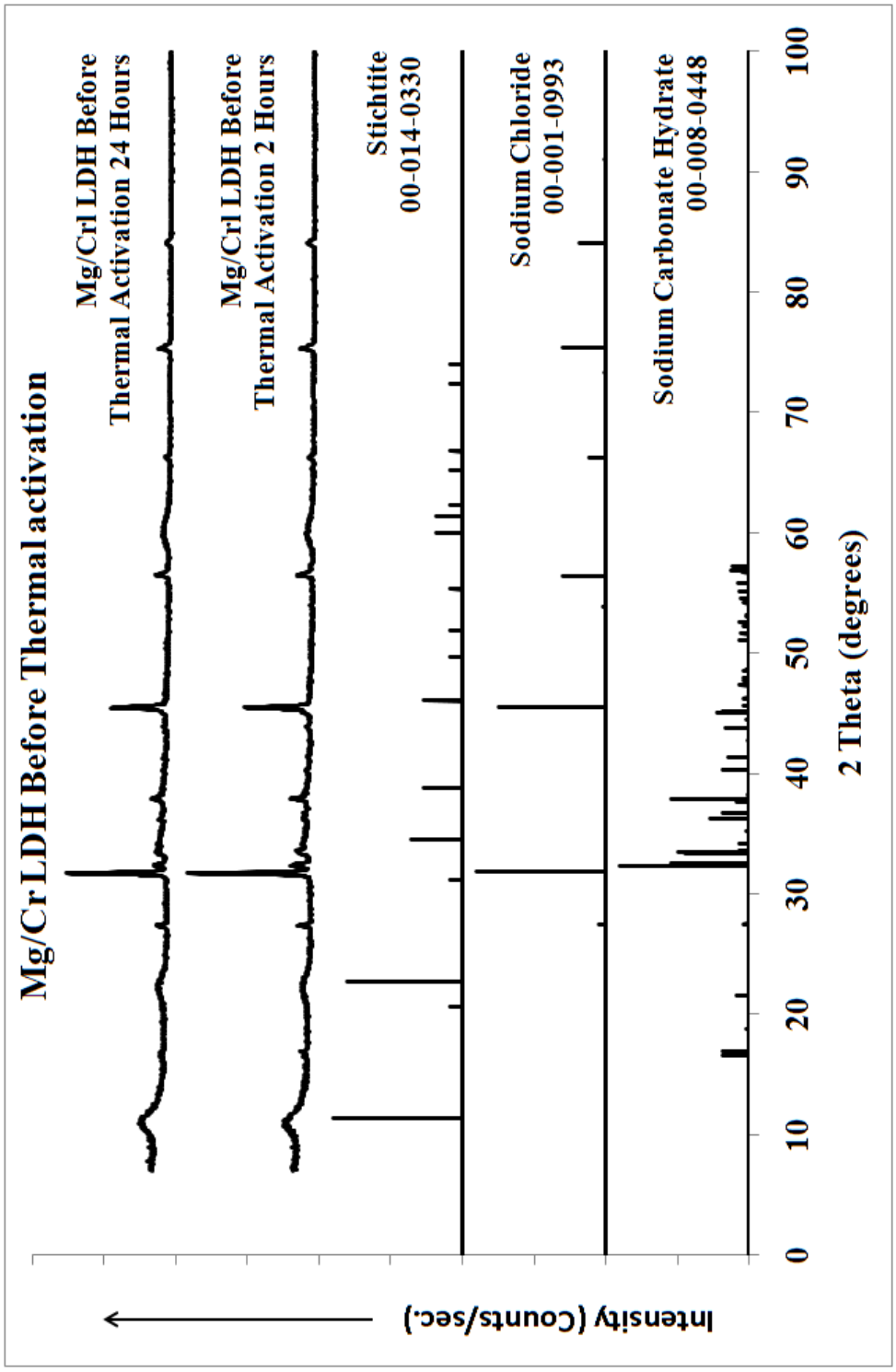

Figure. 4.5: Comparison of powder XRD of synthetic stichtite with 2 and 24 hours stirring after addition of the caustic solution

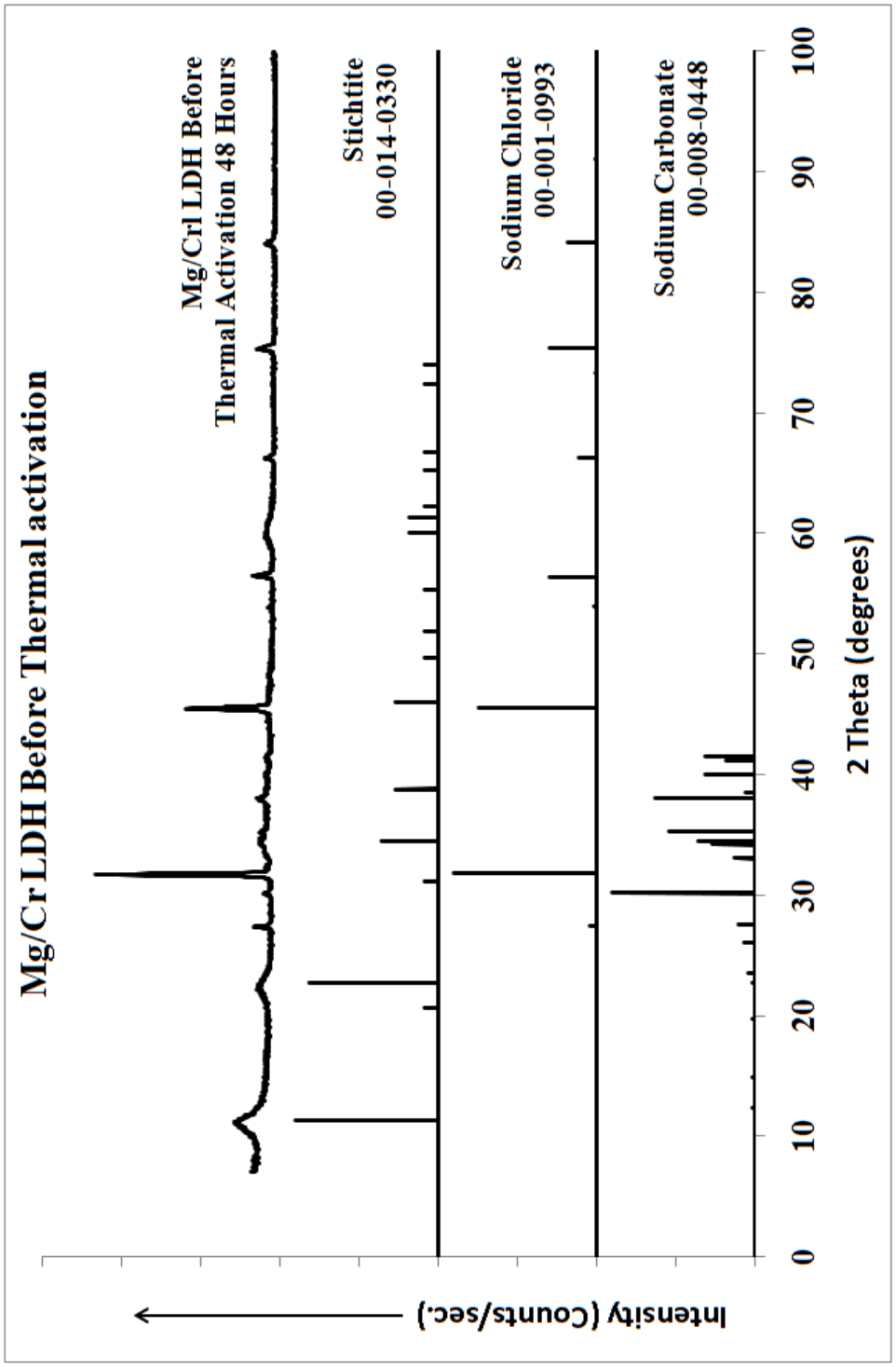

Figure. 4.6: Powder XRD of synthetic stichtite with 48 hours stirring after addition of the caustic solution

Appendix 2: Supplementary material for chapter 3.

Appendix 2 contains the supplementary material prepared for the paper *"Zinc Aluminium Layered Double Hydroxides for the Removal of Iodine and Iodide from Aqueous Solutions"*, which chapter 3 of this thesis is based on.

***Stoichiometric* Reactions**

Reaction of iodide and iodate to form triiodide

$$IO_3^- + 8I^- + 6H^+ \rightleftharpoons 3I_3^- + 3H_2O$$

Reaction of triiodide with thiosulphate

$$I_3^- + 2S_2O_3^{2-} \rightleftharpoons 3I^- + S_3O_6^{2-}$$

Calculations

Calculation of the initial concentration of iodide in the potassium iodide solution

Mass of potassium iodide used = *3.6555g*

Molecular mass potassium iodide = *166.01g/mol*

Volume of potassium iodide solution = *250mL = 0.25L*

$$n = \frac{m}{M_r}$$

$$n = \frac{3.6555}{166.01}$$

$$n \approx 0.2202\ mol$$

$$n = cv$$

$$c = \frac{n}{v}$$

$$c = \frac{0.2202}{0.25}$$

$$c \approx 0.08809\ mol/L$$

Standardisation of the sodium thiosulphate solution

Concentration of potassium iodide solution = *0.08809mol/L*

Volume of potassium iodide solution used = *20mL = 0.02L*

Average mass of potassium iodate = *1.0788g*

Molecular mass potassium iodate = *214.00g/mol*

Average volume of sodium thiosulphate = *45.2g*

$$n = cv$$

$$n = 0.02(0.08809)$$

$n = 1.7618 \times 10^{-3} mol$ of potassium iodide in the solution

$$n = \frac{m}{M_r}$$

$$n = \frac{1.0788}{214.00}$$

$n = 5.0411 \times 10^{-3}$ *mol* of potassium iodate in the solution

Potassium iodate is present in excess therefore the maximum concentration of triiodide that can be formed will depend on the concentration of potassium iodide.

$$mols\ I_3^- = 3\left(\frac{mol\ I^-}{8}\right)$$

$$n = 3\left(\frac{1.7618 \times 10^{-3}}{8}\right)$$

$$n = 6.60675 \times 10^{-4}\ mol$$

$$mols\ S_2O_3^{2-} = 2(mols\ I_3^-)$$

$$n = 2(6.60675 \times 10^{-4})$$

$$n = 1.32125 \times 10^{-3}\ mol$$

$$n = cv$$

$$c = \frac{n}{v}$$

$$c = \frac{1.32125 \times 10^{-3}}{0.0452}$$

$$c \approx 0.0292\ mol/L$$

Calculation of the concentration of iodide remaining in solution after treatment with Zn/Al LDH

Concentration of the sodium thiosulphate solution = *0.0292mol/L*

Average volume of sodium thiosulphate solution used = *18.6mL = 0.0186L*

$$n = cv$$

$$n = 0.0292(0.0186)$$

$$n \approx 8.3512 \times 10^{-4}\ mol$$

$$mol\ I_3^- = \frac{mol\ S_2O_3^{2-}}{2}$$

$$n = \frac{8.3512 \times 10^{-4}}{2}$$

$n \approx 4.1756 \times 10^{-4}\ mol$ of triiodide needed to react with all the thiosulphate solution used.

From the equation

$$mols\ I^- = 8\left(\frac{mol\ I_3^-}{3}\right)$$

$$n = 8\left(\frac{4.1756 \times 10^{-4}}{3}\right)$$

$$n \approx 1.11349 \times 10^{-3}$$

$$n = cv$$

$$c = \frac{n}{v}$$

$$c = \frac{1.11349 \times 10^{-3}}{0.02}$$

$$c \approx 0.0557 mol/L$$

Determining percentage removal of iodide after treatment with Zn/Al LDH

$$\%\ \text{iodide remaining} = 100\left(\frac{0.0557}{0.08809}\right)$$

% iodide remaining = 63.2%

% iodide removed = 100 – 63.2 = 36.8%

Calculation of the initial concentration of iodine in solution

Average mass of potassium iodide = *0.5794g*

Average mass of potassium iodate = *0.1421g*

Molecular mass potassium iodide = *166.01g/mol*

Volume of potassium iodide solution used = *20mL = 0.02L*

Solution volume = *20mL = 0.02L*

Concentration of potassium thiosulphate solution = *0.0292mol/L*

$$n = \frac{m}{M_r}$$

$$mols\ \mathrm{I^-} = \frac{0.5794}{166.01}$$

$n = 3.4902 \times 10^{-3}$ *mols* of iodide in the solution

$$mols\ \mathrm{IO_3^-} = \frac{0.1421}{214.00}$$

$n = 6.6402 \times 10^{-4}$ *mol* of iodate in the solution

The yield limiting reagent is potassium iodate. The maximum concentration of triiodide will depend on the concentration of iodate.

$$mols\ \mathrm{I_3^-} = 3(mol\ \mathrm{IO_3^-})$$

$$n = 3(6.6402 \times 10^{-4})$$

$$n = 1.99 \times 10^{-3} mol$$

$$n = cv$$

$$c = \frac{n}{v}$$

$$c = \frac{1.99 \times 10^{-3}}{0.02}$$

$$c \approx 0.0995\ mol/L$$

Calculation of the concentration of iodine remaining in solution after treatment with Zn/Al LDH

Average volume of potassium thiosulphate solution = *6.4mL = 0.00064L*

Solution volume = *20mL = 0.02L*

$n = cv$

$mols\ S_2O_3^{2-} = 0.0292(0.00064)$

$n = 1.8688 \times 10^{-5}$

$mols\ I_3^- = \frac{mols\ S_2O_3^{2-}}{2}$

$n = \frac{1.8688 \times 10^{-5}}{2}$

$n = 9.344 \times 10^{-6}$

$n = cv$

$c = \frac{n}{v}$

$c = \frac{9.344 \times 10^{-6}}{0.02}$

$c \approx 4.672 \times 10^{-4}$

Determining percentage removal of iodine after treatment with Zn/Al LDH

$$\%\ \text{iodide remaining} = 100\left(\frac{4.672 \times 10^{-4}}{0.0995}\right)$$

% iodide remaining = 0.47

% iodide removed = 100 – 0.47 = 99.5%

Determining the theoretical number of mols of Zn/Al LDH present in the sample

Mass of Zn/Al LDH = *45.330mg = 0.04533g*

Molecular mass of Zn/Al LDH = *557.10g/mol*

$$n = \frac{m}{M_r}$$

$$n = \frac{0.04533}{557.10}$$

$$n = 8.137 \times 10^{-5}$$

Theoretical mass loss resulting from removal of interlayer water from Zn/Al LDH

Mols of Zn/Al LDH = *8.137×10^{-5}*

Molecular mass of water = *18.02g/mol*

$$mol\ \mathrm{H_2O} = 4(mol\ \mathrm{LDH})$$

$$n = 4(8.137 \times 10^{-5})$$

$$n = 3.2548 \times 10^{-4} mol$$

$$n = \frac{m}{M_r}$$

$$m = n(M_r)$$

$$m = 18.02(3.2548 \times 10^{-4})$$

$$m = 5.8 \times 10^{-3} g$$

$$m = 5.864\ mg$$

$$\%\ mass\ loss = 100\left(\frac{5.864}{45.330}\right)$$

$$\%\ mass\ loss = 12.94\%$$

Theoretical mass loss resulting from dehydroxylation and decarbonation of Zn/Al LDH

Mols of Zn/Al LDH = *8.137×10^{-5}*

Molecular mass of water = *18.02g/mol*

Molecular mass of carbon dioxide = *44.01g/mol*

$mols\ \mathrm{CO_2} = mol\ \mathrm{LDH}$

$n_{\mathrm{CO_2}} = 8.137 \times 10^{-5}$

$n = \frac{m}{M_r}$

$m = n(M_r)$

$m_{\mathrm{CO_2}} = 44.01(8.137 \times 10^{-5})$

$m_{\mathrm{CO_2}} = 3.581 \times 10^{-3} g$

$m_{\mathrm{CO_2}} = 3.58\ mg\ of\ \mathrm{CO_2}\ released$

$\%\ mass\ loss\ \mathrm{CO_2} = 100\left(\frac{3.58}{45.330}\right)$

$\%\ mass\ loss\ \mathrm{CO_2} = 7.90\%$

$mols\ \mathrm{H_2O} = 8(mol\ \mathrm{LDH})$

$n_{\mathrm{H_2O}} = 8(8.137 \times 10^{-5})$

$n_{\mathrm{H_2O}} = 6.5096 \times 10^{-4}$

$n = \frac{m}{M_r}$

$m = n(M_r)$

$m_{\mathrm{H_2O}} = 18.02(6.5096 \times 10^{-4})$

$m_{\mathrm{H_2O}} = 1.172 \times 10^{-2} g$

$m_{\mathrm{H_2O}} = 11.72\ mg$

$$\%\ mass\ loss\ \mathrm{H_2O} = 100\left(\frac{11.72}{45.330}\right)$$

$$\%\ mass\ loss\ \mathrm{H_2O} = 25.87\%$$

$$Total\ \%\ mass\ loss = 7.90 + 25.87$$

$$Total\ \%\ mass\ loss = 33.77\%$$

$$= 25.87\%$$

$$Total\ \%\ mass\ loss = 7.90 + 25.87$$

$$Total\ \%\ mass\ loss = 33.77\%$$